Preface

Special Issue on Electronic, Telecommunications, Automation, and Informatics with Computer Science (ETAI)

The Guest Editors are honored and proud to present this *Special Issue of* ***Acta Polytechnica Hungarica*** comprising the final selection of nine *best papers of the International Conference ETAI-2018,* which have been considerably extended and modified. The manuscripts that appear in this special issue were finally selected following additional three rounds of reviews of the initially recommended collection of the 12 best ETAI-2018 papers, recommended by the Editorial Board. The finally selected manuscripts have been additionally upgraded with new authentic research ingredients hence potential overlaps with ones in the conference proceedings has been further reduced to much less than the required standard of the journal. The underlying criteria for this selection were the essential novelty of contributions, quality of research, potential interest of the world-wide scientific and professional community as well as clarity of the presentation. Each expanded manuscript was reviewed by internationally recognized experts in the respective technical fields. Thus, we are convinced the scientific values of these selected manuscripts will enhance broadening the existing knowledge and deepening the understanding in the corresponding expertize areas of all potentially interested readers.

The thematic Conferences on Electronic, Telecommunications, Automation, and Informatics with Computer Science (ETAI) became fully International in 2003 after the independence the Republic of North Macedonia. However initially these were established in 1982 during former S.F.R. of Yugoslavia as all-Yugoslav ones created and organized in Macedonia. Traditionally, the ETAI Conferences all have taken place in the natural ambient of exceptional beauty of Ohridean Lake region and cradle of cultural heritage of Ohrid City, which make the world-wide is a well-known UNESCO protected region for both cultural and natural heritage of the mankind. The ETAI 2018 was the fourteenth one in this series of conferences. International ETAI Conferences have thus grown and matured as one of the largest international meetings of professional experts and researchers from academic, business and industrial community in countries of Balkan region, which are dedicated to the ETAI fields and their mutual cross-fertilizing synergies.

This special issue begins with the symbol ***E*** novel contribution (Electrical-Electronics fields) to the ever interesting and intriguing field of Electromagnetic Compatibility. Although more than century and a half has elapsed since celebrated Maxwell's Equations were published still their exact application in some areas appears to be a challenge. The approximation if often used in order to enable fast

yet accurate modeling. Article *"**Accurate Low-Frequency Approximation for Wires within a Two-Layered Earth**"* is authored by Blagoja Markovski, Leonid Grcev, Vesna Arnautovski-Toseva, and Andrijana Kuhar, and it is focused on approximating the electromagnetic model based on transverse Hertz vector potentials as applied to wires embedded in two-layered earth. The authors show that this approximation is more accurate than the one based on Sommerfeld's resolution for frequencies within the range 10 kHz – 10 MHz. Therefore their novel approximation is made applicable in transient analysis where currents with significant high frequency contents are involved, such as the ones initiated by subsequent lightning strikes. Their result has been validated for a range of different wire geometries and soil characteristics. The development of the proposed low-frequency approximation model is based on exact solution for the spatial domain Green's functions, which are cast in an appropriate form.

The subsequent two articles present research novelties within the symbol ***T*** (Telecommunications) field. The first one is dedicated to considerations in the currently rather hot topic of 5G mobile broadband networks, while the second one explored further the elastic optical networks. It should be noted in addition, these manuscripts contribute certain cross-fertilization synergies of communications networks and systems with computer science and information signal processing.

The new 5G concept of mobile broadband networks raises very high interest and expectations not only in the scientific community, but also in the broader community. The forthcoming networks are analyzed from many different aspects. The security and quality-of-service (QoS) is investigated in the paper *"**Future 5G Mobile Broadband Networks using Cloud-based Services with Advanced Security and QoS Framework**"* is authored by Mitko Bogdanoski, Tomislav Shuminoski, Metodi Hadji-Janev, Aleksandar Risteski, and Toni Janevski. The paper presents a Security and Quality of Service (QoS) framework that provides safety based on high level of security features. The framework, conveniently named ASECQUA, assures QoS for different multimedia services in the presence of different types of disturbances and Denial of Service attacks, by providing the highest level of multimedia secure access probability ratio and highest aggregated throughputs for each multimedia service over secure traffic tunnels.

The contribution *"**Analysis of Latency, Blocking Probability and Network Utilization for Specific Routing and Spectrum Assignment Algorithm in Elastic Optical Networks**"*, which is authored by Teodora Kocevska, Pero Latkoski, Marko Porjazoski, and Borislav Popovski, is focused on coping with the problem of ever increasing traffic volumes. Understanding the limitations and inappropriateness of the currently used technologies to meet the heterogeneous and variable traffic demands, they research new intelligent routing and spectrum allocation algorithms that support different class of service (CoS). The proposed algorithm assumes a coexistence of two traffic categories in the network, and a central Software Defined Networking (SDN) controller. The priority of different classes is determined by a dynamic RSA algorithm with two controlling

coefficients. The paper presents a simulation tool for analysis of the impact of controlling algorithm's coefficients on the network conditions. The results of the simulation could enable network operators to perform fine tuning of the utilization of the network, its blocking probability and data traffic latency, which is essential for the forthcoming 5G communication networks.

This journal issue continues with a rather important contribution in the field symbolized by letter ***A*** (Automation and Control), which is entitled *"**Stability of Nonlinear Descriptor Systems and Application to Stabilization of Quadcopters**"*. It has been authored by Drilon Bunjaku, Jovan D. Stefanovski, and Georgi M. Dimirovski. The authors argue that in some cases stability can be achieved via employing solely the differentiation of functions, and thus solving of combined nonlinear differential equations and nonlinear algebraic equations was shown unnecessary. Their approach is based on nonlinear descriptor systems, for which they present new sufficient Lyapunov-like stability conditions and new sufficient Lyapunov-like stabilizability conditions. Thus this original result appears extremely important for various applications of nonlinear descriptor system models. In order to validate their result, they apply the conditions to very popular problem of quadcopter's flight stabilization, for which they elaborate a new representation of the quadcopter as a nonlinear descriptor system. The numerical simulations show that the achieved stabilization is better than the one achieved with pure tracking control. This result appears to imply great practical importance since it enables simple and efficient stability control design. This article does bring certain cross-fertilization synergy of systems science, control theory and advanced computing.

The following three articles consider different machine learning techniques applied to relevant problems in different domains; hence largely contribute innovations in the field symbolized by letter ***I*** (Informatics with Computer Science). Though, it should be noted, these manuscripts also bring cross-fertilization synergies of computational intelligence with computer and systems sciences.

This group of contributions begins with article *"**Feature Space Reduction Using PCA in the Algorithm for Epilepsy Detection Using Adaptive Neuro-Fuzzy Inference System and Comparative Analysis**"* is authored by Marjan Stoimchev and Vesna Ojleska Latkoska. The research presented in this article is a problem specific one. This article considers the application of Adaptive Neuro-Fuzzy Inference System as a classifier for detection of epilepsy from EEG signals. The feature extraction is performed using statistical moments of the wavelet transform of the signal. This approach has been previously used with success, and the paper presents an attempt to further improve the performance and lower probability of over-fitting through reduction of the number of features based on Principal Component Analysis (PCA). The experimental results clearly show the advantages of using PCA. The paper also includes algorithms performance

analysis when different data splitting methods and different input space partitioning methods are used.

The subsequent article is entitled *"**Option Predictive Clustering Trees for Multi-label Classification**"* and authored by Tomaž Stepišnik, Dragi Kocev, and Sašo Džeroski. This article investigates the feasible possibilities of performance improvement of general classifiers. The research presented in the paper considers the application of clustering trees for the problem of multi-label classification. The presented algorithm is an attempt to overcome the shortsightedness of the standard tree induction algorithm, regardless of the type of the classification problem that is considered. The approach is based on allowing for alternative splits in the internal nodes of the tree and introduction of option nodes (thus entitled 'Option Predictive Clustering Trees'), which in essence broadens the space of trees that is searched during the tree induction procedure. The performance evaluation of the algorithm is conducted by means of processing 12 benchmark MLC datasets from completely different domains, which range from text to biology and multimedia, in order to demonstrate its applicability to different classification problems. The achieved performance of the Option Predictive Clustering Trees as ensembles is closing that of bagging ensembles in Predictive Clustering Trees.

The third paper in this group *"**Feature Ranking for Hierarchical Multi-Label Classification with Tree Ensemble Methods**"* is authored by Matej Petković, Saso Dzeroski, and Dragi Kocev and explores the timely topic of hierarchical multi-label classification. The techniques in this group are gaining increased attention due to their potential for application in text document classification and functional genomics. The focus of the research is on the feature ranking for hierarchical multi-label classification. The authors propose a group of feature ranking methods based on three established ensemble methods of predictive clustering trees: Bagging, Random Forests and Extra Trees, and the usage of three scoring functions for calculating the feature importance: Symbolic, Genie3 and Random Forest. The performances of the proposed methods are evaluated on 30 benchmark HMLC datasets. The results show that first two scoring functions, Symbolic and Genie3 scores, yield relevant rankings and that most suitable ensemble method for them is Random Forests ensemble. Moreover, when coupled with the suitable ensemble method, all three scores outperform the existing HMLC-Relief feature ranking.

The last, but not the least of the papers in this special issue of the journal APH is entirely devoted to model-based information processing ***I***. This article investigates the challenging and rather interesting topic of model development and forecasting the demand in hospitality and tourism business. Modeling and forecasting the tourist demand has been in the focus of multi-disciplinary research for a long time, yet reaching the goal of accurate forecast appears still not in the grasp of the researchers. Article *"**Modelling, Forecasting and Testing Decisions on Seasonal Time Series in Tourism**"* by authors Cvetko Andreeski and Daniela Meckaroska is focused on time series analysis applied to tourist demand forecasting problem.

This research considers data from two closed-continental different-size countries North Macedonia and Serbia, also having considerably different economies. Though for both these countries the authors claim that they have accentuated seasonal component and accentuated trend in the last several years. Thus, they are amenable for modeling the tourism demand, but also appeared to possess rising variances that makes the modeling challenging. The model of choice for time series analysis is ARIMA. Several model parameters have been analyzed and then the best choice forecast and decision test is generated. The applied analysis and performance testing is quite comprehensive and the obtained application results are very interesting in terms of comprehension information.

We remain hopping that each and every interested reader shall find some article of her/his personal specific interest. Thank you.

Zoran Ivanovski[1], Georgi Dimirovski[1,2], Dimitar Taskovski[1]

Guest Editors

[1] Faculty of Electrical Engineering and Information Technologies, SS Cyril and Methodius University, Skopje, Republic of Macedonia, dimir@feit.ukim.edu.mk

[2] Faculty of Engineering, Dogus University of Istanbul, Istanbul, Republic of Turkey, gdimirovski@dogus.edu.tr

Accurate Low-Frequency Approximation for Wires within a Two-Layered Earth

Blagoja Markovski, Leonid Grcev, Vesna Arnautovski-Toseva, Andrijana Kuhar

Ss. Cyril and Methodius University in Skopje, Faculty of Electrical Engineering and Information Technologies, Rugjer Boshkovik 18, 1000 Skopje, Macedonia, bmarkovski@feit.ukim.edu.mk, lgrcev@feit.ukim.edu.mk, atvesna@feit.ukim.edu.mk, kuhar@feit.ukim.edu.mk

Abstract: Rigorous electromagnetic models and approximations are traditionally based on the Sommerfeld's resolution for Hertz vector potentials. However, another resolution, based on transverse Hertz vector potentials, also exists. This paper shows that a low frequency approximation, based on this resolution, for wires embedded in a two-layered earth, is more accurate than the existing alternative. The accuracy of proposed approximation is validated for a range of different wire geometries, frequencies and earth characteristics.

Keywords: Electromagnetic model; Grounding; Green's functions; Modeling

1 Introduction

Analysis of wires embedded in earth, for frequency ranges from DC to tens of MHz, is of interest in a number of engineering analyses, such as those related to grounding in power systems [1], EMC [2], lightning protection [3] and subsurface communications [4]. The electromagnetic model based on the mixed potential integral equation (MPIE) [5] and the method of moments [6], is generally the preferred choice for such analyses.

When the corresponding Green's functions are based of mathematically exact solution for the electric field in planar-layered media, electromagnetic modeling involves evaluation of Sommerfeld-type integrals by complex numerical procedures. Alternatively, simpler models for analysis with reasonable loss of accuracy can be obtained by approximating the mathematically exact equations. Amongst existing variants, the low-frequency (LF) or often cited image approximations in analytical form, are mostly preferred in practice, due to their simplicity, ease in development and implementation.

It is important to note that existing image approximations are based on the Sommerfeld's resolution for Hertz vector potentials from horizontal electric dipole [7], also known as traditional choice of potentials. This resolution is widely accepted in electromagnetic modeling of grounding systems, antenna theory and other EMC related studies. However, other resolutions also exist [8], for example the transverse resolution or so-called alternative choice of potentials. Both resolutions are basis for development of different formulations of potentials in MPIE [9]. Recent analysis for wires embedded in uniform earth have shown that LF approximation derived from the transverse resolution for potentials is substantially more accurate than other image approximations based on Sommerfeld's resolution [10].

In this paper, we propose new LF approximation of the Green's functions for MPIE modeling of wires within a single layer in two-layered earth. This approximation is derived from a rigorous full-wave solution based on the alternative choice of potentials for planar-layered media [11], implemented in formulation A of potentials in MPIE. The proposed approximation is compared with the existing image approximation for a two-layered earth, which is based on the traditional formulation of potentials, for a range of different wire geometries, frequencies and earth characteristics. The accuracy of the proposed and the existing approximations are evaluated by comparison with results obtained by the commercial electromagnetic simulation software FEKO. This software incorporates an exact Sommerfeld integral formulation for analysis of wires in a layered media [12].

2 Formulation of Electric Field by MPIE

In MPIE, the scattered electric field vector $\vec{E}^s(\vec{r})$ from a straight thin wire with longitudinal current $I(\vec{r}')$, can be expressed in terms of magnetic vector and electric scalar potentials, $\vec{A}(\vec{r})$ and $\Phi(\vec{r})$ respectively:

$$\vec{E}^S_{m,i}(\vec{r}) = -j\omega\vec{A}_{m,i}(\vec{r}) - \nabla\Phi_{m,i}(\vec{r}) \tag{1}$$

$$\vec{A}_{m,i}(\vec{r}) = \frac{\mu_m}{4\pi}\int_{\ell'}\overline{\overline{G}}_{A_{m,i}}(\vec{r},\vec{r}')I(\vec{r}')\,d\ell' \tag{2}$$

$$\Phi_{m,i}(\vec{r}) = \frac{j\omega}{4\pi\underline{\sigma}_i}\int_{\ell'}G_{\Phi_{m,i}}(\vec{r},\vec{r}')q(\vec{r}')d\ell' \tag{3}$$

$$q(\vec{r}') = \frac{-1}{j\omega}\nabla' I(\vec{r}') \tag{4}$$

where $\overline{\overline{G}}_{A_{m,i}}$ and $G_{\Phi_{m,i}}$ are dyadic magnetic vector and electric scalar potential Green's functions for source in layer *m* and observation point in layer *i*. The position of electric dipole with strength $I(\vec{r}')d\ell'$, on the axis ℓ' of a $(\hat{x}', \hat{y}', \hat{z}')$- directed straight wire is denoted by $\vec{r}'$, and position of the observation point for $(\hat{x}, \hat{y}, \hat{z})$- directed electric field vector is denoted by $\vec{r}$.

Green's functions for potentials $\overline{\overline{G}}_{A_{m,i}}$ and $G_{\Phi_{m,i}}$ in MPIE are not unique. Among several possibilities, the Green's functions for the traditional formulation and formulation A of potentials, and their LF approximations for source and observation points within same layer are of particular interest for the analysis in this paper.

The traditional formulation is based on the Sommerfeld's resolution [7] that postulates that for source and observation points within same layer, *x*- directed horizontal electric dipole (HED) has *x*- and *z*- component of magnetic vector potential, as illustrated on Fig. 1a). Formulation A is based on the transverse resolution [8], where *y*-component accompanies the primary *x*-component, as illustrated on Fig. 1b). The *z*- components of magnetic vector potentials in both formulations are identical for source and observation points in same layer, and the scalar potential Green's function for formulation A is identical with the scalar potential Green's function for vertical electric dipole (VED) from the traditional formulation.

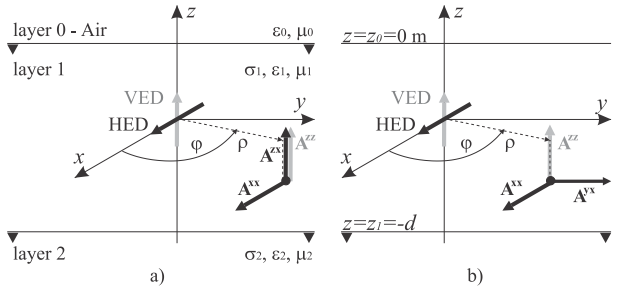

Figure 1

Components of magnetic vector potentials associated to HED and VED for source and observation points within same layer in two-layered earth for: (a) traditional formulation and (b) formulation A

Green's functions for traditional formulation of potentials can be obtained from [13], while exact mathematical solution for spatial domain Green's functions for formulation A and related parameters for general planar-layered media are provided in Annex A. These Green's functions are basis for development of the corresponding LF approximations for a two-layered earth.

3 LF Approximations for Source and Observation Points within Same Layer in Two-layered Earth

3.1 Traditional Formulation of Potentials in MPIE

Dyadic Green's function for magnetic vector potential is expressed as:

$$\overline{\overline{G}}_A = \left(\hat{x}'\hat{x} + \hat{y}'\hat{y}\right) G_A^{xx} + \hat{x}'\hat{z} G_A^{zx} + \hat{y}'\hat{z} G_A^{zy} + \hat{z}'\hat{z} G_A^{zz} \tag{5}$$

Details of development of LF approximations for traditional formulation of potentials can be found in [14]-[15], and here they are rewritten for completeness:

$$G_{A(LF)}^{xx} = \begin{cases} g_d^0 & ,m=0 \\ g_d^1 & ,m=1 \\ g_d^2 & ,m=2 \end{cases} \tag{6}$$

$$\begin{matrix} G_{A(LF)}^{zx} \\ \hline \cos\varphi \\ \\ G_{A(LF)}^{zy} \\ \hline \sin\varphi \end{matrix} = \begin{cases} -R_{1,0}\tilde{g}_{1,0}^0 - \sum_{p=1}^{\infty} (R_{1,0}R_{1,2})^p [R_{1,0} - \frac{1}{R_{1,0}}] \tilde{g}_{1,p}^0 & ,m=0 \\ -R_{1,0}\tilde{g}_{3,0}^1 + \sum_{p=1}^{\infty} (R_{1,0}R_{1,2})^p [\frac{1}{R_{1,0}} \tilde{g}_{1,p}^1 + \tilde{g}_{2,p}^1 - R_{1,0}\tilde{g}_{3,p}^1 - \tilde{g}_{4,p}^1] & ,m=1 \\ R_{1,2}\tilde{g}_{5,0}^2 + \sum_{p=1}^{\infty} (R_{1,0}R_{1,2})^p [R_{1,2} - \frac{1}{R_{1,2}}] \tilde{g}_{5,p}^2 & ,m=2 \end{cases} \tag{7}$$

$$G_{A(LF)}^{zz} = \begin{cases} g_d^0 + R_{1,0}g_{1,0}^0 + \sum_{p=1}^{\infty} (R_{1,0}R_{1,2})^p [R_{1,0} - \frac{1}{R_{1,0}}] g_{1,p}^0 & ,m=0 \\ g_d^1 - R_{1,0}g_{3,0}^1 + \sum_{p=1}^{\infty} (R_{1,0}R_{1,2})^p [-\frac{1}{R_{1,0}} g_{1,p}^1 + g_{2,p}^1 - R_{1,0}g_{3,p}^1 + g_{4,p}^1] & ,m=1 \\ g_d^2 + R_{1,2}g_{5,0}^2 + \sum_{p=1}^{\infty} (R_{1,0}R_{1,2})^p [R_{1,2} - \frac{1}{R_{1,2}}] g_{5,p}^2 & ,m=2 \end{cases} \tag{8}$$

$$G_{\Phi(LF)} = \begin{cases} g_d^0 - R_{1,0}g_{1,0}^0 - \sum_{p=1}^{\infty} (R_{1,0}R_{1,2})^p [R_{1,0} - \frac{1}{R_{1,0}}] g_{1,p}^0 & ,m=0 \\ g_d^1 + R_{1,0}g_{3,0}^1 + \sum_{p=1}^{\infty} (R_{1,0}R_{1,2})^p [\frac{1}{R_{1,0}} g_{1,p}^1 + g_{2,p}^1 + R_{1,0}g_{3,p}^1 + g_{4p}^1] & ,m=1 \\ g_d^2 - R_{1,2}g_{5,0}^2 - \sum_{p=1}^{\infty} (R_{1,0}R_{1,2})^p [R_{1,2} - \frac{1}{R_{1,2}}] g_{5,p}^2 & ,m=2 \end{cases} \tag{9}$$

Details for $R_{m,m\pm1}$, g_d^m, $g_{l,p}^m$ and $\tilde{g}_{l,p}^m$ are provided in Appendices A and B.

3.2 Formulation A of Potentials in MPIE

Dyadic Green's function for magnetic vector potential is expressed as:

$$\overline{\overline{K}}_A = \hat{x}'\hat{x}K_A^{xx} + \hat{y}'\hat{y}K_A^{yy} + \left(\hat{x}'\hat{y} + \hat{y}'\hat{x}\right)K_A^{yx} + \hat{z}'\hat{x}K_A^{xz} + \hat{z}'\hat{y}K_A^{yz} + \hat{z}'\hat{z}G_A^{zz} \tag{10}$$

The key steps in development of LF approximation of Green's functions for formulation A are provided in Appendix B. Components of magnetic vector potential, for source and evaluation points in same layer with index *m*, are expressed as:

$$K_{A(LF)}^{xx} = \begin{cases} g_d^0 + \frac{1}{2}\left\{ \begin{aligned} &-R_{1,0}g_{1,0}^0 - \sum_{p=1}^{\infty}(R_{1,0}R_{1,2})^p[R_{1,0} - \frac{1}{R_{1,0}}]g_{1,p}^0 \\ &+cs\left[R_{1,0}\hat{g}_{1,0}^0 + \sum_{p=1}^{\infty}(R_{1,0}R_{1,2})^p[R_{1,0} - \frac{1}{R_{1,0}}]\hat{g}_{1,p}^0\right] \end{aligned}\right\} & ,m=0 \\ g_d^1 + \frac{1}{2}\left\{ \begin{aligned} &R_{1,0}g_{3,0}^1 - cs[R_{1,0}\hat{g}_{3,0}^1] \\ &+\sum_{p=1}^{\infty}(R_{1,0}R_{1,2})^p[\frac{1}{R_{1,0}}g_{1,p}^1 + g_{2,p}^1 + R_{1,0}g_{3,p}^1 + g_{4,p}^1] \\ &-cs\sum_{p=1}^{\infty}(R_{1,0}R_{1,2})^p[\frac{1}{R_{1,0}}\hat{g}_{1,p}^1 + \hat{g}_{2,p}^1 + R_{1,0}\hat{g}_{3,p}^1 + \hat{g}_{4,p}^1] \end{aligned}\right\} & ,m=1 \\ g_d^2 + \frac{1}{2}\left\{ \begin{aligned} &-R_{1,2}g_{5,0}^2 - \sum_{p=1}^{\infty}(R_{1,0}R_{1,2})^p[R_{1,2} - \frac{1}{R_{1,2}}]g_{5,p}^2 \\ &+cs\left[R_{1,2}\hat{g}_{5,0}^2 + \sum_{p=1}^{\infty}(R_{1,0}R_{1,2})^p[R_{1,2} - \frac{1}{R_{1,2}}]\hat{g}_{5,p}^2\right] \end{aligned}\right\} & ,m=2 \end{cases} \tag{11}$$

$$K_{A(LF)}^{yx} = \begin{cases} \frac{1}{2}sn\left[R_{1,0}\hat{g}_{1,0}^0 + \sum_{p=1}^{\infty}\left(R_{1,0}R_{1,2}\right)^p[R_{1,0} - \frac{1}{R_{1,0}}]\hat{g}_{1,p}^0\right] & ,m=0 \\ -\frac{1}{2}sn\left[\begin{aligned} &R_{1,0}\hat{g}_{3,0}^1 + \\ &\sum_{p=1}^{\infty}\left(R_{1,0}R_{1,2}\right)^p[\frac{1}{R_{1,0}}\hat{g}_{1,p}^1 + \hat{g}_{2,p}^1 + R_{1,0}\hat{g}_{3,p}^1 + \hat{g}_{4,p}^1] \end{aligned}\right] & ,m=1 \\ \frac{1}{2}sn\left[R_{1,2}\hat{g}_{5,0}^2 + \sum_{p=1}^{\infty}\left(R_{1,0}R_{1,2}\right)^p[R_{1,2} - \frac{1}{R_{1,2}}]\hat{g}_{5,p}^2\right] & ,m=2 \end{cases} \tag{12}$$

Note that $K_{A(LF)}^{xz} = K_{A(LF)}^{yz} = 0$, $K_{A(LF)}^{yy}$ is similar to $K_{A(LF)}^{xx}$, but with changed sign before the *cs* term, while $G_{A(LF)}^{zz}$ and $G_{\Phi(LF)}$ are identical with (8) and (9), respectively. In above equations, terms *cs* and *sn* are for $\cos(2\varphi)$ and $\sin(2\varphi)$.

4 Comparison of Accuracy of the LF Approximations

Accuracy of the proposed and existing LF approximations is compared for a set of numerical tests. We consider four cases, illustrated on Figs. 2-5:

- Energized 10-m long horizontal wire

- Passive 5-m long horizontal wire that parallels the energized wire

- Passive 5-m long horizontal wire that is perpendicular to the energized wire

- Passive 1.5-m long vertical wire near the horizontal energized wire

All wires in Figs. 2-5 are with 7 mm radius and are buried at a depth of 0.5 m in two-layer earth, with thickness d =2.5 m of the earth's upper layer. Characteristics of the two-layered earth are expressed in terms of the reflection factor K [16]:

$$K = (\rho_2 - \rho_1)/(\rho_2 + \rho_1) \tag{13}$$

where the resistivity of the top earth layer is fixed to either ρ_1 = 100 Ωm or ρ_1 = 1000 Ωm, and the resistivity of the bottom layer is varied accordingly to K = -0.9, 0.0 or +0.9. Relative permittivities and permeabillities are set to $\varepsilon_{r1} = \varepsilon_{r2} = 10$ and $\mu_{r1} = \mu_{r2} = 1$, respectively. In the case of the passive vertical wire in Fig. 5, its upper point is at a depth of 0.5 m. The wires are energized by a harmonic voltage generator with an RMS value of 1 V connected serially at the midpoint of the 10 m horizontal wire.

Figs. 2-5 show the computed error for the longitudinal current distribution obtained by the new LF approximation and the existing image model based on traditional formulation of potentials, with reference to results obtained by commercial electromagnetic simulation software FEKO [12]. RMS error for the longitudinal current along the conductor [17] is computed as follows:

$$\varepsilon_{\mathrm{RMS}} = \left[\frac{\sum_{n=1}^{N} \left| \hat{I}_n^A - \hat{I}_n^R \right|^2}{\sum_{n=1}^{N} \left| \hat{I}_n^R \right|^2} \right]^{1/2} \cdot 100\ (\%) \tag{14}$$

Here, $\hat{I}_n^R$ is the phasor of the current samples along the conductor computed by rigorous model, and $\hat{I}_n^A$ is the phasor of the current samples obtained using approximate solutions. N is total number of segments along the conductor.

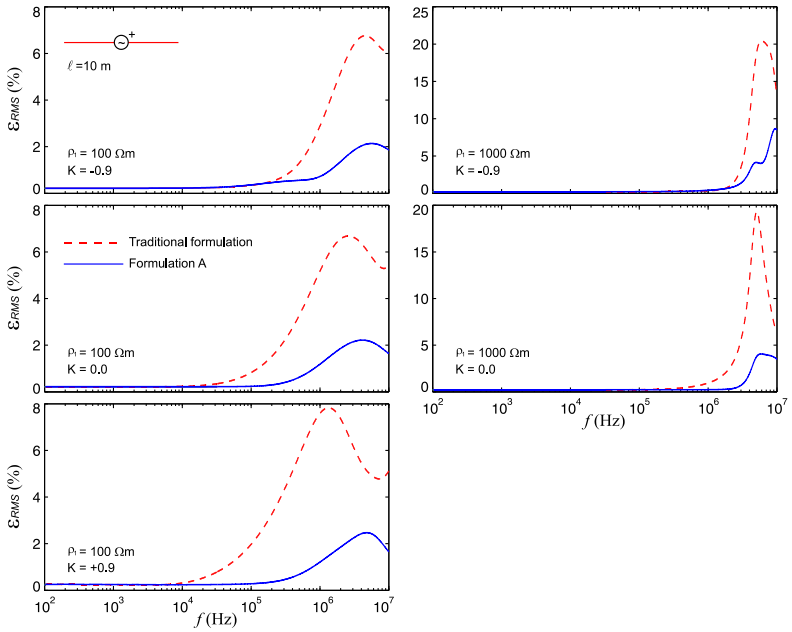

Figure 2

ε_{RMS} error for currents in energized 10-m long horizontal wire

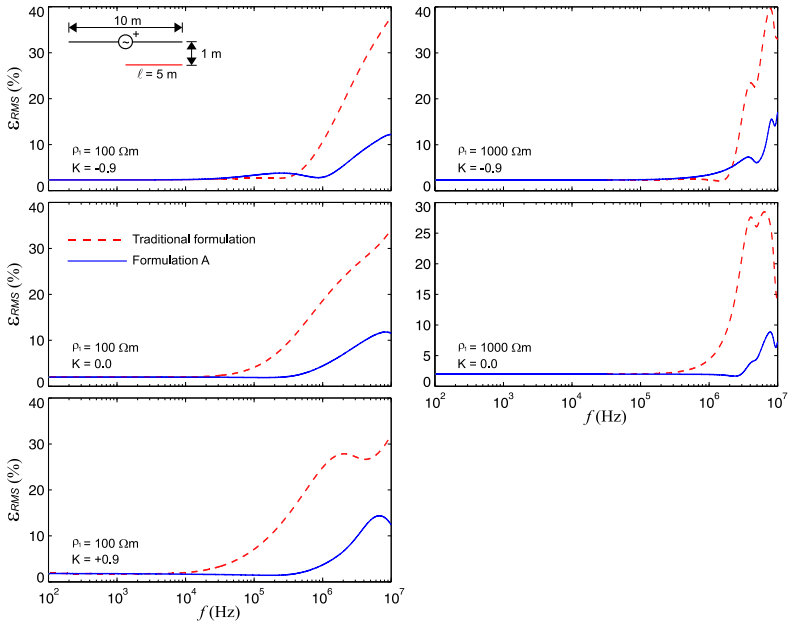

Figure 3

ε_{RMS} error for currents in passive 5-m long horizontal wire that parallels energized wire

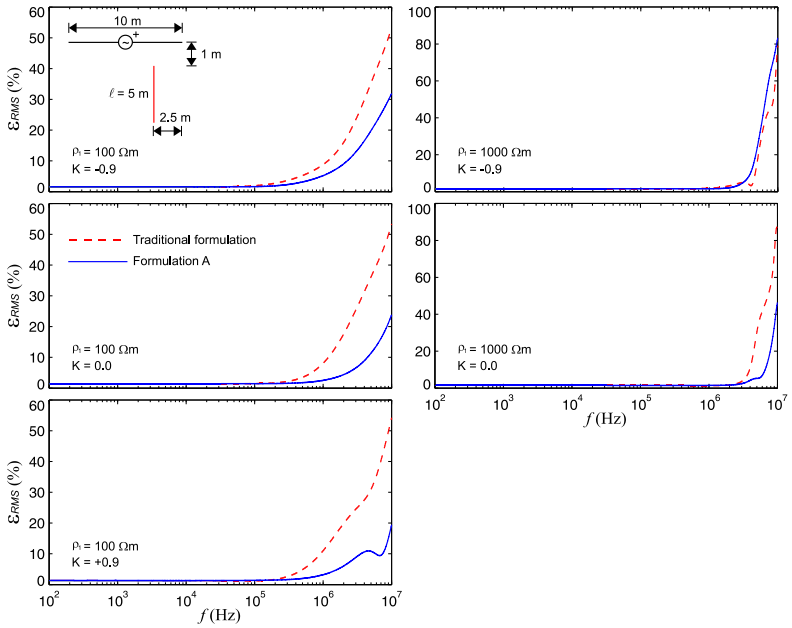

Figure 4

ε_{RMS} error for currents in passive 5-m long horizontal wire that is perpendicular to energized wire

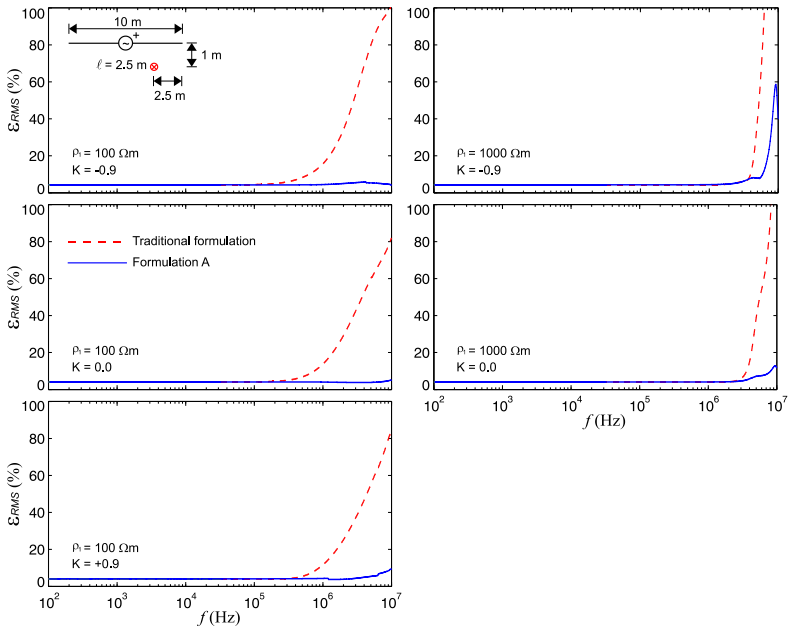

Figure 5

ε_{RMS} error for currents in passive 1.5-m long vertical wire near horizontal energized wire

Conclusions

This paper provides LF approximations for the electromagnetic modeling of wires above or within a two-layered earth, based on the alternative choice of potentials. Accuracy of the proposed approximation is validated for source and observation points within the earth's upper layer and for a range of different wire geometries, frequencies and soil characteristics.

The results illustrated in Figs. 2-5, show that both approximations provide good and nearly equal accuracy for frequencies up to 10 kHz. However, the proposed LF approximation derived from formulation A, is more accurate than existing LF approximation derived from the traditional formulation, for frequencies within the range 10 kHz – 10 MHz, for nearly all cases. Such improvement of accuracy may widen the application of LF approximations in transient analysis where currents with significant high frequency contents are involved, such as, those related to subsequent lightning strikes or due to manipulations in the electrical power systems. The introduced error in transient analysis is not within the scope of this paper, but its evaluation will be considered as a continuation of this work in the future.

The paper also provides a mathematically exact solution for the spatial domain Green's functions for formulation A, for source and observation points within the same layer of general planar-layered media, cast in a form which is appropriate for the development of the proposed LF approximation.

Appendix A – Exact Green's Functions for Formulation A in Planar-Layered Media

Exact form of Green's functions for formulation A of potentials in MPIE, for source and observation points within same layer, in terms of transmission line parameters and in spectral domain, can be found in [11]. Here, Green's functions are cast in a form that is more appropriate for development of the proposed approximation:

$$K_A^{xx} = g_d^m + \frac{1}{2}\left[I_1 + \cos(2\varphi) I_2\right] \tag{15}$$

$$K_A^{yy} = g_d^m + \frac{1}{2}\left[I_1 - \cos(2\varphi) I_2\right] \tag{16}$$

$$K_A^{xy} = K_A^{yx} = \sin(2\varphi)\frac{1}{2} I_2 \tag{17}$$

$$G_A^{zz} = g_d^m + I_3 \tag{18}$$

$$G_\Phi = g_d^m + I_4 \tag{19}$$

where g_d^m is direct term related to a spherical wave due to electric dipole in an unbounded medium with characteristics of the layer *m*:

$$g_d^m = \frac{e^{jk_m r_d}}{r_d}, \qquad r_d = \sqrt{\rho^2 + |z - z'|^2} \tag{20}$$

and I_1, I_2, I_3 and I_4 are Sommerfeld-type integrals related to the up- and down-going waves reflected from interfaces, for example at z_0 and z_1 illustrated on Fig 1.

$$I_1 = \int_0^\infty \left[\left(A_h - B_h\right) \frac{e^{jk_{m,z}(z-z')}}{jk_{m,z}} + \left(C_h + D_h\right) \frac{e^{-jk_{m,z}(z-z')}}{jk_{m,z}} \right] J_0(k_\rho \rho) k_\rho dk_\rho \tag{21}$$

$$I_2 = \int_0^\infty \left[\left(A_h + B_h\right) \frac{e^{jk_{m,z}(z-z')}}{jk_{m,z}} + \left(C_h - D_h\right) \frac{e^{-jk_{m,z}(z-z')}}{jk_{m,z}} \right] J_2(k_\rho \rho) k_\rho dk_\rho \tag{22}$$

$$I_3 = \int_0^\infty \left[A_v \frac{e^{-jk_{m,z}(z-z')}}{jk_{m,z}} + B_v \frac{e^{jk_{m,z}(z-z')}}{jk_{m,z}} \right] J_0\left(k_\rho \rho\right) k_\rho dk_\rho \tag{23}$$

$$I_4 = \int_0^\infty \left[C_v \frac{e^{-jk_{m,z}(z-z')}}{jk_{m,z}} + D_v \frac{e^{jk_{m,z}(z-z')}}{jk_{m,z}} \right] J_0\left(k_\rho \rho\right) k_\rho dk_\rho \tag{24}$$

Coefficients $A_{h,v}$, $B_{h,v}$, $C_{h,v}$ and $D_{h,v}$, and related parameters are expressed as:

$$\tilde{M}_m^{TE,TM} = [1 - \tilde{R}_{m,m-1}^{TE,TM} \tilde{R}_{m,m+1}^{TE,TM} e^{-jk_{m,z} 2\Delta_m}]^{-1} \tag{25}$$

$$\tilde{R}_{m,m\pm1}^{TE,TM} = \left(R_{m,m\pm1}^{TE,TM} + \tilde{R}_{m\pm1,m\pm2}^{TE,TM} e^{-jk_{m\pm1,z} 2\Delta_{m\pm1}} \right) \tilde{M}_{m\pm1}^{TE,TM} \tag{26}$$

$$A_h = \tilde{R}_{m,m-1}^{TE} e^{-jk_{m,z}(\Delta_m - (z'-z_m))} \left[e^{-jk_{m,z}(\Delta_m - (z'-z_m))} + \tilde{R}_{m,m+1}^{TE} e^{-jk_{m,z}(\Delta_m + (z'-z_m))} \right] \tilde{M}_m^{TE} \tag{27}$$

$$B_h = -D_v = \tilde{R}_{m,m-1}^{TM} e^{-jk_{m,z}(\Delta_m - (z'-z_m))} \left[e^{-jk_{m,z}(\Delta_m - (z'-z_m))} - \tilde{R}_{m,m+1}^{TM} e^{-jk_{m,z}(\Delta_m + (z'-z_m))} \right] \tilde{M}_m^{TM} \tag{28}$$

$$C_h = \tilde{R}_{m,m+1}^{TE} e^{-jk_{m,z}(z'-z_m)} \left[e^{-jk_{m,z}(z'-z_m)} + \tilde{R}_{m,m-1}^{TE} e^{-jk_{m,z}(2\Delta_m - (z'-z_m))} \right] \tilde{M}_m^{TE} \tag{29}$$

$$D_h = C_v = \tilde{R}_{m,m+1}^{TM} e^{-jk_{m,z}(z'-z_m)} \left[-e^{-jk_{m,z}(z'-z_m)} + \tilde{R}_{m,m-1}^{TM} e^{-jk_{m,z}(2\Delta_m - (z'-z_m))} \right] \tilde{M}_m^{TM} \tag{30}$$

$$A_v = \tilde{R}_{m,m+1}^{TM} e^{-jk_{m,z}(z'-z_m)} \left[e^{-jk_{m,z}(z'-z_m)} + \tilde{R}_{m,m-1}^{TM} e^{-jk_{m,z}(2\Delta_m - (z'-z_m))} \right] \tilde{M}_m^{TM} \tag{31}$$

$$B_v = \tilde{R}_{m,m-1}^{TM} e^{-jk_{m,z}(\Delta_m - (z'-z_m))} \left[e^{-jk_{m,z}(\Delta_m - (z'-z_m))} + \tilde{R}_{m,m+1}^{TM} e^{-jk_{m,z}(\Delta_m + (z'-z_m))} \right] \tilde{M}_m^{TM} \tag{32}$$

In above equations, geometric quantities z and z' are positions of observation and source points with respect to z- axis with origin at the earth's surface, Δ_m is the thickness of m-th layer and z_m is depth of the interface of the m-th and $m+1$-th layers.

Generalized reflection coefficients $\tilde{R}_{m,m\pm1}^{TE,TM}$ for layer m are obtained by iterative procedure, starting from the lowermost half-space n (semi infinite earth) for evaluation of $\tilde{R}_{m,m+1}^{TE,TM}$ and the topmost half-space with index 0 (air) for evaluation of $\tilde{R}_{m,m-1}^{TE,TM}$, considering that $\tilde{R}_{n,n+1}^{TE,TM}=0$ and $\tilde{R}_{0,-1}^{TE,TM}=0$, respectively.

Other required parameters are expressed as:

$$R_{m,m\pm1}^{TE}=\frac{\mu_{m\pm1}k_{m,z}-\mu_m k_{m\pm1,z}}{\mu_{m\pm1}k_{m,z}+\mu_m k_{m\pm1,z}},\ R_{m,m\pm1}^{TM}=\frac{\underline{\sigma}_{m\pm1}k_{m,z}-\underline{\sigma}_m k_{m\pm1,z}}{\underline{\sigma}_{m\pm1}k_{m,z}+\underline{\sigma}_m k_{m\pm1,z}}$$

$$\underline{\sigma}_m=\sigma_m+j\omega\varepsilon_m,\ k_m=\sqrt{-j\omega\mu_m\underline{\sigma}_m},\ k_{m,z}=\sqrt{k_m^2-k_\rho^2} \tag{33}$$

Appendix B – Development of LF Approximation of Green's Functions for Formulation A

The LF approximations of Green's functions for formulation A of potentials in MPIE, for a two-layered earth are developed following the procedures provided in [14] [15]. Here, some key steps in development are briefly provided for completeness.

For two-layered earth, generalized reflection coefficients are reduced to:

$$M_1^{TE,TM}=[1-R_{1,0}^{TE,TM}R_{1,2}^{TE,TM}e^{-2jk_{1,z}d}]^{-1} \tag{34}$$

$$\tilde{R}_{0,-1}^{TE,TM}=0;\ \tilde{R}_{1,0}^{TE,TM}=R_{1,0}^{TE,TM};\ \tilde{R}_{2,1}^{TE,TM}=\left(R_{2,1}^{TE,TM}+R_{1,0}^{TE,TM}e^{-2jk_{1,z}d}\right)M_1^{TE,TM};$$

$$\tilde{R}_{2,3}^{TE,TM}=0;\ \tilde{R}_{1,2}^{TE,TM}=R_{1,2}^{TE,TM};\ \tilde{R}_{0,1}^{TE,TM}=\left(R_{0,1}^{TE,TM}+R_{1,2}^{TE,TM}e^{-2jk_{1,z}d}\right)M_1^{TE,TM} \tag{35}$$

where d is thickness of topmost earth layer. The first key simplification is to obtain LF approximation of the reflection coefficients $R_{m,m\pm1}^{TE}$ and $R_{m,m\pm1}^{TM}$. For frequencies approaching 0 Hz the following approximation is valid: $k_{0,z}\approx k_{1,z}\approx k_{2,z}$ since $k_n^2\to 0$ for n = 0, 1, 2.

Then reflection coefficients become constants and can be extracted from the Sommerfeld integrals. Considering that in practical cases $\mu_1=\mu_2=\mu_0$, the LF approximations of TE and TM related reflection coefficients can be expressed as:

$$R_{m,m\pm1(LF)}^{TE}\to 0;\ R_{m,m\pm1(LF)}^{TM}\to -R_{m,m\pm1}\ \text{while}\ M_{1(LF)}^{TE}\to 1 \tag{36}$$

The second key simplification is to expand $M_{1(LF)}^{TM}$ in following series [18]:

$$M_{1(LF)}^{TM}\to[1-R_{1,0}R_{1,2}e^{-2jk_{1,z}d}]^{-1}\approx\sum_{p=0}^{\infty}\left(R_{1,0}R_{1,2}\right)^p e^{-jk_{1,z}2dp} \tag{37}$$

Additionally, in development of LF approximations for layers 0 and 2, wave numbers of different layers can appear in equations. In such case it is impossible to obtain simple closed-form approximation of Green's function. To circumvent this problem, third key simplification is introduced, by which, $k_{0,z}$, $k_{1,z}$ and $k_{2,z}$ are substituted with unique wave number $k_{m,z}$ related to the observation layer.

In the final step of development, following identities are used to obtain closed-form solutions of the Green's functions:

$$g_{l,p}^{m} = \int_0^{\infty} \frac{e^{-jk_{m,z}h_{l,p}}}{jk_{m,z}} J_0(k_\rho \rho) k_\rho dk_\rho = \frac{e^{-jk_m r_{l,p}}}{r_{l,p}} \tag{38}$$

$$\hat{g}_{l,p}^{m} = \int_0^{\infty} \frac{e^{-jk_{m,z}h_{l,p}}}{jk_{m,z}} J_2(k_\rho \rho) k_\rho dk_\rho = \frac{2(e^{-jk_m h_{l,p}} - e^{-jk_m r_{l,p}})}{jk_m \rho^2} - \frac{e^{-jk_m r_{l,p}}}{r_{l,p}} \tag{39}$$

$$r_{l,p} = \sqrt{\rho^2 + h_{l,p}^2},\ l = 1,2,3,4.,\ h_{1,p} = 2dp + (z + z'),\ h_{2,p} = 2dp + (z - z'),$$
$$h_{3,p} = 2dp - (z + z'),\ \ h_{4,p} = 2dp - (z - z'). \tag{40}$$

where subscript l is related to the vertical distance $h_{l,p}$ between the observation point and source image with index p, from the infinite series of images.

Note that when $\sigma_1 = \sigma_2$, $\varepsilon_{r1} = \varepsilon_{r2}$ and $\mu_1 = \mu_2 = \mu_0$, image approximations can be further reduced to ones valid for uniform earth, proposed in [10].

References

[1] J. He, R. Zeng and B. Zhang: Methodology and Technology for Power System Grounding, New York: Wiley, 2013

[2] E. B. Joffe, K-S Lock: Grounds for Grounding: A Circuit to System Handbook, New York: Wiley, 2011

[3] Y. Baba, R. A. Rakov: Electromagnetic Computation Methods for Lightning Surge Protection Studies, New York: Wiley, 2016

[4] R. W. P. King and G. S. Smith: Antennas in Matter, Cambridge, MA: MIT Press, 1981

[5] K. A. Michalski: The mixed-potential electric field integral equation for objects in layered media, Archiv für elektronik und übertragungstechnik, Vol. 39, No. 5, Sep./Oct. 1985, pp. 317-322

[6] R. F. Harrington: Field Computation by Moment Methods, New York: Macmillan, 1968; New York: Wiley, 1993

[7] A. Sommerfeld: Partial Differential Equations in Physics, Chapter VI, New York: Academic Press, 1949

[8] A. Erteza and B. K. Park: Non-uniqueness of resolution of Hertz vector in presence of a boundary, and a horizontal dipole problem, IEEE Trans. Antennas Propagat., Vol. AP-17, May 1969, pp. 376-378

[9] K. A. Michalski: On the scalar potential of a point charge associated with a time-harmonic dipole in a layered medium, IEEE Trans. Antennas Propagat., Vol. AP-35, Nov. 1987, pp. 1299-1301

[10] B. Markovski, L. Grcev, V. Arnautovski-Toseva: Accurate low-frequency approximation for wires within a conducting half-space, IEEE Trans. Electromagn. Compat., doi: 10.1109/TEMC.2018.2881932, pp. 1-4

[11] K. A. Michalski and D. Zheng: Electromagnetic scattering and radiation by surfaces of arbitrary shape in layered media, Part I: Theory, IEEE Trans. Antennas Propagat., Vol. 38, No. 3, Mar. 1990, pp. 335-344

[12] EM Software and Systems-S.A. (Pty) Ltd., FEKO, Stellenbosch, South Africa, 2009 [Online] Available: http://www.feko.info

[13] G. Dural, M. I. Aksun: Closed-form Green's functions for general sources and stratified media, IEEE Trans. on Microwave Theory and Techniques, Vol. 43, No. 7, Jul. 1995, pp. 1545-1552

[14] V. Arnautovski-Toseva and L. Grcev: Electromagnetic analysis of horizontal wire in two-layered soil, J. Comput. Appl. Math., Vol. 168, Nos. 1-2, Jul. 2004, pp. 21-29

[15] V. Arnautovski-Toseva, L. Grcev: Image and exact models of a vertical wire penetrating a two-layered earth, IEEE Trans. Electromagn. Compat, Vol. 53, No. 4, Nov. 2011, pp. 968-976

[16] F. Dawalibi, D. Mukhedikar: Influence of ground rods on grounding grids, IEEE Trans. on Power Apparatus and Systems, Vol. PAS-98, No. 6, Nov./Dec. 1979, pp. 2089-2097

[17] A. Poggio, R. Bevensee and E. K. Miller: Evaluation of some thin wire computer programs, IEEE Antennas Propag. Symp., Vol. 12, Jun. 1974, pp. 181-184

[18] L. M. Brekhovskikh, Waves in Layered Media. New York: Academic, 1960

Future 5G Mobile Broadband Networks Using Cloud-based Services with Advanced Security and QoS Framework

Mitko Bogdanoski[1], Tomislav Shuminoski[2], Metodi Hadji-Janev[1], Aleksandar Risteski[2], Toni Janevski[2]

[1]Military Academy "General Mihailo Apostolski" University of Goce Delcev, an associated member, Str. Vasko Karangeleski BB 1000, Skopje, Macedonia
[2]Ss. Cyril and Methodius University, Faculty of Electrical Engineering and Information Technologies, Rugjer Boshkovik 18, PO Box 574, 1000 Skopje, Macedonia
E-mails: mitko.bogdanoski@ugd.edu.mk, tomish@feit.ukim.edu.mk, metodi.hadzi-janev@ugd.edu.mk, acerist@feit.ukim.edu.mk, tonij@feit.ukim.edu.mk

Abstract: The work suggests a potential solution to contemporary Corporate and National security concerns, with regards to the use in the future of 5G technologies. In today's digital age, individuals, groups and some states, (ab)use the easy access to modern technologies to further their economic and political objectives. In these endeavors, among others, these actors utilize jamming attacks (i.e. electronic warfare tactics exclusively used by the military in the past), in order to produce the well-known effect of DoS (Denial of Service). Up to now there is no communication technology that is immune to the jamming attacks, so there is no expectation that the new 5G concept, that is still under development will be fully resistant to well-known traditional jamming and other types of attacks. The proposed Security and Quality of Service (QoS) framework provides high levels of security features and safety, through high-performance mobile broadband networks, using Mobile Cloud computing. It guarantees QoS provisioning for different broadband services, with present jamming, as well as, other types of distributed DoS (DDoS) attacks. Moreover, the trend of integrating various criminal activities in the cyberspace is also presented. The performance of the proposed security and QoS framework is evaluated through simulations and analysis with multimedia traffic, in a heterogeneous mobile broadband Cloud environment with the coexistence of multiple radio technologies.

Keywords: 5G; Cloud; Cyber; Jamming; DoS; Quality of Service (QoS); Security

1 Introduction

The advancement of modern mobile and wireless technology and its usage in attending political objectives have changed threat perceptions, definitions of weapon systems and the way of achieving strategic-political objectives. Although the use of modern-day technologies and cyberspace provide many benefits there are numerous examples where individuals, groups and even states have abused modern technologies and cyberspace in achieving strategic ends. These tendencies have urged countrywide and corporate security risk management teams to change the approach to the threat vectors. Consequently, new threat vectors in the digital age are blurring the line between peace and war. This is understandable giving that modern technologies have changed the idea of weaponry arsenal at potential adversaries' disposal. The cyber-attack(s) understood as syntactic (straight forward-viruses, worms, Trojans, etc.), semantic (the modification and dissemination of correct and incorrect information) or combination, can be serious weapon system. This weapon system can be used for achieving different end-states. The threat level that these weapons can cause in time, space and effects are significant.

One example that has a widespread implementation in modern battlespace activities and is as old as the emergence of radio equipment, it is called the "jamming" process. This process, because of its nature and method of operation belongs to the well-known group of attacks called DoS (Denial of Service). Up to now there is no communication technology that is immune to the jamming attack, so there is no expectation that the novel 5G concept that is still under development will be fully resistant to the well-known traditional jamming attacks. The importance of defining the security measures for the new 5G device-centric based technology [1-8] that is at the front door is obvious. Considering mentioned, this technology is expected to take a significant part of the Next Generation Mobile Broadband network, not bypassing the military networks [9, 10]. Taking suitable measure against different disruption in the proper functionality of the 5G technology, including the appropriate answer against the jamming attack, need to be one of the key areas during the development phase.

Indubitably, the future 5G networks would require smarter devices capable of providing a broad range of multimedia services to cell customers, with the enormous spectrum for advanced capabilities. The 5G security of wireless cellular systems is expected to be divided in the security issues for the main three services:

1. Enhanced Mobile BroadBand (eMBB)
2. Ultra-Reliable Low-Latency Communications (URLLC)
3. Machine-Type Communications (mMTC) [11-14]

The concept of our framework, presented herein, is a 5G based terminal that has access to various different radio access technologies (RATs), at the same time and

to be able to combine different secured flows from different technologies using advance security and QoS algorithms, vertical multi-homing and multi-streaming [15] [16].

The paper is organized as follows. Section 2 discusses some background researches on converging jamming and hacking in the age of cyber warfare in mobile and wireless networks and provides an overview of different types of jamming attacks. Section 3 describes the System Model together with the proposed security and QoS algorithm and a proposed method to mitigate the jamming effects. In Section 4 the simulation results and analysis are discussed. Finally, Section 5 gives some conclusions of our work.

2 Related Works

Contemporary dynamics in military affairs confirm that cyberwarfare has expanded beyond the digital realm. As the wireless networks become a norm so does the ability to attack a target simultaneously in multiple ways from multiple domains. Among others, national and corporate security risk assessment teams produce guidance that urges leadership to merge cyber warfare and traditional electronic warfare type of activities. Although jamming technologies was once the exclusive province of the military, today these technologies have become so commonplace that can be purchased online.

Parallel with the above, along with the improved performances and QoS, the brand new 5G concept should undoubtedly provide the capability to ensure security, trust, identity, reliability, and privacy, that are highly vital [17-20]. The [21] presents that any eventual security solution in the 5G should take into considerations the needs for low latency, low power, and high reliability. Moreover, there will be a very wide range of 5G use cases with different requirements, that will need to be secured and overviewed. Significant importance in nowadays and future telecommunication networks' security is to focus on mobile broadband networks and to prove the vulnerabilities in the implementation and configuration of those networks. Additional exposure of future mobile and wireless networks to attacks must be expected from the trend [22-25] away from imposing advanced RAT functions using proprietary algorithms. One challenging fact is that the 5G networks, due to the new networks of Internet of Things (IoTs) [26], Mobile Cloud Computing (MCC) [27], Software-defined networking (SDN) [28,29] and Network Function Virtualization (NFV) [30] are open doors to novel security threats [19]. Therefore, the security architectures of the 3G and 4G will not fulfill the security requirements of the 5G networks, and the securely using above-mentioned technologies and providing user privacy in future 5G networks are bringing new concerns, new demanding situations and new challenges. Moreover, the MCC in 5G has emerged as a key and most significant paradigm,

promising to augment the capability of mobile terminals through provisioning of computational resources on demand, and enabling cell users to offload their processing and storage requirements to the Cloud servers [31].

In that way, a converged access-agnostic core (where identity, mobility, security, etc. are decoupled from the access technology), which integrates fixed and mobile core, is envisioned as a direction of IMT-2020 [32, 33]. Therefore, the IMT-2020 network architecture proposed by ITU (International Telecommunication Union), should be studied to support a true fixed and mobile convergence ensuring a seamless user experience within the fixed and mobile domains. The most significant example of 4.5G: LTE-Advanced Pro provides a smooth transition to 5G New Radio (NR) to meet IMT-2020 requirements given from ITU [34].

Different from the other related works, this paper provides Security and Quality of Service (QoS) framework that can result in a high level of security features and safety through high-performance mobile broadband networks. The proposed framework guarantees QoS provisioning for different multimedia services (including video, audio, and data), with present jamming and distributed denial-of-service (DDoS) attacks (i.e. the jamming attacks).

However, before we provide an explanation for our proposal it would be useful to take a brief summary of the different types of jamming attacks.

2.1 Types of Jamming Attacks

There are several distinct classifications of the jamming attacks [35-37]. In the classification we adopt [38-40], seven jamming models are defined. The most common model is the constant jamming. This model describes the continuous signal or noise transmission to interfere with other ongoing transmissions. Deceptive jamming is very similar to the constant jamming, and the similarity is that both constantly transmit bits. Unlike the constant jamming, the transmitted bits in deceptive jamming are not random. The deceptive jamming continually injects regular packets on the channel without any gaps between the transmissions. Busy jamming is the type of jamming where a very short pulse of noise is created for every interval that is less than DIFS (Distributed Inter-Frame Space), so the nodes are fooled into thinking that the medium is busy. In order to save energy and reduce the probability of detection, other jamming techniques as bursty or random jamming are used, where jamming signals transmission is less frequently. On the other hand, reactive and corruption jamming are the most “intelligent” jamming techniques which only transmit whenever an ongoing transmission or a certain message is sensed. None of the recent known mechanisms are capable enough to handle the jamming attack on wireless networks [41]. An ideal jamming attack should have high energy efficiency (i.e., consume low power), low probability of detection, achieve high levels of DoS (i.e., disrupt communications to the desired extent) and be resistant to PHY layer anti-jamming techniques [42].

3 System Model and ASECQUA Algorithm

The system model of our proposed framework for secure 5G node is shown in Figure 1. The 5G node is using network aggregation and is using all available RAT interfaces. The entire framework is placed in both nodes: the mobile terminal node and fixed node (secure and QoS server) in the core network, with several (n) interfaces (each for distinctive RATs) as shown in Fig. 1. The developed determined framework is based on advanced Security and QoS provisioning algorithm, set within a module on network layer with advanced user-centric aggregation algorithm using vertical multi-homing and multi-streaming capabilities [15] [16] and [43-45]. According to network congestion and security conditions, it selects the most suitable, most reliable and most secure RAT/RATs per used service. We refer to it as Advanced Security QoS-based User-centric Aggregation (ASECQUA) algorithm, which is defined independently from any existing or future technology below network layer. The functionalities with more information and details for the QoS part of the AQUA module are elaborated in [43] and [44], and for the security part in the [45].

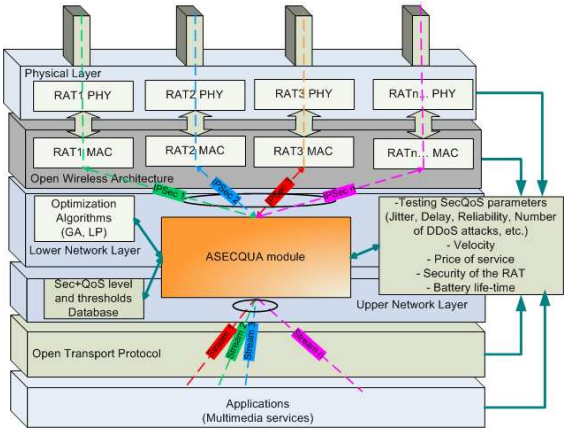

Figure 1

System model for the Secure 5G node with ASECQUA algorithm

The fundamental novelty and distinction from our previous works [43-45] is the development of new advanced Security and QoS Module with improved testing parameter module, IPSec key entity, and Sec+QoS level and thresholds Database, using vertical multi-homing and multi-streaming security features. It uses Multi-RAT interfaces and IPSec encapsulation, where IPSec key entity helps with holding parameters (such as keys) that are used to encrypt and authenticate a particular flow, in the process of forming the IPSec security associations. The information for the network congestion, security, and overall conditions is stored in ASECQUA Cloud server (the Sec+QoS level and thresholds Database) that is a fixed node placed in the core part of the network, due to higher processing and

memory requirements. This information can be: number of users connected per RAT, number of jamming (as one particular type of DDoS attack) attacks per RAT, jamming attack information, the volume of used capacity per RAT, RAT reliability, RAT availability, level of the security threats and etc. Also, the mobile node can have a smaller similar Database, only with collected and necessary information. The module considers the predefined thresholds for the observed parameters, in order to choose the most appropriate optimization algorithm (i.e. the GA (Genetic Algorithm) or LP (Linear Programming) algorithm, stored in the Optimization Algorithms database). To emphasize, ASECQUA is a novel crucial component in our system model, complementary to our previous work in this field ([43-45]), but improved with new security features. That gives profound advantages and better security traffic control for real-time and non-real-time broadband services. It uses different IPSec encapsulation and keys for each different traffic streams (IPSec flow 1, IPSec flow 2, etc.) in Tunnel or Transport mode. Optionally, the mobile node can use one overall IPSec encapsulation (in transport mode) in the Upper IP Layer for better security in an uplink. The ASECQUA proxy server, on the other side (in the core network), will do the IPSec de-capsulation for all streams and will forward the traffic streams in the core part of the network, Internet or other legacy cellular networks.

3.1 ASECQUA Algorithm

Looking the ASECQUA algorithm, one might also be aware the data measurements for different selection criteria, which include user requirements, Security and QoS requirements, operator requirements, as well as radio link conditions, DDoS attacks, jamming attacks (see the following subsection) and other security threats in different RATs presented with n inputs as n sets of parallel criteria functions (CFs), one set per each RAT (from RAT 1 to RAT *n*). One RAT CF is shaping and filtering the outputs from the previous components into adequate interior threshold functions. The ASECQUA module has capability to select one Optimization Algorithm (OA), which as inputs uses: the outputs of the *n* sets of parallel CFs, five values from each RATs (5*n in total) and the output of the threshold CF for battery support (one value) which shapes and filtrates the outputs from the user's mobile battery lifetime. In the process of choosing the algorithm (GA, LP, or other OA) for optimization of the weighted factors, the ASECQUA module is doing the optimal and appropriate choice of algorithm, depending on the different input criteria and conditions for each RAT, for given service, by coordination of the other entities and mentioned Database.

Finally, the ASECQUA module, besides other mentioned functions, is centered for the selection of RATs, so the outcome choice should select the high-quality and most suitable (stable and secure) RAT or RATs with the highest value for a RAT ranking function (1). The *i*-th RAT ranking function is calculated as follows:

$$RF_{RAT(i)} = \frac{SECt_i \cdot W_{SEC} + QoSt_i \cdot W_{QoS}}{W_{SEC} + W_{QoS} + W_C + W_V + W_{SS} + W_B} + \frac{Ct_i W_C + Vt_i \cdot W_V + SSt_i \cdot W_{SS} + Bt_i \cdot W_B}{W_{SEC} + W_{QoS} + W_C + W_V + W_{SS} + W_B} \quad (1)$$

for $1 \le i \le n$ and $W_{SEC} + W_{QoS} + W_C + W_V + W_{SS} + W_B = 1$ (2)

where $W_{SEC}, W_{QoS}, W_C, W_V, W_{SS}, W_B$ are assigned weight factors for the CFs of: Security attack parameter, QoS parameter, service price, velocity of the MT, signal strength, and ME battery support, respectively. Those values of weight factors are assigned using a particular method of optimization. On the other hand, after passing the interior threshold functions for *i*-th RAT CF, the outputs (shaped values as real numbers within the limits [0, 1]): $SECt_i$ are regarding for the Security parameters, QoS parameters are QoSti, from service price are Ct_i, from velocity support are Vt_i, and from detected signals strength are SSt_i. The shaped output value of the threshold CF for battery support is Bt_i. So, the final step is selection of the optimal and the most secure RAT(s) for a given service or stream (if we have done multi-streaming before):

$$\max_{service\_m} \left\{ Optimal\left(RF_{RAT(i)} \right) \right\} \quad (3)$$

subject to: $W_{SEC} \le 1, W_{QoS} \le 1, W_C \le 1, W_V \le 1, W_{SS} \le 1, W_B \le 1$ (4)

and (2), for $1 \le i \le n$; $1 \le m \le 3$ (5)

Above we have defined the optimization problem, where service_m is the given service (i.e. m=1 for audio, m=2 for video and m=3 for data), and Optimal (RF_{RAT_i}) is the optimal function value for the *i*-th RAT RF, calculated by OA (which reaches the global optimum).

3.2 Adaptive Transmission Power and Receiver Sensitivity Adjustment Algorithm with ASECQUA

Despite many proposed countermeasures against low power jamming attacks, the best results are achieved by the combination of increased transmission power on the transmitter side, decreased receiver sensitivity (reception power threshold) and the used spread spectrum technique (iDSSS). DSSS in many scenarios is set as a default spread spectrum technique on wireless nodes and WiFi Access Points, whereby transmission power and receiver sensitivity were manually set to the given level. In our ASECQUA module, we are considering the possibility of adaptive transmission power and receiver sensitivity adjustment. In order to achieve this, we propose an algorithm working within the ASECQUA module, using the amendment 5, part 11, of the 802.11h-2003 standard [46], which considers transmitting power management, when there is a jamming attack in some particular RAT. Considering the fact that, in wireless and mobile communications, the Medium Access Control (MAC) layer is responsible for

Transmit Power Control (TPC), we are proposing this adaptive transmission power and receiver sensitivity adjustment mechanism to be implemented at the IP layer, but to have tight cross-layer connections with the Layer Two. The examined scenario in our simulation works in infrastructure mode so that most of the computation will be done by RAT AP (or Base Station if this is not WLAN RAT), which does not mean that the wireless and mobile client terminals are not able to implement this standard. All work is supported by three elements which are used for TPC solution. These three elements are TPC request element, TPC report element and Power constraint element [46]. As can be seen in [46], there are 4 octets in the TPC Report element. The information about transmission power (used to send TPC Report element back to the node, or in our case AP) and actual link margin (received transmission power from the client stations measured at the side of the AP minus sensitivity for the time when related TPC Request element was received) is contained in the last two octets. This information follows as a response to a TPC Request element. Received TPC reports are stored in AP's database, and these reports are used for the purpose of power control. Fig. 2 shows the process of measurement of the TPC for the AP. Based on the information from the TPC Report elements the AP calculates the minimum transmit power it needs to set for downlink (DL) communication with each of the wireless client stations (STAs). The AP also calculates the transmit power for each of the client stations which they should set for uplink (UL) communication with the AP. The management frame containing information about the minimum and maximum transmit power is than sent to the client stations [46].

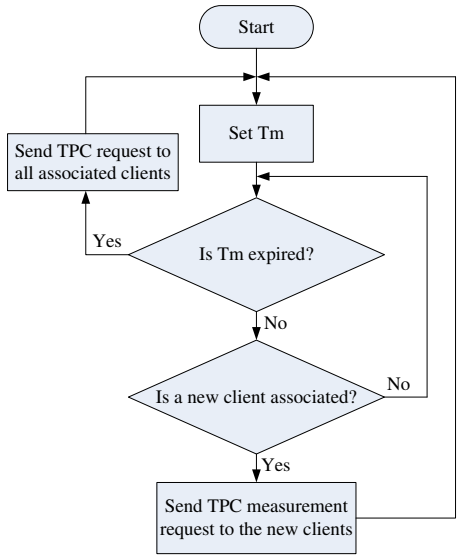

Figure 2
TPC measurement process in ASECQUA algorithm

Considering the client n, in order to guarantee QoS, desired received power P_{rn} is equal to:

$$P_{rn} = S_{inn} + D \tag{6}$$

where S_{inn} is the receiver's sensitivity and D is the margin to be above the receiver's sensitivity. If we replace all losses, including Free space path loss (FSPL), shadowing effects and jamming with L_n then the transmit power can be calculated as:

$$P_{RSSIn} = P_{tn} = L_n + S_{inn} + D = I_n + D \tag{7}$$

The link margin $M_n(i)$ in the TPC Report for the i-th measurement is:

$$M_n(i) = P_{rn}(i) - S_{inn} \tag{8}$$

The transmit power by the AP used to transmit data frames to client n is equal to P_{RSSI} or desired P_{tn}.

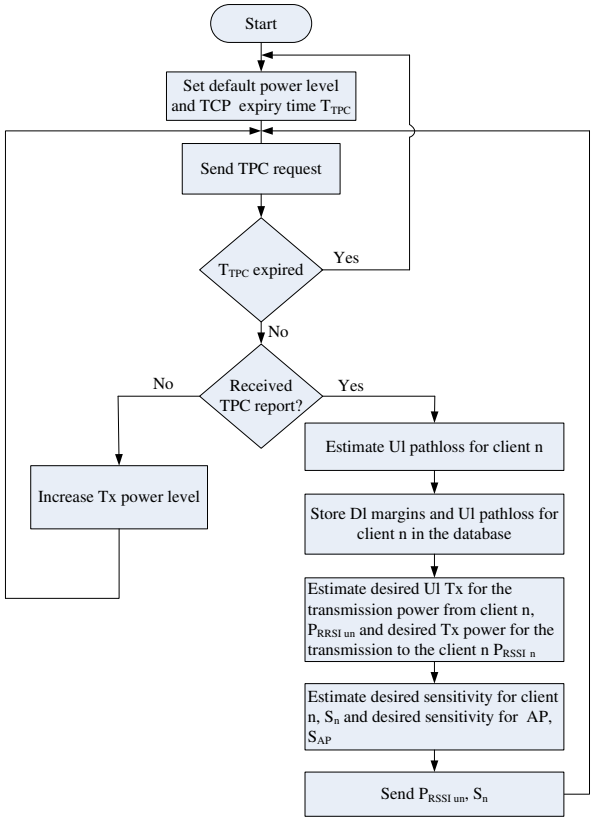

Figure 3
TPC decision based on TPC report elements from the adequate terminals in ASECQUA

The power is controlled per each client station, so for each station different transmitter power is used. Fig. 3 shows algorithm decision on AP side based on measurement reports from wireless client stations. It should be mentioned that many mobile and wireless cards do not support a change of the transmit power on the AP side, so the AP sets its transmit power based on the mobile and wireless client terminal that facing worst link conditions. In this way, the AP transmits sufficient power so the STA with worst conditions successfully receives wireless packets. If the AP is associated with many STAs, the AP's transmit power is:

$$P_t = \max_n(P_{tn}) = \max_n(P_{RSSIn}) \tag{9}$$

When the AP initializes, it transmits at default power level, that is: $P_t(0) = \max P$.

As it is shown in Fig. 3, the AP estimates path loss for client n (which will include FSPL, shadowing effects, and jamming effects), stores DL margins and UL path loss for client station, estimates its own transmission power and sensitivity, as well as STA transmission power and sensitivity. The AP also sends the estimated STA transmission power and sensitivity to the appropriate STA. If the link experiences some problems, in our case if a jamming attack occurs, the AP will not receive TPC Report, and it will iteratively increase its transmit power (each iteration will increase the power for 0.005 W). On the wireless and mobile client side, the situation is same. TPC Request/Report elements can be also implemented on STA side [46], so the STA can also iteratively increasing the power level until TCP Report from the AP is received. As it is shown in equations (6) and (7), the receiver sensitivity is also connected with transmission power, so the AP can estimate and send the best transmission power-receiver sensitivity ratio, which means that if transmission power on one site is increased, the receiver sensitivity on the opposite side can be decreased, so any noise which occurs in communication link, including the jamming signal produced by low power jammers, can be squelched.

4 Simulation Results and Analysis

The obtained simulation results for average aggregated system throughput, as well as average multimedia secure access probability values for different 5G and heterogeneous mobile and wireless broadband network conditions (with different security threats per different RATs), are presented furthermore. The jamming and DDoS attacks and the effects of these attacks are simulated in OPNET Modeler environment [40] [47-52]. The performance of the proposed ASECQUA framework is evaluated through simulations done in both MATLAB and OPNET. For solving the optimization problem (3) we are using MATLAB functions: GA when using genetic algorithm and LP when using linear programming, for finding

the optimal (maximal) RAT ranking function (1) for a given service. Moreover, the adaptive transmission power and receiver sensitivity adjustment algorithm proposed in subsection 3.2 is written in MATLAB scripts. After that, the calculations and results from MATLAB scripts and functions, using the technology of the MATLAB engine interface are integrated into OPNET, where the system model is placed.

The average aggregated system throughput is the average sum of all throughputs per mobile node, and the multimedia secure access probability ratio is calculated as the ratio of all successful and secure multimedia service access attempts from the users and the total number of all multimedia service access attempts (including not secure multimedia service access attempts due to the jamming attacks, DDoS attacks or other cyber and security threats). Our simulation scenario is a multi-cell scenario, plotted in the dense urban area, with random initial locations of MTs uniformly distributed within the entire observed area. The scenario consists of three kinds of RATs. All base stations are positioned in various locations within the simulation area, and their positions (per cell), together with their network coverage areas and capacities are given in Tab. 1. The values are carefully chosen in order to correspond with the certain standardized capacities of LTE, IEEE 802.11n and IEEE 802.11ac.

All RATs are constantly attacked by a different kind of DDoS attacks (TCP SYN flood, UDP flood, and ICMP Ping Distributed DoS (DDoS) attacks and jamming attacks). Those DDoS attacks are causing inability to access any service from the MTs and the jamming attacks are preventing the MTs to communicate by occupying the channel that they are communicating. Moreover, in RAT1 (LTE) we have adaptive modulation and coding, i.e., at different destination points from the RAT1 (LTE) base stations we are using different modulation and coding schemes. For mobile nodes physical mobility, we have adopted 2-dimensional implementation of the Gauss-Markov Mobility model considering average speeds in the range of 20-320 km/h. This mobility model provides a high level of randomness for user mobility. Also, when a group of mobile nodes is leaving the RAT1 (macro) cell, it is supposed that the same number of mobile nodes is incoming in the observed cell from other neighboring cells, so the number of mobile nodes per cell remains constant over the simulation time. The multimedia service flow model consists of three types of services as follows:

1st service type: Video conference with a low bit rate (128 kbit/s) and small latency.

2nd service type: Video-streaming with medium bit rate (256 kbit/s) and low propagation time, plus jitter sensitive.

3rd service type: Data service with high bitrate (512 kbit/s) or larger latency, but has requirements for zero packet delivery errors.

During the simulation for a given number of ordinary active mobile users N, each user is randomly assigned to one of the three types of services defined above.

When the users have MT with ASECQUA module within, for each user are randomly assigned all three types of multimedia services. We have done five cases for this scenario:

Case 1: All MTs are enhanced with ASECQUA module with GA optimizations in our three-RAT MT with three interfaces.

Case 2: All MTs are enhanced with ASECQUA module with LP optimization algorithm, instead of having GA. We refer to this kind of MT as MT with LP module (ASECQUA_LP).

Case 3: All MTs are using only RAT1 technology (only LTE interface), without ASECQUA module within.

Case 4: All MTs are using only RAT2 technology (only IEEE 802.16n interface), without ASECQUA module within.

Case 5: All MTs are using only RAT3 technology (only IEEE 802.16ac interface), without ASECQUA module within.

The simulation results regarding the achievable average aggregated throughput (R) are shown in Fig. 4, which provides results on the average throughput (per cell) versus the number of MTs for all five cases.

Table 1

Parameter Values for the RATs

	Position(s) (meter, meter)	**Network Radius (meter)**	**Network Capacity [kbps]**
RAT 1	(0,0)	2100	300000
RAT 2	(0,0), (120,120), (-120,120), (-120,-120), (120, -120), (0, -255), (0, 255)	70	600000
RAT 3	(0,0), (0, 120), (-120, 0), (120,120), (-120,120), (-120,-120), (120, -120)	40	7000000

The average velocity of the MTs is set to 40 km/h and the total simulation time is 120 seconds (according to [53] it is default service duration for getting valuable statistical results from the Security and QoS measurements for any multimedia services). As one can notice, the throughput for our MT, with ASECQUA module, for any number of used MTs, is much higher than the average throughput values in the case when we use only MTs that can access only RAT1 (R_RAT1_MT), or in the case when we use only MTs that access RAT2 (R_RAT2_MT) or RAT3 (R_RAT3_MT).

Comparing the throughput for the R_ASECQUA_LP curve (where the LP is used as OA) and the throughput in the case when GA is used as OA within the ASECQUA module of MT (R_ASECQUA_GA), the MT with LP is achieving the

highest throughput for any number of ME. This indicates that the MT with LP can be used for middle to high traffic congestion scenarios (more than 360 MTs) because gives overall better yields then GA OA.

Furthermore, in Fig. 5 are presented the average multimedia secure access probability ratio per cell (Pm_sec_acc) values for different velocities of the MTs, with 500 MTs and simulation time of 120 seconds. For the first case, when we use MTs with ASECQUA modules with LP algorithm, the average Pm_sec_acc values are higher than the MTs with ASECQUA modules with the GA algorithm for any average speed of MTs. As it was expected, for the first two Cases (with ASECQUA module) the values for Pm_sec_acc are higher than the values obtained for the cases when we used MTs that can access only one RAT. The difference between MTs with ASECQUA module with GA OA and those with LP OA is in range of 0.125 or less for the Pm_sec_acc per cell. In case of higher velocity (when the average velocity of MTs is more than 200 km/h), the preference should be given to LP OA for all cases where this Secure-QoS parameter (Pm_sec_acc) is crucial for the services. Generally, the higher value for Pm_sec_acc further results in lower packet error ratio, higher service availability, reliability and security, as well as in higher aggregated bit rates due to vertical multi-homing, multi-streaming and RAT aggregation. Finally, Fig. 6 depicted the values for Pm_sec_acc per cell versus the number of MTs, when all MTs are moving with an average speed of 50 km/h and simulation time of 120 seconds. For the cases when we use MTs with ASECQUA modules with LP or GA algorithm, the average Pm_sec_acc values are higher than the other cases when the MTs are without ASECQUA modules.

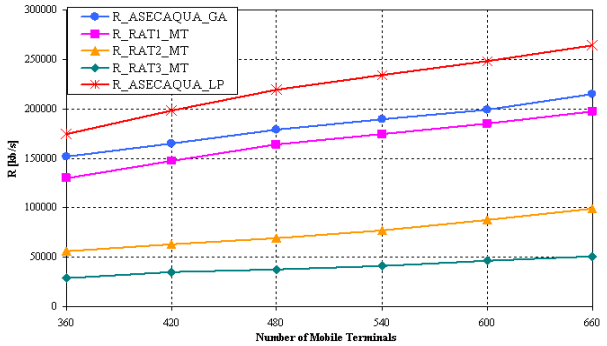

Figure 4
Average throughput per cell versus number of MTs

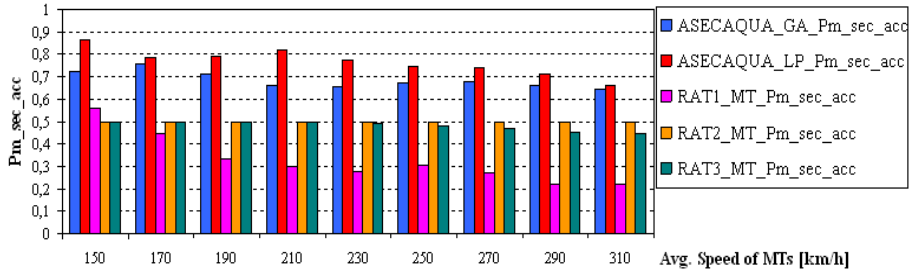

Figure 5

Average Pm_sec_acc per cell versus velocity of MTs

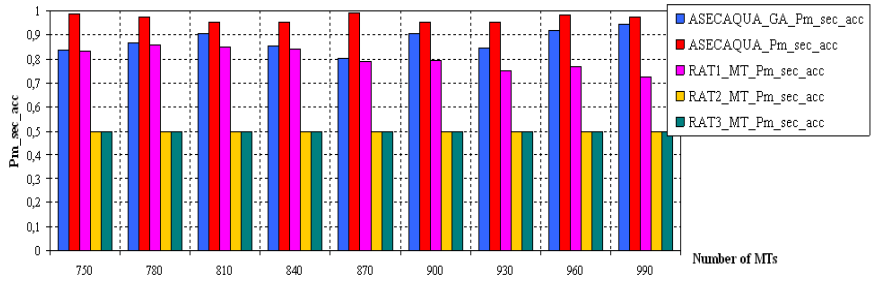

Figure 6

Average Pm_sec_acc per cell versus number of MTs

The difference between those two cases is 0.1 or less in the average multimedia secure access probability ratios. As can be seen, the number of MTs is very high, and this scenario is for dense network conditions.

So, if we have MTs with the ASECQUA module within, with two options for choosing LP or GA optimization algorithms, in those network conditions, where there are high dense networks (where mobile nodes are above hundreds) - we will use LP. However, it is always wise to have a backup and shared combinations of Secure and QoS optimization algorithms for different network conditions and environments. Undoubtedly, the 5G nodes with ASECQUA are achieving superior results regarding the aggregated average aggregated throughput and multimedia secure access probability ratio per service with optimal secure RAT(s) selections.

Conclusions

The trend of integrating criminal and warfare methods with inexpensive technologies to achieve individual, criminal or national security objectives can pose serious challenges to the implementation of future ICT technologies. The expected and promising 5G based technology will not be immune to these threats. Including the jamming process. Solutions that will mitigate the upcoming 5G devices' vulnerabilities from jamming attacks, build trust among the end-users (individuals, corporate, public stakeholders). The presented framework herein

could be adapted to serve corporate or national security purposes. As we have shown, this framework, called the ASECQUA module, can provide future Security and QoS provisioning within the 5G network capacity aggregation with vertical multi-homing and multi-streaming features. The presented results prove that this framework provides the highest level of multimedia, secure access probability ratio and highest aggregated throughputs for each multimedia and broadband service, over secure traffic tunnels. Moreover, the proposed, combined anti-jamming mechanisms, within ASECQUA show results that are almost the same as in the case when no jammer is used. Here we also propose an algorithm for adaptive transmission power and receiver sensitivity control, in order to achieve desired transmission power and receiver sensitivity adjustment. In that manner, optimal, secure and QoS-based usage of available wireless and mobile broadband resources is essential for the excellent provision of any broadband service, with a high level of security.

In one future 5G, a possible scenario for using various broadband services from the end users over the 5G and other heterogeneous wireless and mobile broadband networks, the 5G mobile node and ASECQUA proxy server with vertical multi-homing and multi-streaming security features are able to handle simultaneously multiple RAT connections. Moreover, there will be high speed wireless and mobile connections for each broadband service (e.g., web, video streaming, ftp, etc.) by transmitting each object of each service in a separate IPSec stream, to achieve the highest level of secure communications and satisfied end-users.

Finally, the given advanced framework for 5G and heterogeneous wireless and mobile broadband networks can be one of the key solutions for future network architectures, not only 5G, but beyond. Because of the fact that the presented framework achieves maximal aggregated throughput and multimedia secure access probability ratio, and consequently better overall security and QoS performances. The given advanced framework for 5G could be easy extended for mobile cloud computing and security plus QoS orchestration mechanisms in all network entities, including the smart mobile devices, i.e. the cloud computing would be extended at the edge of the network in a form of intelligent multi-access edge computing. The time is near, where more and more virtual network functionality, including blockchain technology, will be executed in a mobile cloud and edge computing environment, including many parts of our given advanced framework. They together, would provide ubiquitous computing and broadband service to the users, where devices, smart terminals, laptops, machines, but also, smart things and robots would become innovative tools that would produce and use different services and data, i.e. they would be able to provide “Anything as a Service” (AaaS) as well.

References

[1] Federico Boccardi et al.: Five Disruptive Technology Directions for 5G, IEEE Communications Magazine, Vol. 52, No. 2, 2014, pp. 74-80

[2] Naga Bhushan et al.: Network Densification: The Dominant Theme for Wireless Evolution into 5G, IEEE Communications Magazine, Vol. 52, No. 2, 2014, pp. 82-89

[3] Boyd Bangerter, Shilpa Talwar, Reza Arefi, and Ken Stewart: Networks and Devices for the 5G Era, IEEE Communications Magazine, Vol. 52, No. 2, 2014, pp. 90-96

[4] Cheng-Xiang Wang et al.: Cellular Architecture and Key Technologies for 5G Wireless Communication Networks, IEEE Communications Magazine, Vol. 52, No. 2, 2014, pp. 122-130

[5] Toni Janevski: 5G Mobile Phone Concept, IEEE Consumer Communications and Networking Conference (CCNC) 2009, Las Vegas, USA, 2009

[6] Willie W. Lu: An Open Baseband Processing Architecture for Future Mobile Terminals Design, IEEE Wireless Communications, April 2008

[7] Aleksandar Tudzarov and Toni Janevski: Design for 5G Mobile Network Architecture, International Journal of Communication Networks and Information Security, Vol. 3, No. 2, August 2011, pp. 112-123

[8] Josef Noll, Mohammad. M. R Chowdhury: 5G – Service Continuity in Heterogeneous Environments, Wireless Personal Communications, DOI: 10.1007/s11277-010-0077-6, Published online: 31 July 2010

[9] Kris Osbornnov: Samsung works with U.S. military to prototype new high-speed 5G network, Defense Systems, accessed: November 28, 2018 at: https://defensesystems.com/articles/2017/11/02/samsung-5g-halvorsen.aspx

[10] Anirudh Bhagwandas Rathi, Snehal Kalam: 5G Technology and Advancement in Telecommunication at Military Level, Scholars Journal of Engineering and Technology (SJET), 4(1):49-52, 2016

[11] M. Shafi et al.: 5G: A Tutorial Overview of Standards, Trials, Challenges, Deployment, and Practice, IEEE Journ. Sel. Areas in Commun., Vol. 35, No. 6, Jun. 2017, pp. 1201-1221

[12] R. Kassab, O. Simeone, and P. Popovski: Coexistence of URLLC and eMBB Services in the C-RAN Uplink: An Information-Theoretic Study, in Proc. IEEE Globecom, Abu Dhabi, December 2018

[13] P. Popovski et al.: Ultra-Reliable Low-Latency Communication (URLLC): Principles and building blocks, IEEE Network, Vol. 32, No. 2, Mar. 2018, pp. 16-23

[14] 3GPP: Study on new radio (NR) access technology physical layer aspects, TR 38.802, Mar. 2017

[15] Recommendation ITU-T Y.2052 (02/2008): Framework of multi-homing in IPv6-based NGN

[16] Recommendation ITU-T Y.2056 (08/2011): Framework of vertical multihoming in IPv6-based Next Generation Networks

[17] Next Generation Mobile Network Alliance: 5G White Paper, Version 1.0, Feb 17, 2015

[18] D. Kutscher: It's the network: Towards better security and transport performance in 5G, 2016 IEEE Conference on Computer Communications Workshops (INFOCOM WKSHPS), San Francisco, CA, 2016, pp. 656-661

[19] Ahmad, Ijaz et al.: 5G security: Analysis of threats and solutions. 2017 IEEE Conference on Standards for Communications and Networking (CSCN), 2017, pp. 193-199

[20] I. Ahmad, T. Kumar, M. Liyanage, J. Okwuibe, M. Ylianttila and A. Gurtov: Overview of 5G Security Challenges and Solutions, in IEEE Communications Standards Magazine, Vol. 2, No. 1, March 2018, pp. 36-43

[21] SIMalliance: An analysis of the security needs of the 5G market, A SIMalliance 5G Working Group marketing white paper, 2016

[22] Symantec: Internet Security Threat Report, Volume 21, April 2016

[23] P. Schneider and G. Horn: Towards 5G Security, 2015 IEEE Trustcom/BigDataSE/ISPA, Helsinki, 2015, pp. 1165-1170

[24] M. Hadji-Janev, and Bogdanoski, M.: Handbook of Research on Civil Society and National Security in the Era of Cyber Warfare, Hershey, PA, IGI Global, 2016

[25] A. Risteski, M. Bogdanoski, M. Stoilkovski, M. Jovanovic: Cyber Security Issues of Telecommunication Infrastructure, Chapter, Book: Cyber Security and Resilience Policy Framework, IOS Press, NATO Science for Peace and Security Series - D: Information and Communication Security, September 2014

[26] Ejaz, Waleed et al.: Internet of Things (IoT) in 5G Wireless Communications, IEEE Access. 4. 10310-10314, January 2016

[27] Z. Zhang and S. Li: A Survey of Computational Offloading in Mobile Cloud Computing, 2016 4th IEEE International Conference on Mobile Cloud Computing, Services, and Engineering (MobileCloud), Oxford, 2016, doi: 10.1109/MobileCloud.2016.15, pp. 81-82

[28] Singh, S. & Jha, R. K. Jha: A Survey on Software Defined Networking: Architecture for Next Generation Network, Journal of Network and Systems Management, Vol. 25, 321-374, April 2017, https://doi.org/10.1007/s10922-016-9393-9

[29] I. Ahmad, S. Namal, M. Ylianttila, and A. Gurtov: Security in Software Defined Networks: A Survey, IEEE Communications Surveys Tutorials, Vol. 17, No. 4, Fourthquarter 2015, pp. 2317-2346

[30] Bo Han and al.: Network Function Virtualization: Challenges and Opportunities for Innovations, IEEE Communications Magazine, 53(2), February 2015, pp. 90-97

[31] A. Aissioui, A. Ksentini, A. M. Gueroui and T. Taleb: Toward Elastic Distributed SDN/NFV Controller for 5G Mobile Cloud Management Systems, in IEEE Access, Vol. 3, 2015, pp. 2055-2064

[32] ITU-R: ITU-R M. - Minimum requirements related to technical performance for IMT- 2020 radio interface(s), Report ITU-R M.2410-0, Nov. 2017

[33] ITU Recommendation Y.3101: Requirements of the IMT-2020 network, January 2018

[34] Qualcomm: Accelerating the 5G ecosystem expansion today with LTE Advanced Pro, May 2018. <available link> https://www.qualcomm.com/invention/5g/lte-advanced-pro

[35] Liu, Z., Liu, H., Xu, W., and Chen, Y.: Exploiting jamming-caused neighbor changes for jammer localization, Parallel and Distributed Systems, IEEE Transactions on, 23(3), 2012, pp. 547-555

[36] Wilhelm M., Martinovic I., Schmitt J. B., and Lenders V. Short paper: reactive jamming in wireless networks: how realistic is the threat?. In Proceedings of the fourth ACM conference on Wireless network security (WiSec '11) 2011, ACM, 47-52. DOI=10.1145/1998412.1998422

[37] Chaturvedi P., Gupta K.: Detection and Prevention of various types of Jamming Attacks in Wireless Networks, IRACST – International Journal of Computer Networks and Wireless Communications (IJCNWC), ISSN: 2250-3501, Vol. 3, No. 2, April 2013

[38] Xu, W., Trappe, W., Zhang, Y. & Wood, T.: The Feasibility of Launching and Detecting Jamming Attacks in Wireless Networks, In Proceedings of the 6th ACM international symposium on Mobile ad hoc networking and computing, ACM MOBIHOC, 2005, pp. 4657

[39] Acharya, M., Sharma T., Thuente, D., and Sizemore, D.: Intelligent jamming in 802.11b wireless networks, In Proceedings of OPNETWORK-2004 Conference, Washington D.C., USA, 2004

[40] Mitko Bogdanoski, Aleksandar Risteski, Pero Latkoski, Tomislav Shuminoski: Power Control as an Effective Method Against Low Power Jamming, CICSyN2014, Tetovo, Republic of Macedonia, May 27-29, 2014

[41] Khan, S., Loo, K. K., Naeem, T. and Khan, M. A.: Denial of Service Attacks and Challenges in Broadband Wireless Networks, IJCSNS International Journal of Computer Science and Network Security, 2008

[42] Acharya, M. and Thuente, D.: Intelligent Jamming Attacks, Counterattacks and (Counter)2 Attacks in 802.11b Wireless Networks, In Proceedings of the OPNETWORK-2005 Conference, Washington DC, USA, August 2005

[43] Tomislav Shuminoski, Toni Janevski: Radio Network Aggregation for 5G Mobile Terminals in Heterogeneous Wireless and Mobile Networks, Wireless Personal Communications, Vol. 78, Issue 2, 2014, pp. 1211-1229

[44] T. Shuminoski, T. Janevski: 5G mobile terminals with advanced QoS-based user-centric aggregation (AQUA) for heterogeneous wireless and mobile networks, Wireless Networks, 22(5), July 2016, pp. 1553-1570

[45] Tomislav Shuminoski, Toni Janevski, Aleksandar Risteski and Mitko Bogdanoski: Security and QoS framework for 5G and Next Generation Mobile Broadband Networks, IEEE EUROCON 2017, Ohrid, Macedonia, 6-8 July 2017

[46] IEEE 802.11h Standard, Part 11: Wireless LAN Medium Access Control (MAC) and Physical layer (PHY) specifications, Amendment 5: Spectrum and Transmit Power Management Extensions in the 5 GHz band in Europe, December 2003

[47] Mitko Bogdanoski, Aleksandar Risteski: Wireless Network Behavior under ICMP Ping Flood DoS Attack and Mitigation Techniques, International Journal of Communication Networks and Information Security (IJCNIS), Vol. 3, No. 1, 2011

[48] Mitko Bogdanoski, Tomislav Shuminoski, Aleksandar Risteski: Analysis of the SYN Flood DoS Attack, International Journal of Computer Network and Information Security, Vol. 5, No. 8, June 2013, pp. 1-11

[49] Mitko Bogdanoski, Aleksandar Toshevski, Dimitar Bogatinov, and Marjan Bogdanoski: A novel approach for mitigating the effects of the TCP SYN flood DDoS attacks, World Journal of Modelling and Simulation, 12 (3), 2016, pp. 217-230

[50] Boris Mihajlov, Mitko Bogdanoski: Analysis of the WSN MAC Protocols under Jamming DoS Attack, International Journal of Network Security, Vol. 16, No. 4, July 2014, pp. 304-312

[51] Mitko Bogdanoski, Pero Latkoski, and Aleksandar Risteski: Analysis of the Impact of AuthRF and AssRF Attacks on IEEE 802.11e-based Access Point, Mobile Networks and Applications, Volume 22, Issue 5, October 2017, pp. 834-843

[52] Peco Stojanoski, Mitko Bogdanoski, Aleksandar Risteski: Wireless Local Area Network Behavior under RTS flood DoS attack, 20th

Telecommunications Forum TELFOR 2012, IEEE Conference, 20-22 November 2012

[53] Recommendation ITU-T E.804 (02/2014): QoS aspects for popular services in mobile networks

Analysis of Latency, Blocking Probability and Network Utilization for a Specific Routing and Spectrum Assignment Algorithm, in Elastic Optical Networks

Teodora Kocevska, Pero Latkoski, Marko Porjazoski, Borislav Popovski

Faculty of Electrical Engineering and Information Technologies, Ss. Cyril and Methodius University, 1000 Skopje, Macedonia
{teodora, pero, markop, borop}@feit.ukim.edu.mk

Abstract: The emergence of new ICT applications has triggered significant growth in data traffic volumes. As a result, novel flexible and adaptive concepts for optical network management has emerged, in order to meet the heterogeneous and variable traffic demands. Efficient spectrum usage has become one of the most important issues, since the optical spectrum is not an infinite resource. Today's WDM (Wavelength Division Multiplexing) technology is inappropriate, due to the fixed spectrum grid it uses. The elastic optical networks (EON) will overcome these problems. Finding an efficient RSA (Routing and Spectrum Allocation) algorithm is very important for resourceful use of the network. This paper extends the current research knowledge regarding the intelligent RSA algorithm with support for different Class of Service (CoS). It assumes a coexistence of two traffic categories in the network, along with a central Software Defined Networking (SDN) controller. Furthermore, a dynamic RSA algorithm is used with two controlling coefficients to determine the priority of different classes. The performance of the algorithm and the impact of the controlling coefficients on several performance metrics (e.g. average latency for data traffic, blocking probability, network utilization and network efficiency) has been examined through MATLAB simulations. The obtained results indicate some complex influence of the data traffic load and spectrum-controlling RSA coefficient over the performance metrics. The results can help network operators not only define different CoS in their network, but to also finely tune its utilization, blocking probability and data traffic latency, which is crucial for the emerging 5G communication networks.

Keywords: Elastic Optical Networks; Software Defined Networking; RSA; 5G; MATLAB

1 Introduction

Today, communication networks are an inseparable part of people's lives. They provide support for various personal daily activities (work, social life, entertainment, etc.), as well as, for most of the industrial sectors (engineering, marketing, trade, medicine, business, etc.). The future will introduce even a more noticeable role of communication networks in everyday life. With 5G, every person and every device, from anywhere, at any time, is expected to have access to information and to be able to share data. Network operators in the future are expected to offer a number of services with different features, such as extended Mobile Broadband (eMBB), Ultra-Reliable Low-Latency Communications (URLLC) and massive Machine-Type of Communications (mMTC). This requires for a new network architecture and a new traffic engineering strategy in all parts of the communication network.

The present optical transport networks are based on DWDM (Dense WDM) technology. Although this is a relatively mature optical transmission technology, it is not suitable for traffic demands in future optical networks, because it uses a uniform division of the spectrum, i.e. fixed frequency grid. This approach leads to spectral inefficiency. A new adaptive and flexible concept for optical networks management is needed in order to deal with future trends: flexible resource allocation, heterogeneous traffic demands, energy efficient solutions and reliability.

Flexible optical networks, also known as elastic optical networks, use the spectrum by dividing it into a large number of narrow frequency slices. In this way, the elastic optical networks can use wider spectral channels in order to serve the traffic requirements that need high bit rates (400 Gb/s, 1 Tb/s and more).

This paper extends the research findings made in [1] by introducing a variety of network relevant performance metrics and by discussing the importance of spectrum management for all classes of traffic. The paper also assumes a SDN controller to optimize the usage of network resources, thus, the spectrum allocation will be based on the network state information and the characteristics of the previously served traffic requests. This central entity can orchestrate the requests that must be served immediately, with regard to the requests that can tolerate a certain delay. Such an orchestration is particularly important to control the blocking probability for the requests that must be served immediately, as well as, to provide efficient network utilization. In order to analyze, evaluate and validate the proposed algorithm, many simulations were conducted in a custom-made MATLAB software tool. The simulations evaluate the influence of the priority control mechanism on the average latency of the traffic, the blocking probability, network utilization and network efficiency.

2 Related Work

Since the introduction of the elastic optical networks concept, there have been numerous research on the subject. The literature on elastic optical networks shows a variety of approaches. Only a part of the recent work has been selected here.

Most of the research has focused on elastic optical inter-datacenter networks because they are targeting high-bandwidth and low-latency requirements. Since resource availability is considered as one of the main constraints in today's optical networks, failure recovery is extremely important. So far, several studies have been performed within these two topics [2]-[6]. The research on protection in Elastic Optical Networks (EONs) has become very popular, as well. The authors of [7] propose a new dedicated path protection mechanism for link-failure survivability in EONs. Further, they used modified version of the Dijkstra's algorithm for calculation of the link-disjoint routes. Other well-known algorithms were used for the sake of comparison with the proposed algorithm.

The RSA problem must be considered in order to properly analyze, design, plan, and operate flex-grid networks [8]. In recent years, the RSA issue has attracted considerable attention from research teams, since the development of efficient methods for solving realistic problem instances in reasonable time has become an imperative. Several papers investigated RSA in spectrum sliced EONs. The reference [9] reviews and classifies different routing and spectrum allocation approaches. Additionally, the authors presented fragmentation, modulation, quality-of-transmission, traffic grooming, survivability, energy saving, and networking cost, as important aspects related to RSA. Authors of [10] studied the problem complexity when different technological options for the EON realization are used. In [11], authors proposed a technique which improves resource allocation efficiency and lowers the call blocking for scheduled demands. Paper [12], focuses on minimizing the maximum spectrum usage for a set of traffic demands and proposes new cost functions that are pluggable into an auxiliary layered-graph framework to solve the routing, fiber, waveband, and spectrum assignment problem. The work in [13], proposes a dynamic RSA algorithm that uses Back Propagation Neural Network (BPNN) to predict the arrival time and the holding time of future arrival requests. Authors of [14] have designed an algorithm that minimizes the process of selection with priority-based encoding for selecting optimized path in the existing routes. In [15], a novel heuristic algorithm for the problem of routing, spectrum, transceiver and regeneration allocation is proposed. Moreover, a trade-off between spectrum usage and transceiver usage was investigated through simulations. In [16] two virtualized functions for routing and frequency allocation (RFA) are proposed and different ordering policies were investigated. The development of an efficient mechanism that is able to handle traffic requests that need to be served immediately and others that can be reserved in advance has gained importance in recent years. The coexistence of immediate and advanced reservation request is an important issue since advanced reservation

(AR) requests tend to reserve future resources which can cause a blocking of the immediate reservation (IR) requests. The concept of advanced reservation was first introduced in [17]. In [18], the authors summarized related research into EONs and resource-allocation methods for IR and AR requests, and proposed dynamic RSA method to reduce spectrum fragmentation, while controlling the service level of IR and AR requests. In [1], *Shahsavari et al.* proposed multi-quality of service routing and spectrum assignment algorithm in EONs considering the bandwidth usage and the holding time of established connections. Moreover, authors suggested use of two controlling coefficients to determine the ratio of time and spectrum slots which can be assigned to big data traffic (BDT) requests and demonstrated the influence of this coefficients on the blocking probability.

In this paper, we take into consideration, the previously mentioned related work, especially the work provided in [1], and extend the research in the area of network utilization and data latency, as two key metrics related to the network management, in addition to the blocking probability.

3 Problem Description

Traffic demands that arrive to a network, can be classified into two categories: Priority Real-time Traffic (category 1) and Big Data Traffic (category 2). Finding an algorithm that will reduce the blocking probability of the first category traffic is essential since 5G communication networks are expected to support critical services such as self-driving vehicles, factory automation, remote health care (generally 5G URRLC and eMTC). Moreover, it is necessary to find a strategy for parallel handling of data traffic which can tolerate some delay (e.g. 5G eMBB, exchange of data between data centers, etc.). On the other hand, it is very important to improve the efficiency in the network resources utilization. In the case of optical networks, it is particularly difficult to support the coexistence of these two categories of traffic, since data traffic while more robust, can increase the blocking probability of the category 1 traffic.

The solution lays in the usage of a logically centralized SDN controller that has a global picture of the network state, based on which it can make strategic changes in the routing and spectrum allocation. This centralized entity can orchestrate the traffic demands from different CoS and improve the overall service. The focus of this paper is finding a way to determine the priority of the traffic requirements belonging to the first category, in relation to those of the second category, based on network conditions. An efficient method and performance metrics have been proposed in order to allow the network controller to handle traffic requirements that have different quality of service requirements.

3. 1 Network Model

The network model discussed in this paper is an extended and improved version of the network model presented in [1]. Graph *G(J, L)* is used to denote the elastic optical network, where *J* is the set of switching nodes and *L* is the set of optical links between the nodes in the set *J*. The number of nodes in the network is denoted as $N_j = | J |$, and the number of bidirectional links is denoted as $N_l = | L |$. Each link is bidirectional, composed of a pair of optical fibers, one for each direction. Each optical fiber has capacity *C*. The optical fiber capacity is divided into N_{fs} frequency slices, where each frequency slice has capacity equal to $M \times C / N_{fs}$, where *M* represents the modulation level (in this paper BPSK is taken into account, *M*=1). Each optical fiber can be represented as ordered set $F = \{f_1, f_2, f_3, \ldots, f_{Nfs}\}$ of frequency slices. The value of N_{fs} is set by the network designer.

The time duration of each connection is expressed in the number of time slots, because the usage of the spectrum is divided into time slots (*TS*). Each time slot lasts *T* seconds.

Two types of requests are arriving in the network: requests that do not tolerate delay and must be served immediately (Fixed Rate Immediate traffic), denoted as FRI and requests that can tolerate delay (Bulk Data Traffic), denoted as BDT. Each FRI request is represented as f (s, d, t_a, n_{rfs}), where s is the source node index, d is the index of the destination node, t_a is the time point in which the request arrives in the network, and n_{rfs} is the number of required frequency slices. The service duration is not known in advance and the allocated bandwidth is released when the service is terminated. The BDT requests are denoted as b (s, d, t_s, t_e, n_{rb}), where s is the source node index, d is the index of the destination node, t_s is the arrival time of the request, t_e is the latest time moment in which the request can be accepted in the network and n_{rb} is the number of required resource blocks. The maximum tolerable delay after which the request is blocked is denoted as $t_e - t_s$. The duration of the BDT requests is specified in advance.

3. 2 Simulation Scenario

A custom-made, MATLAB simulation tool is used for the analysis, evaluation and validation of the proposed algorithm. In particular, each network node is connected with the SDN controller that controls and optimizes the spectrum allocation. It is assumed that the SDN controller has all the information about the network state (bandwidth usage and duration of the established connections). For the purposes of the simulation, the topology of the National Science Foundation Network (NSFNET), with 14 nodes and 22 bidirectional links [19], has been used. The NSFNET topology is shown in Figure 1.

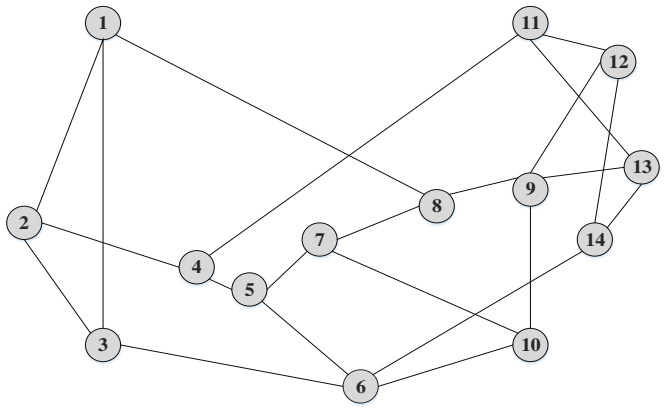

Figure 1
NSFNET topology

Each optical fiber has a capacity C=2.5 THz corresponding to N_{fs}=200 frequency slices with a bandwidth of 12.5 GHz (for M=1). In time domain, it is assumed that the duration of one TS is T=0.01s [1].

All traffic demands are generated from uniformly distributed sources and are addressed to uniformly distributed destinations. The arrival time of traffic demands is generated using the Poisson model with a mean duration of 100 T. The number of frequency slices required by the FRI traffic demands is uniformly distributed in the range from 1 to 17. The FRI traffic load is fixed at 60 E (Erlang). The number of resource blocks in the time-frequency domain and the maximum tolerable delay in number of time slots are uniformly distributed within [100, 600] and [400, 700] intervals, respectively. The simulations are repeatedly executed for five values of the BDT traffic load (50, 75, 100, 125 and 150 E).

The average duration of FRI connections, as well as the average number of frequency slots assigned to the FRI connections, are calculated based on 100 served FRI demands. In all simulations, the following performance metrics are analyzed: average latency for BDT traffic, blocking probability for both traffic types, network utilization and network efficiency.

4 Routing and Spectrum Allocation Algorithm with Support for QoS

4.1 Symbols Used

The symbols used in the algorithm described below are summarized in Table 1.

Table 1
Used symbols

Symbol	Description
s	Source node index
d	Destination node index
K	Number of shortest paths between s and d
C	Optical fiber capacity
M	Modulation level
N_j	Number of nodes in the network
N_l	Number of bidirectional links in the network
N_{fs}	Number of frequency slices
T	Duration of one time slot (in seconds)
n_t	Number of simulated time slots
t_a	Arrival moment of the FRI request
n_{rfs}	Number of required frequency slices by the FRI request
n_{ts}	Number of required time slots by the FRI request
t_s	Arrival moment of the BDT request
t_e	Latest time moment in which the BDT request can be accepted in the network
n_{rb}	Number of required resource blocks by the *BDT* request
q_{time}	Control coefficient $0 \leq q_{time} \leq 1$
$T_{F,i}$	Duration of the i^{th} FRI connection
N_F	Number of FRI connections that are taken into account in the calculation of the average duration of the served FRI connections and the average number of frequency slots assigned to the served FRI connections
R_{avt}	Average duration of the FRI connections
R_t	Maximum number of time slots that can be assigned to a BDT request
q_{freq}	Control coefficient $0 \leq q_{freq} \leq 1$
$L_{F,i}$	Number of frequency slices assigned to the i^{th} FRI connection
R_{avf}	Average number of frequency slices assigned to the FRI connections
R_f	Maximum number of frequency slices that can be assigned to a BDT request

$t_{backoff}$	Backoff interval
numBlockFri	Number of blocked FRI requests
numBlockBdt	Number of blocked BDT requests

4.2 RSA Algorithm Description

Requests arriving in the network are represented by the set *D* defined with the Equation (3), which is a union of the *FRI* requests *F* (Equation (1)) set and the set of *BDT* requests *B* (Equation (2)). Each request is actually a connection between a pair of nodes in the network.

$$F = \bigcup_{\substack{s,d \in J \\ t_a \in \{1,2,\ \ldots,\ n_t\} \\ n_{rfs} \in Z^+}} f(s, d, t_a, n_{rfs}) \tag{1}$$

$$B = \bigcup_{\substack{s,d \in J \\ t_s \in \{1,2,\ \ldots,\ n_t\} \\ n_{rb} \in Z^+}} b(s, d, t_s, t_e, n_{rb}) \tag{2}$$

$$D = F \cup B \tag{3}$$

During the initialization of the simulation controlling process, all the parameters obtain values and the process goes to the state WAIT expecting to arrive either a FRI or a BDT request. If a FRI request arrives, the process goes to the SERVE_FRI state, and if a BDT request arrives, the process goes to the SERVE_BDT state, as is shown in Figure 2.

All requests that arrive in the network are placed in a queue, which is represented by a matrix. Matrix rows are sorted according to time slots (e.g. TS_1, TS_2, ..., TS_{nt}) in which the requests are arriving. Same type request that arrive in a time slot are recorded one after another in the matrix. If multiple requests, that belong to different categories arrive within the same timeslot, the FRI requests are served before the BDT requests.

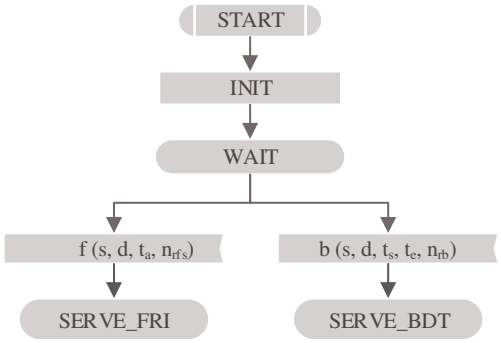

Figure 2
Formal description of the controlling process (initial transition)

The considered network has 22 bidirectional links and each link is composed of a pair of optical fibers. Further, each optical fiber (44 optical fibers) is represented by a $N_{fs} \times n_t$ matrix. The columns represent the frequency slices of the optical fiber spectrum, and the rows are representing the time slots in which the frequency slices are used. The set of links can be represented as a 3D matrix of dimensions $N_{fs} \times n_t \times 2N_l$.

For each pair (s, d), there are K shortest paths that can be calculated using an algorithm for finding the K shortest paths between pairs of nodes [20]. The path between any pair of nodes can be represented as a 3D matrix, where the planes are actually 2D matrices that represent the constitutive links on the path represented by the 3D matrix. If the traffic request is represented as a rectangle, then the spectrum allocation comes down to simple search for free space in this 3D matrix in which this rectangle can be accommodated. Contiguity and continuity constraints must be met in order to serve traffic requests in an elastic optical network. This means that the request can be served only if the rectangle can be placed at the same position in all planes of the matrix representing the path between the source and the destination.

The sequence after the SERVE_FRI state symbol describes the algorithm operation while serving the priority real time traffic (category 1). This is shown in Figure 3, using a flowchart.

For each FRI request, the set P containing K shortest paths from the source s to the destination d is found using [20]. In Equation (4), P denotes the set of paths corresponding to one request f (s, d, t_a, n_{rfs}), and p_{sd} denotes the k^{th} path from the source s to the destination d, $1 \leq k \leq K$.

$$P = \bigcup_{(s,d) \in J^2} p_{sd} \tag{4}$$

In order to serve the request, the controller is searching for free resources among the first path (k=1), i.e. the controller is searching for free frequency slots blocks (B_l={f_{ij} | f_{ij} = [f_i, f_j], $n_{rfs} \leq f_j - f_i$}). Next, the controller checks whether there are available resources along the path that correspond to the request. The first n_{rfs} frequency slots are then assigned to the connection.

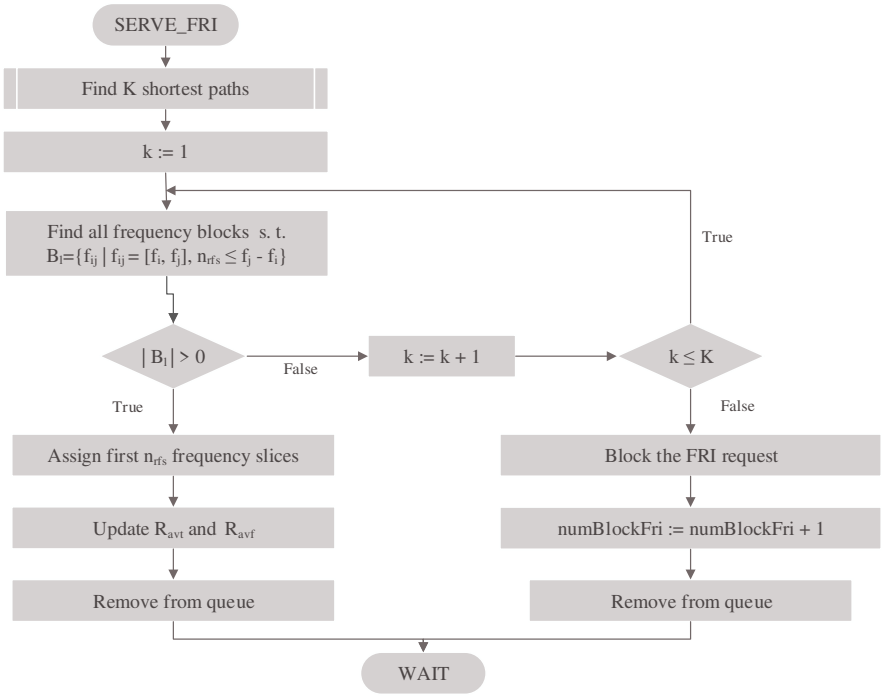

Figure 3

A flowchart that describes the operation of the algorithm, while serving a priority traffic request

Once the FRI request is served, the SDN controller makes a record about the amount of network resources allocated to this request. The average number of frequency slices assigned to the FRI connections (R_{avf}) is calculated using Equation (5). The average number of frequency slots assigned to the FRI connections is calculated after each served FRI request and it is referring to the last N_F served requests.

$$R_{avf} = \frac{1}{N_F} \sum_{i=1}^{N_F} L_{F,i} \tag{5}$$

The average duration of the FRI connections (R_{avt}) is calculated using the Equation (6). The average duration of the FRI connections is calculated after each served FRI request and it is referring to the latest N_F requirements.

$$R_{avt} = \frac{1}{N_F} \sum_{i=1}^{N_F} T_{F,i} \tag{6}$$

Once the R_{avf} and R_{avt} values are updated, this request is removed from the queue and the process goes to the *WAIT* state where it is waiting for the next request.

If free resources cannot be found along the first path, then the same check is made for the next path. This procedure is repeated as long as $k \leq K$ or until appropriate block of free resources is found. If the controller could not find a block of available resources along all K paths that belong to the set P for the request to be served, a record is made that this request is blocked, the number of blocked *FRI* requests is increased by one, this request is removed from the queue and the process goes to the state *WAIT* where it is waiting for a new request to arrive.

The sequence after the *SERVE_BDT* state symbol describes the algorithm behavior while serving big data traffic request (category 2). This is illustrated using flowchart in Figure 4.

Similar to the serving of FLRs algorithm, for each BDT request described as b (s, d, t_s, t_e, n_{rb}), the K shortest paths are calculated using [20].

Only a fixed part of the available network resources is allocated to the BDT requests in regards to the priority category 1 by the SDN controller. The maximum number of frequency slices that can be assigned to a BDT request (R_f) is part of the average number of frequency slices assigned to the served FRI connections (R_{avf}). The size of this part depends on the coefficient q_{freq}. Similarly, the number of time slots that can be occupied by a BDT request (R_t) is part of the average duration of the served FRI connections (R_{avt}) and the size of this part depends on the coefficient q_{time}. When a BDT request arrives in the network, the SDN controller calculates R_f and R_t using Equations (7) and (8).

$$R_f = \lceil q_{freq} \times R_{avf} \rceil \tag{7}$$

$$R_t = \lceil q_{time} \times R_{avt} \rceil \tag{8}$$

The BDT request will be blocked if, and only if, it arrives after the maximum tolerable delay ($t_s \geq t_e$). Then, the controlling process makes a record that this request was blocked, the number of blocked BDT requests is increased by one, the request is removed from the queue, and the process goes to a *WAIT* state, waiting a new request to arrive at the network, as can be seen in Figure 4.

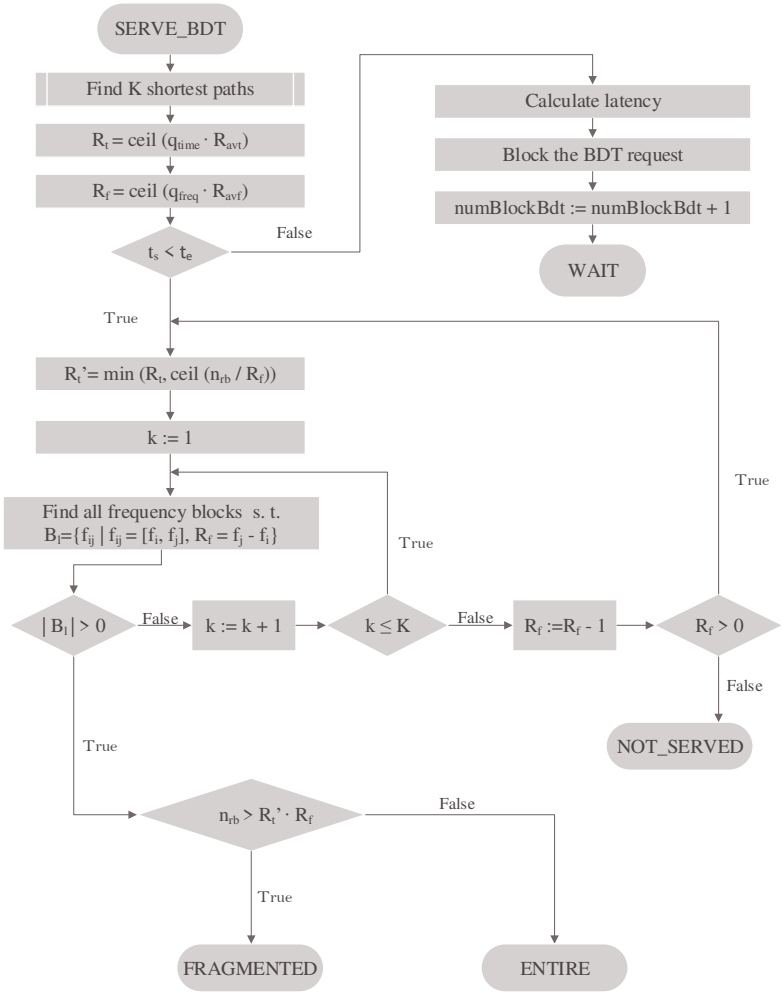

Figure 4

A flowchart that describes the operation of the algorithm, while serving a big data traffic

The network controller tries to assign a maximum possible number of frequency slices to the BDT request that requires n_{rb} resource blocks. If less than R_t time slots are needed for serving n_{rb} resource blocks using R_f frequency slices, a lower and appropriate time is assigned to the request. The number of time slots that will be assigned to the BDT request (R'_t) is calculated using Equation (9).

$$R_t^{'} = min(R_t, \left\lceil \frac{n_{rb}}{R_f} \right\rceil) \tag{9}$$

In order the request to be served, the controller is searching for free resources along the first path (k=1), i.e. the controller is searching for free frequency slots blocks (B_l={f_{ij} | f_{ij} = [f_i, f_j], $n_{rfs} \leq f_j - f_i$}). Next, the controller is checking whether there are available resources along the path that correspond to the request. This is repeated until R_f >0. If a block of free frequency slices is found (| B_l | = 0), the controller checks if R_f frequency slices and R'_t time slots are enough for the request to be served entirely. If $n_{rb} > R_t' \cdot R_f$, then the process goes to the state *FRAGMENTED*, otherwise the process goes in the state *ENTIRE*. If $R_f = 0$ and there is no suitable block of free frequency slots that can be used for serving the request, the process goes to the state *NOT_SERVED*.

The frequency slices with smallest indices are always assigned to the connection. If in the first path, there is no appropriate block of frequency slices for the request to be served (| B_l | = 0), the same search is repeated for the next path. This procedure is repeated as long as $k \leq K$. Finally, if all K paths from the set P are searched and no appropriate resources are found, the controller is trying to serve the request with a smaller number of frequency slices. Namely, the value of R_f is decreased by one. For the new value of R_f, a new value for R'_t is calculated and again all K paths are searched for suitable block of frequency slices (corresponding to the new values of R_f and R'_t).

If the process is in the state *FRAGMENTED*, the number of resource blocks that can be assigned to the request is lower than the number of resource blocks it requires. In that case, the request will be partially served as it is depicted in Figure 5 (a). If a BDT request is served partially, it is transformed into a new request and its arriving moment will change according to Equation (10).

$$t_s \leftarrow t_s + R_t^{'} + t_{backoff} \tag{10}$$

Also, the number of resource blocks it requires will be updated according to the Equation (11). The number of required RBs will be equal to the initial number of required RBs minus the number of served RBs. The number of served RBs is equal to the product of time spent for serving the block and the number of frequency slots assigned to the *BDT* request. After that, the process goes in the state *WAIT* where it is waiting for a new request to arrive in the network.

$$n_{rb} \leftarrow n_{rb} - (R_t^{'} \cdot R_f) \tag{11}$$

When all the fragments of one request are handled, it is considered to be served.

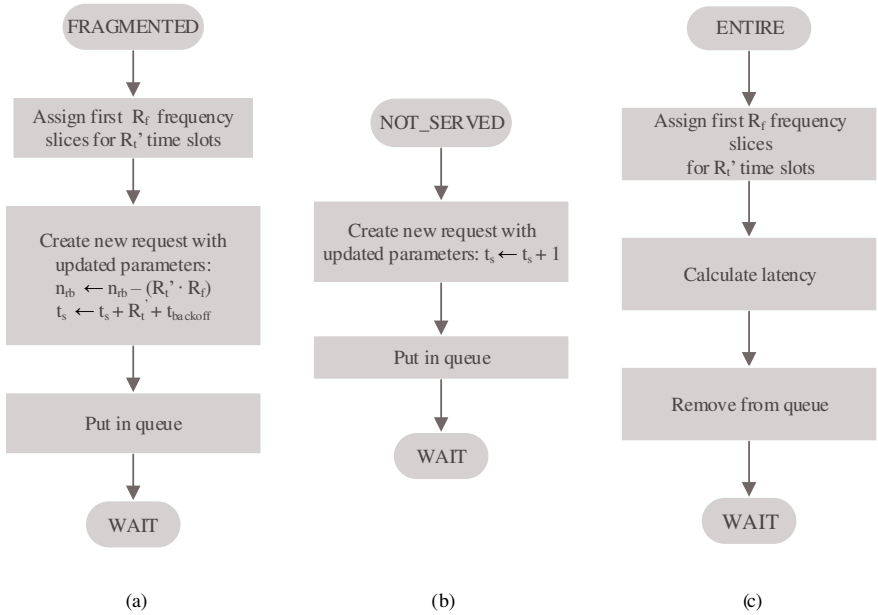

Figure 5

A flowchart that describes the operation of the algorithm while serving a big data traffic (a) BDT request is served partially (b) there are no available free resources for the BDT request to be served (c) BDT request is served entirely

If the controller cannot find free resources for the BDT request among all k paths for all possible values of R_f, the BDT request is not blocked but it is put back in the queue with new arrival moment:

$$t_s = t_s + t_{backoff} \tag{12}$$

Once the request arrival time is updated, the process returns to the state *WAIT* where it waits for a new request to arrive in the network as shown in Figure 5 (b).

If the number of resource blocks that may be assigned to the BDT is greater than or equal to the number of resource blocks it requires, an attempt is made for serving the request without fragmentation, as shown in Figure 5 (c). In this case, R_f frequency slices are assigned to the request for R_t time slots and the latency is calculated. If this request is created as part of any previous request that could not be fully served, the latency is calculated starting from the moment when the initial request arrived in the network. Once the request is served, it can be removed from the queue and the process goes back to the state *WAIT*, where it waits for a new request to arrive in the network.

5 Results and Discussion

In this section, the simulation results are presented for the purpose of analysis, evaluation and validation of scheduling scheme for spectrum assignment in elastic optical networks. For simplicity, we use k=1.

Figure 6 shows the average latency of the BDT traffic as a function of q_{freq}. It is obvious that latency decreases for greater values of the parameter q_{freq}. As mentioned, a greater value of q_{freq} allows for larger portion of the spectrum resources to be available for serving BDT requests. Thus, BDT requests are served with less fragmentation that directly reduces the latency. In other words, if q_{freq} has a small value, the request needs to be fragmented several times into smaller blocks, before it can be served, resulting in greater latency or, in the extreme, breach the maximum tolerable delay. According to Figure 6, as the BDT load increases the latency becomes slightly higher. Obviously, heavy BDT loads congest the network and there are less free resources, but the average BDT latency is not affected significantly.

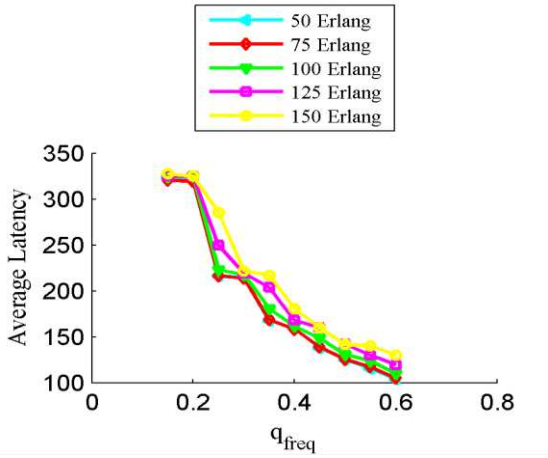

Figure 6
Average latency (in TS) as a function of q_{freq} for different BDT traffic loads

Figure 7 plots the FRI blocking probability versus q_{freq} for different BDT traffic loads. As can be seen, higher data traffic load causes higher blocking probability for FRIs. On one hand, network operators want higher network utilization, while aiming smaller blocking probability for the critical services. Clearly, a tradeoff must be considered by the carriers. Figure 7 further shows that the blocking probability of FRIs can be slightly controlled by the change of design parameter q_{freq}. The change of q_{freq} has not such influence over the FRI blocking probability, compared to the BDT load influence.

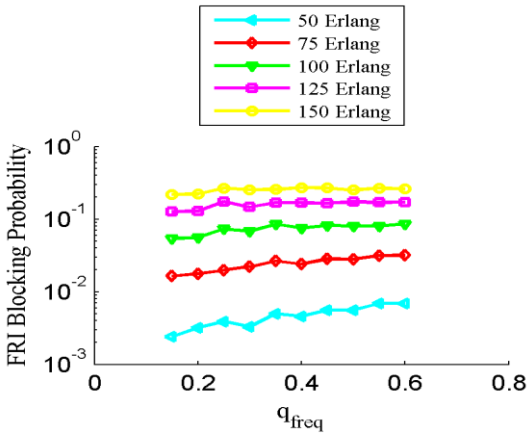

Figure 7

FRI blocking probability as a function of q_{freq} for different BDT traffic loads

BDT requests tend to reserve spectrum resources in advance. Therefore, the current resources available for FRI requests are wasted. This behavior leads to higher blocking probability for FRIs compared with BDT, as can be seen from Figures 7 and 8. In Figure 8 the BDT blocking probability is plotted as a function of q_{freq}. The blocking probability decreases as the value of q_{freq} increases. When q_{freq} is larger, there are more resources available for the arriving BDT requests, and thus the probability that the request will not be served before the maximum tolerable delay expires, becomes low.

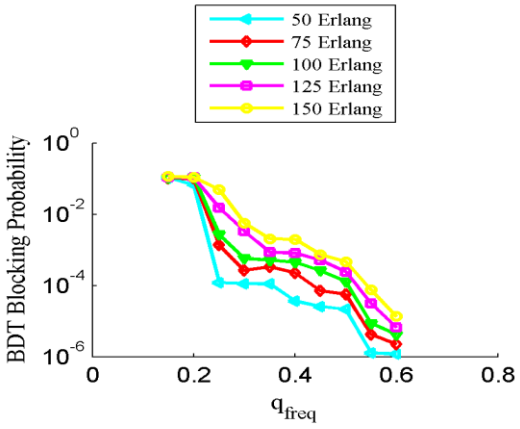

Figure 8

BDT blocking probability as a function of q_{freq} for different BDT traffic loads

Figure 9 shows the effect of the coefficient q_{freq} and the BDT traffic load on the network utilization defined as a percentage of the time-frequency slots that are successfully used for caring traffic (FRI or BDT). It can be seen that the average network utilization does not change with respect to the coefficient q_{freq}, while it is significantly influenced by the volume of the BDT traffic. The results reveal higher network utilization, for the case of higher BDT traffic loads. Thus, it can be concluded that for fixed FRI traffic loads, adding more BDT traffic will cause increased network utilization.

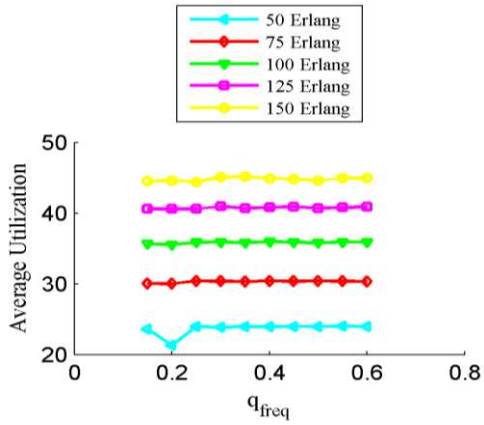

Figure 9

Average network utilization (in %) as a function of q_{freq} for different BDT traffic loads

Based on these results, we can summarize that this paper enhances the previous research, by proposing an improved RSA method for parallel handling of data traffic in EON, as well as, investigating the average network latency and utilization in case of multiple traffic categories. These findings are important for efficient coexistence of different classes of services. The obtained results have direct practical relevance. Namely, a network operator can improve the overall network conditions choosing appropriate values for the controlling coefficients, as well as, data traffic loads.

Conclusions

RSA is one of the most intriguing research topics in the field of flexible optical networks. Designing an algorithm that efficiently deals with the traffic requests in an EON, can significantly improve the performance of the network. This is particularly challenging in the case of a network, in which, different categories of traffic coexist.

This paper presents a simulation tool, along with a formal description of the controlling algorithm, in SDN-based EON. In this work new performance metrics are introduced and the impact of the controlling algorithm's coefficients on the network conditions is analyzed. In the simulations, we highlighted the coefficient

that determines the portion of the frequency slots that can be assigned to BDT requests. From the obtained results, it can be concluded that this coefficient significantly impacts the BDT blocking probability and BDT latency, while it has small influence over the FRI blocking probability and network utilization. This proves that through q_{freq} the network operator can actively control the BDT performance, with a possibility to introduce different sub-classes of service.

Conversely, the results revealed that the BDT traffic load has a significant impact over the blocking probability (for both FRI and BDT requests), and it is a crucial parameter to control the overall network utilization.

Further research of this issue will target different RSA algorithms, in order to find more efficient spectrum management schemes, which can reduce the blocking probability and improve the network capacity utilization. The future work will involve optimization of the controlling coefficients calculation, as well as, analysis of the influence of the suggested algorithm on the network fragmentation. Clearly, more study is needed to find an appropriate approach for reducing the FRI traffic degradation at high intensity of BDT traffic. One possible solution may be to consider a smaller number of possible paths while serving the BDT traffic. This raises the question of how many paths must be considered while searching for free resources for the first and second traffic category, as well as, how the decision will be made for which of the *K*-shortest paths will be considered and why.

References

[1] S. Shahsavari, H. Beyranvand, and J. A. Salehi, "Multi-quality of service routing and spectrum assignment in elastic optical networks", IEEE ICC Optical Networks and Systems Symposium, pp. 1-6, Paris, France, May 2017

[2] Y. Xiong, Y. Li, X. Dong, Y. Gao, and G. N. Rouskas, "Exploiting SDN principles for extremely fast restoration in elastic optical datacenter networks", IEEE Global Communications Conference, Washington, DC, USA, February 2017

[3] Y. Xiong, Y. Li, B. Zhou, R. Wang, and G. N. Rouskas, "SDN enabled restoration with triggered precomputation in elastic optical inter-datacenter networks", J. Opt. Commun. Netw., Vol. 14, No. 1, pp. 24-34, January 2018

[4] D. Amar, E. Le Rouzic, N. Brochier, and C. Lepers, "Class-of-service-based multilayer architecture for traffic restoration in elastic optical networks", J. Opt. Commun. Netw., Vol. 8, No. 7, pp. 34-44, July 2016

[5] H. Xuan, Y. Wang, Sh. Guan, and Z. Xu, "A new optimization model and algorithm for a network scheduling problem in inter-datacenters elastic optical networks", International Conference on Computational Intelligence and Security, Hong Kong, December 2017

[6] W. Fang, M. Zeng, X. Liu, W. Lu, and Z. Zhu, "Joint spectrum and it resource allocation for efficient vnf service chaining in inter-datacenter elastic optical networks," IEEE Communications Letters, Vol. 20, No. 8, pp. 1539-1542, 2016

[7] A. V. S. Xavier, R. C. Almeida Jr., J. F. Martins-Filho, D. A. R. Chaves, and C. J. A. Bastos-Filho, "Spectrum contiguity and continuity based dedicated protection for flexible optical networks", Journal of Microwaves, Optoelectronics and Electromagnetic Applications, Vol. 16, No. 2, pp. 481-493, June 2016

[8] L. Velasco, M. Ruiz, K. Christodoulopoulos, M. Varvarigos, M. Żotkiewicz, and M. Pióro, "Routing and spectrum allocation", in Elastic optical networks: architectures, technologies, and control, Springer, Switzerland, pp. 55-80, 2016

[9] B. C. Chatterjee, N. Sarma, and E. Oki, "Routing and spectrum allocation in elastic optical networks: A tutorial", IEEE Communication Surveys and Tutorials, Vol. 17, No. 3, pp. 1776-1799, 2015

[10] R. Goéscié, K. Walkowiak, and M. Klinkowski, "On the complexity of routing and spectrum allocation in survivable elastic optical network with unicast and anycast traffic", 8th International Workshop on Resilient Networks Design and Modeling, pp. 166-173, Halmstad, Sweden, September 2016

[11] P. Afsharlar, A. Deylamsalehi, J. M. Plante, J. Zhao, and V. M. Vokkarane, "Routing and spectrum assignment with delayed allocation in elastic optical networks", J. Opt. Commun. Netw., Vol. 9, No. 3, pp. 101-111, March 2017

[12] J. Wu, M. Xu, S. Subramaniam, H. Hasegawa, "Routing, fiber, band, and spectrum assignment (RFBSA) for multi-granular elastic optical networks", IEEE ICC 2017 Optical Networks and Systems Symposium, Paris, France, May 2017

[13] W. Jia, Z. Xu, Z. Ding, and K. Wang, "Routing and spectrum assignment algorithm with prediction for elastic optical networks under self-similar traffic", 15th International Conference on Optical Communications and Networks, pp. 1-3, Hangzhou, China, September 2016

[14] C. L. Triveni, P. C. Srikanth, and T. Srinivas, "An optimized routing algorithm for elastic optical network", International Conference on Electrical, Electronics, and Optimization Techniques, pp. 3873-3878, Chennai, India, March 2016

[15] M. Klinkowski1 and K. Walkowiak, "A heuristic algorithm for routing, spectrum, transceiver and regeneration allocation problem in elastic optical networks", 18th International Conference on Transparent Optical Networks, pp. 1-4, Trento, Italy, July 2016

[16] Q. P. Van et al., "Virtualized routing and frequency allocation functions in elastic optical networks", 42nd European Conference and Exhibition on Optical Communications, pp. 1-3, Dusseldorf, Germany, September 2016

[17] H. Zheng and H. T. Mouftah, "Supporting advance reservations in wavelength-routed WDM networks," in IEEE Int. Conf. on Computer Communications and Networks, pp. 594-597, October 2001

[18] S. Sugihara, Y. Hirota, S. Fujii, H. Tode, and T. Watanabe, "Dynamic resource allocation for immediate and advance reservation in space-division-multiplexing-based elastic optical networks", J. Opt. Commun. Netw., Vol. 9, No. 3, pp. 183-197, March 2017

[19] National Science Foundation, "A partnership for high - speed networking: final report 1987-1995," pp. 20-39, Available: https://web.archive.org/web/20170202190225/http://nsfnet-legacy.org/about.php

[20] J. Y. Yen, "Finding the k shortest loopless paths in a network," Management Science, Vol. 17, No. 11, pp. 712-716, 1971

Stability of Nonlinear Descriptor Systems and Applications to Stabilization of Quadcopters

Drilon Bunjaku[1], Jovan D. Stefanovski[2], Georgi Dimirovski[3]

[1]Faculty of Electrical and Computer Engineering at University of Prishtina, Kodra e Diellit p.n., 10000 Prishtina, Republic of Kosovo, drilon.bunjaku@uni-pr.edu

[2]Control & Informatics Div. JP "Strezevo", Boulevard 1st of May b. b., 7000 Bitola, R. N. Macedonia, jovanstef@t.mk

[3]Dogus University Acibadem-Kadikoy, 34722 Istanbul, Republic of Turkey, gdimirovski@dogus.edu.tr

Abstract: In this paper, new sufficient Lyapunov-like stability conditions and new Lyapunov-like, stabilizability conditions for nonlinear descriptor systems, with control, are presented along with their applications to quadcopter's flight stabilization. Most of these results are rather practical because they do not need solving nonlinear differential equations and nonlinear algebraic equations. Thus, the usage of these new results requires only the differentiation of functions. The numerical simulation results prove that the stabilization of the quadcopter is improved, in comparison with pure tracking control.

Keywords: Nonlinear descriptor system; Lyapunov-like stability; Nonlinear hybrid control; Quadcopter stabilization

1 Introduction

Considerable new developments appeared over the last couple of decades, within the literature, on various hybrid dynamical systems [1], [2]. Certain segments of these developments are called differential-algebraic systems while others hybrid systems, one subclass of which obeys switching law in terms of algebraic part hence known as switched systems, while another subclass is referred to as nonlinear descriptor systems and is of main concern in this study. Nonetheless, the word is about an equivalent case of nonlinear dynamical continuous-time systems to linear descriptor systems. These can be best envisaged by the original system created in 1951 by A. I. Lurye [3] at the Control Science Institute of Academy of Sciences in Moscow. Namely, Lurye's nonlinear systems had a feedback architecture with one static sector nonlinearity and a linear dynamic component, classical one, which could be conceptualized as descriptor, linear as in Figure 1.

The herein considered, nonlinear descriptor systems can be readily envisaged as a generalization of Lurye by assuming the linear part is described by descriptor state-variable and output equation as depicted in Fig. 1. Obviously, this figure highlights the underlying control physics of nonlinear descriptor systems. Feedback systems having such an architecture became known as Lurye-type of systems (also called nonlinear control systems with separable nonlinearity) while their stability as the Lurye stability problem. Ultimately LaSalle and Lefschetz solved it in [4], by proving that Lurye's candidate Lyapunov function was indeed a proper Lyapunov function, for his class of nonlinear systems [3]. Many years later, in 2000, the essential fundamental result on the stability of multivariable Lurye systems [5] appeared.

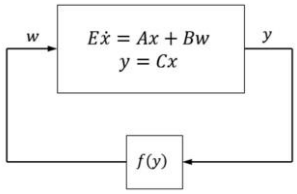

Figure 1
Lurye-type of nonlinear descriptor systems

To date, the most thorough recent study for Lurye-type subclass of nonlinear descriptor systems was contributed by M. Ikeda and collaborators of Graduate Scholl of Engineering his at Osaka University; see [6]-[8] and references therein. In 2004, they have derived absolute stability criteria for Lurye systems with asymmetric nonlinearities [6], and in 2006 they published stability theory for descriptor system with non-smooth nonlinearities [7]. Furthermore, in 2008, they solved the absolute stability problem for multivariable Lurye-type descriptor systems [8]. Thus, we consider, nowadays, the concept of nonlinear descriptor systems is well established and their mathematical description generalized to differential-algebraic equations like (1) and (2) presented below.

In the sequel, the following combined differential and algebraic equations define the descriptor nonlinear systems of interest in this study. Consider the system of differential and algebraic equations (descriptor system)

$$\dot{x}_1(t) = \boldsymbol{f}(x_1(t), x_2(t)), \tag{1}$$

$$0 = \boldsymbol{h}(\mathrm{x}_1(\mathrm{t}), \mathrm{x}_2(\mathrm{t})), \tag{2}$$

where $x_1 = x_1(t) \in \mathbf{N}_1 \subseteq \mathbf{R}^{n_1}$, $x_2 = x_2(t) \in \mathbf{N}_2 \subseteq \mathbf{R}^{n_2}$.

Let denote $x = x(t) := \left[x_1(t)\ x_2(t)\right]^T \in \mathbf{N} = \mathbf{N}_1 \times \mathbf{N}_2 \subseteq \mathbf{R}^n$, $n = n_1 + n_2$. Let denote by $\left[x_{10}\ x_{20}\right]^T = x_0$ the initial condition for the descriptor system (1) and (2).

The function $\boldsymbol{f}(x_1, x_2)$ and $\boldsymbol{h}(x_1, x_2)$ are assumed to have partial derivatives of all orders in $\mathbf{N}$. Even though, the existence of all partial derivatives is not needed in all of our results.

The set $\mathbf{N}$ must be invariant with respect to the dynamics (1) and (2), i.e. once $x_0 \in \mathbf{N}$ we must have $x(t) \in \mathbf{N}$ for all $t > 0$. The importance of the sets $\mathbf{N}$ is illustrated in Example 3. Obtaining the set $\mathbf{N}$ is not easy if there is no physical interpretation of the mathematical model (1) and (2). In that case, estimation mathematical techniques could be applied, as in Example 4 of [4] (pages 68-70).

Assumption 1: $\boldsymbol{f}(0,0) = 0$ and $\boldsymbol{h}(0,0) = 0$

Notice that this assumption is a natural consequence of the fundamental laws of physics.

The systems of the form (1) and (2) became of considerable current interest nowadays; see [2] and references therein. Nonetheless, there are three reasons at least why we consider such systems:

i. If the system includes both linearities and nonlinearities, then it is convenient if we can separate the nonlinearities into algebraic equations of the type $\boldsymbol{h}(x_1, x_2) = 0$. (Obviously, then $\boldsymbol{f}(x_1, x_2)$ is a linear dependence of the form $\boldsymbol{f}(x_1, x_2) = A_1 x_1 + A_2 x_2$ for some constant matrices A_1 and A_2). For example, in electrical circuits containing nonlinear elements (for instance, diodes) the nonlinear block $\boldsymbol{h}(x) = 0$ can be chosen so that it contains the nonlinear elements only.

ii. In many systems, a passive [9] or made passive by feedback [10]-[12] (usually referred to as 'passified'), or else conservative [13] some part could appear separated.

    It is important to mention works [14], [15] and later [16] which marked the beginning of studies in dissipative and passive dynamical systems (the linear ones, in particular), as well as, passivity-oriented reliable control developments.

iii. The holonomic constraints in mechatronic systems are modelled by the algebraic constraints of the type (2) (see [17]). As we shall show in Section 3.1 the descriptor system (1) and (2) is a natural model for the typical quadcopter construction.

In order to motivate our concept, we discuss here the drawbacks of the two well-accepted concepts for stabilization of affine-in-control nonlinear systems that are given by:

$$\dot{x} = \boldsymbol{f}(x) + \boldsymbol{G}(x)u\ ,\ x \in \mathbf{R}^n,\ \ u \in \mathbf{R}^m\ , \tag{3}$$

$$y = h(x) + E(x)u\ , \quad y \in \mathbf{R}^m\ , \tag{4}$$

where u is the control variable and y is the output variable. Namely, these are the concept of feedback passivization [12], [19], [37] (see Section 2.4 in [37]) and the concept of control Lyapunov functions (see Section 3.2 in [37]). The first concept requires the existence of a function $\boldsymbol{v}(x)$ such that:

$$\frac{\partial \boldsymbol{v}(x)}{\partial x}\boldsymbol{g}_i(x) = \boldsymbol{h}_i(x)\ , \quad i = 1, 2, \ldots, m\ , \tag{5}$$

where $[\boldsymbol{g}_1, \boldsymbol{g}_2, \ldots, \boldsymbol{g}_m] := \boldsymbol{G}$ and $[\boldsymbol{h}_1, \boldsymbol{h}_2, \ldots, \boldsymbol{h}_m]^{\mathrm{T}} := \boldsymbol{h}$. In the case of vector control $(m > 1)$, the system of partial differential equations (5) has no solution in the generic case of controllable system. (Also see the Comment (3) on page 1225 in [13]). Therefore, the concept of feedback passivization does not use the controllability property in a positive way.

In the concept of control Lyapunov functions, one has to find a so-called control Lyapunov function $\mathbf{v}(x)$ such that the following implication relationships hold:

$$\frac{\partial \boldsymbol{v}(x)}{\partial x}\boldsymbol{g}_i(x) = 0\ , \ i = 1, 2, \ldots, m \ \Rightarrow \ \frac{\partial \boldsymbol{v}(x)}{\partial x}\boldsymbol{f}(x) = 0\ . \tag{6}$$

Apart of the fact that it is more involved to find a control Lyapunov function than to find a Lyapunov function, in order to check the validity of implication (6), the system on the left in (6) has to be solved in $\boldsymbol{v}$. However, analogous to the case of system (5), this system too has no solution in the generic case.

The contributions of this paper are:

Theorem 1, which is one of the main results of this paper, can be regarded as a generalization of the second part of the Corollary 1 in [18] (i.e., going from linear descriptor systems to nonlinear descriptor systems). Theorem 2, which is also one of the main results in here, does generalize Theorem 4 in [18] (i.e., going from controlled systems to controlled descriptor systems). Also, the four corollaries in this paper guarantee stability and stabilizability as these Theorems 1 and 2 do, respectively. But our conditions, which are based on differentiation of functions, actually do represent observability and controllability; besides, they are more useful in practical applications. In particular, Corollary 4 uses the controllability rather in a positive way.

Theorem 2, is advanced, in this the paper, by its application to the quadcopter flight stabilization problem. In particular:

i. We consider a positive semidefinite Lyapunov-like function, instead of positive definite one, for the reason that the moving of quadcopter in the horizontal direction, in general, requires that at least one of the coordinates does not approach zero when $t \to \infty$. Precisely, if we denote by $x(t)$ the

position of the quadcopter in the moving direction, then we require $x(t)$ to be a ramp signal (then the corresponding velocity is nonzero), instead of $x(t) \to \infty$ when $t \to \infty$. In addition, the motion is possible only if $\theta \neq 0$ or $\phi \neq 0$, where θ and ϕ are quad rotor angles (attitude angles). Therefore, the coordinate x, as well as the attitude coordinates, are not allowed directly in the Lyapunov-like function.

ii. We consider a descriptor system model of the quadcopter for the reason that there is no analytic inversion of the algebraic dependency (see also Remark 1 and the algebraic dependences (27)).

In the applications-oriented research towards electrical power systems, the actual novel contribution is to the so-called coordinated passivation control of nonlinear systems. It was first introduced by work [19] and further extended in [20]-[25]. The works [21]-[25] have expended the ideas of dissipativity and passivity further to control designs for switched dynamical systems.

Quadcopters are known for their highly nonlinear motion dynamics and so nonlinear models are indispensable. A common practical procedure is to linearize the nonlinear quadcopter dynamic model around a hovering mode (the operating steady-state) since, due to its symmetric frame, the linear dynamic model becomes somewhat simplified, and therefore, it is easier to design linear controllers; see ([26-30], [39]). A drawback of such linearized model, however, is the operation in the immediate proximity of the linearizing state point (hovering mode) must be secured. Once the quadcopter is out of this proximity region, the system becomes uncontrollable using linear control strategies, hence, it is highly possible that quadcopter will crash. Often, quadcopters are called under-actuated physical systems, where the translational motion in $x-y$ plane are performed through the rotational motions θ, ϕ. Namely, the 6-DoF flying object could not be controlled with a single loop, and thus, a cascade control system is indispensable. In order to recover and keep vicinity of the aforementioned hovering mode, there are various control approaches developed under the cascade control concept, where the inner loop ought to be designed at least 5 times faster than the outer loop; see [27]-[30], [39].

In this paper, we elaborate a new approach with respect to: (a) representing a quadcopter model as the descriptor system, i.e. system with Differential-Algebraic Equations; (b) designing a nonlinear control. For, recently it was shown in [31] and [40], that the class of descriptor state-vector systems appears more advanced in describing the nature of physical systems than ordinary state-vector systems. It should be noted that, the descriptor system approach has been already applied successfully to aircraft control design [32] (see Example 7.2 in there).

Remarks on the notation. The scalars and vector are denoted by lower-case letters, while the matrices are denoted by upper-case letters. The functions of the

state variable x are denoted by bold-faced letters, and if it is not ambiguous, we omit the dependence on x frequently. If $\boldsymbol{v}$, is a scalar function, the notation $\frac{\partial \boldsymbol{v}}{\partial x}$ means $\left[\frac{\partial \boldsymbol{v}}{\partial x_1},...,\frac{\partial \boldsymbol{v}}{\partial x_n}\right]$ where $x_1,...,x_n$ are the entries of the vector-column x.

2 Main Results

In this section, the following assumption specifies the specific mathematical preliminaries that are required in this study.

2.1 On the Stability of Nonlinear Descriptor Systems

The following assumption specifies certain mathematical preliminaries that are needed in this study.

Assumption 2:

(I) The vector function $\boldsymbol{h}$ has n_2 entries, and the algebraic equation (2) defined in $\mathbf{N}$ is equivalent with the equation $x_2 = \gamma(x_1)$, for some vector function $\gamma(\cdot)$.

(II) The system given by (1) and (2) has unique finite solution $x(t)$ for all $t>0$ and all initial conditions $x(0) = x_0$.

Remark 1. (i) Assumption 2 (I) is a necessary condition for uniqueness of the solution of the descriptor system (1) and (2).

(ii) By replacement of the dependency $x_2 = \gamma(x_1)$ in the formula (1), we obtain a system of ordinary differential equations $\dot{x}_1 = f(x_1, \gamma(x_1))$, on which the standard existence and uniqueness results can be applied (for instance, Existence Theorem on page 23 in [4]). The reason why we consider the descriptor system, and not the ordinary system $\dot{x}_1 = f(x_1, \gamma(x_1))$ is that the explicit dependency $x_2 = \gamma(x_1)$ cannot be found in general.

(ii) Note that under Assumption 2, impulsive solutions at $t = 0$ of the descriptor system (1) and (2) cannot appear. Only finite jumps can appear at $t = 0$, if the initial conditions are not consistent [12].

Remark 2. Assumption 2 is not unrealistic. Indeed, sufficient conditions for Assumption 2 for nonlinear discrete-time descriptor system

$Ex_{k+1} = Ax_k + B\phi(k, x_k)$, where the pair (E, A) is regular and causal, are given by (2) and (8) in [41]. The condition (2) is a Lipschitz-type condition on ϕ, while the condition (8) guarantees, together with (2), the contractivity of a function, needed to apply the fixed-point theorem, instead of the implicit function theorem, used in some papers referenced in [41].

Remark 3. Assumption 2 is natural. Indeed, if the equations (1) and (2) model a real system, then if Assumption 2 is not satisfied, finite escape times can appear in the solution, which cannot appear in practice. In this case, we have to modify the model equations (1) and (2). However, the problem to establish that there are no finite escape times is not easy. It is connected with the problem of obtaining the set $\mathbf{N}$, for which we have already stated that it is not easy. (See Example 3 where we obtain the set $\mathbf{N}$ and checked the existence of finite escape times but, only for a very simple descriptor system.)

Finally, we could give our stability results without Assumption 2, like in Theorem VIII of seminal monograph [4], which restricts only on the bounded solutions for $0 \le t < \infty$. Another possibility is to restrict $\mathbf{N}$ to be a bounded set, like in Theorem VI of [4]. The third possibility is to consider the local asymptotic stability property, i.e. all points x_0 in a neighborhood of the origin satisfy $x(0) = x_0 \Rightarrow x(t) \to 0$ when $t \to \infty$.

An obvious consequence of Assumption 2 (I) is the following proposition.

Proposition 1: Matrix $\partial \boldsymbol{h} / \partial x_2$ is nonsingular in $\mathbf{N}$.

Theorem 1: Under Assumptions 1 and 2, if there exists a function $\boldsymbol{v}(x_1)$ such that

(i) $\boldsymbol{v}(x_1) \ge 0$ for all $x_1 \in \mathbf{N}_1$ and $\boldsymbol{v}(0) = 0$,

(ii) $\boldsymbol{\varphi}(x_1, x_2) := \dfrac{\partial \boldsymbol{v}}{\partial x_1} \boldsymbol{f}(x_1, x_2) = \dot{\boldsymbol{v}} \le 0$ for all $x \in \mathbf{N}$ satisfying (2),

(iii) The solution $x(t)$ of the descriptor system given by

$$\dot{x}_1 = \boldsymbol{f}(x_1, x_2), \ \boldsymbol{h}(x_1, x_2) = 0, \ \boldsymbol{\varphi}(x_1, x_2) = 0 \tag{7}$$

satisfies $x(\infty) = \lim_{t \to \infty} x(t) = 0$ for all initial conditions $x(0) = x_0$, then the solution $x(t)$ of the descriptor systems given by (1) and (2) satisfies $x(\infty) = \lim_{t \to \infty} x(t) = 0$ for all initial conditions $x(0) = x_0$.

Proof. For some $a \ge 0$, define the point set $\mathbf{E}_a = \{x \in \mathbf{N} : 0 \le \boldsymbol{v}(x_1) \le a\}$. Under the condition (i) and (ii), the set $\mathbf{E}_a$ is invariant with respect to dynamics (1) and (2). Indeed, since $0 \le \boldsymbol{v}(x_1(t)) \le \boldsymbol{v}(x_{10}) \le a$, we have $0 \le \boldsymbol{v}(x_1(t)) \le a$. Denote by $\mathbf{M}$

the point set $\mathbf{M} = \{x \in \mathbf{N} : \boldsymbol{\varphi}(x) = 0\}$. By virtue of Theorem VI in [4], all solutions $x(t)$, starting with $x(0) = x_0 \in \mathbf{N}$ must tend to the largest invariant set contained in $\mathbf{M}$.■

Remark 4. That the absence of finite escape time in Theorem 1 is really necessary, we can see by Example 1.1 in [33], i.e.

$$\dot{x} = -0.5(1+z)x^3 \ , \ \ \dot{y} = z \ , \ \ \dot{z} = -2az - a^2 y \ ,$$

for some real number $a > 0$. (The algebraic identities (2) are void.) The initial conditions are $x(0) = x_0$, $\mathrm{y}(0) = 1$ and $\mathrm{z}(0) = 0$. The analytical solution for $x(t)$ satisfies

$$x(t)^2 = x_0^2 \,/\, \{1 + x_0^2[t + (1+at)e^{-at} - 1]\} \ ,$$

therefore, if $x_0^2 > 1$, a finite escape time appears for sufficiently large a. (This kind of dynamic event is called peaking phenomenon in [33].)

On the other hand, the conditions (i), (ii) and (iii) of Theorem 1 are satisfied with

$\mathbf{v} = \begin{bmatrix} y & z \end{bmatrix} \begin{bmatrix} \frac{5}{4a} + \frac{a}{4} & \frac{1}{2a^2} \\ \frac{1}{2a^2} & \frac{1}{4a^3} + \frac{1}{4a} \end{bmatrix} \begin{bmatrix} y \\ z \end{bmatrix}$. Indeed, we have $\boldsymbol{v} > 0$, for all $\begin{bmatrix} y \ , \ z \end{bmatrix} \neq 0$,

and $\dot{\boldsymbol{v}} = -[y \ z] \begin{bmatrix} 1 & 0 \\ 0 & 1 \end{bmatrix} \begin{bmatrix} y \\ z \end{bmatrix} < 0$, for all $\begin{bmatrix} y \ , \ z \end{bmatrix} \neq 0$.

The condition $\dot{\boldsymbol{v}} = 0$ implies that $y = 0$, $z = 0$ and $\dot{x} = -0.5x^3$, whose solution $x(t) \to 0$ when $t \to \infty$.

Example 1. In work [34], the below stated result is proved as Theorem 1. Namely, consider the regular descriptor system

$$E\dot{x} = Ax, \tag{8}$$

and suppose there is a solution P of the following equations:

$$E^T P = P^T E \ , \tag{9}$$

$$A^T P + P^T A + C^T C = 0 \ , \tag{10}$$

for some matrix C. It is proved in [34], if the pair $(A - sE, C)$ is impulse observable and finite mode detectable, and if $E^T P = P^T E \geq 0$ holds, then the descriptor system (8) is asymptotically stable and impulse-free.

Let us now prove this Theorem 1 of [34] by means of our Theorem 1. For this purpose, consider $\boldsymbol{f}(x_1, x_2)$ and $\boldsymbol{h}(x_1, x_2)$ are represented by linear dependencies

$\boldsymbol{f}(x_1, x_2) = A_{11}x_1 + A_{12}x_2$ and $\boldsymbol{h}(x_1, x_2) = A_{21}x_1 + A_{22}x_2$, for some matrices A_{11}, A_{12}, A_{21} and A_{22}. Further, denote

$$E = \begin{bmatrix} I_{n_1} & 0 \\ 0 & 0 \end{bmatrix} \text{ and } A = \begin{bmatrix} A_{11} & A_{12} \\ A_{21} & A_{22} \end{bmatrix}.$$

The absence of impulses of the descriptor system (8) is equivalent to the non-singularity of matrix A_{22}; see article [35].

Next, take $\boldsymbol{v}(x_1) = x^T E^T P x \geq 0,$ where matrix P satisfies the equation (9) and (10) as well as the inequality $E^T P = P^T E \geq 0.$ Then $\boldsymbol{\varphi}(x) = -x^T C^T C x \leq 0,$ and thus the conditions (i) and (ii) of Theorem 1 hold. To prove that condition (iii) also holds, consider the descriptor system (8) extended by the condition $\boldsymbol{\varphi}(x) = 0,$ which appears equivalent to the equation $Cx = 0.$ Since the pair $(A - sE, C)$ is finite mode detectable, by Theorem 1 we have that $x(t) \to 0$ when $t \to \infty.$

Example 2. Take the following nonlinear autonomous system

$$\begin{aligned} &\dot{x} = -xy^2\,,\ \dot{y} = e^z + z - 1\,, \\ &e^z + z = y + 1\,, \end{aligned} \tag{11}$$

with the equilibrium point $(x, y, z) = (0, 0, 0).$ Take the function $\boldsymbol{v}(x) = 0.5x^2.$ We find $\dot{\boldsymbol{v}} = \boldsymbol{\varphi}(x, y) = -x^2 y^2.$ Therefore, the conditions (i) and (ii) of Theorem 1 are satisfied. However, the condition (iii) is not satisfied. Indeed, the equation of the autonomous system plus the equation $\boldsymbol{\varphi}(x, y) = -x^2 y^2 = 0$ admit a solution $x(t) = 0$ and $y(t) = e^t y_0,$ so $y(t) \to \infty$ when $t \to \infty.$

It is easy to check that the true solution of the autonomous system is

$$x(t) = e^{-0.5 y_0^2 (e^{2t} - 1)} x_0 \to 0 \ (t \to \infty)\,,$$

$$y(t) = e^t y_0 \to \infty \ \ (t \to \infty)\,,$$

and $z(t)$ is given by the implicit function (11).

Example 3. Consider the descriptor system given by

$$\dot{x} = -xz\,,\ \dot{y} = z - y\,, \tag{12}$$

$$z^2 - x = 0\,. \tag{13}$$

From the latter equation it follows that the consistent initial values $x(0)=x_0,\ y(0)=y_0$ and $z(0)=z_0$ have to satisfy $z_0^2-x_0=0,$ and that $x(t)\geq 0$ for all t. The equation (13) has two solutions $z=-\sqrt{x}$ and $z=\sqrt{x}$. If we take the former solution, by solving the differential equations (12), we obtain

$$x(t)=1/\left(0.5t+\left(z_0\right)^{-1}\right)^2,\ \ z(t)=1/\left(0.5t+\left(z_0\right)^{-1}\right), \tag{14}$$

($y(t)$ is not presented) therefore, a finite escape time appears (at $t=-2\left(z_0\right)^{-1}$). In this case, we take $\mathbf{N}=\mathbf{N}_1\times\mathbf{N}_2,$ where $\mathbf{N}_1=[0,\infty]\times[-\infty,\infty]$ and $\mathbf{N}_2=[-\infty,0].$ If we take the solution $z=\sqrt{x},$ by solving the differential equation (12), we obtain formally the same solution (14) for $x(t)$ and $z(t),$ then

$$y(t)=e^{-t}y_0+\int_0^t e^{s-t}/\left(0.5s+\left(z_0\right)^{-1}\right)ds\,. \tag{15}$$

Therefore, a finite escape time does not appear. In this case, we take $\mathbf{N}=\mathbf{N}_1\times\mathbf{N}_2,$ where $\mathbf{N}_1$ is the same, and $\mathbf{N}_2=[0,\infty].$

Moreover, we can apply Theorem 1 on the case $\mathbf{N}_2=[0,\infty].$ Take $\boldsymbol{v}(x)=0.5x^2\geq 0$. Then $\dot{\boldsymbol{v}}=-z^5\leq 0$ in $\mathbf{N}$. The equation $\dot{\boldsymbol{v}}=0$ implies that $z=0$ and, by (13), $x=0,$ while the solution of the right equation in (12) is $y=e^{-t}y_0$. The latter solution $(x,y,z)=(0,e^{-t}y_0,0)$ satisfies the condition (iii) of Theorem 1, therefore the solution (12) and (13) tend to the origin when $t\to\infty$ for all initial values, which is already seen by (14) and (15) (That $y(\infty)=0$ can be checked by applying the l'Hopital rule on (15)).

Corollary 1: Consider that the descriptor system (1) and (2) is given, such that Assumptions 1 and 2 hold, and let there exist a function $\boldsymbol{v}(x_1)$ satisfying the condition (i) and (ii) of Theorem 1. If the system of algebraic equations $\boldsymbol{h}(x)=0,$ $\dot{\boldsymbol{v}}=0,\ \ddot{\boldsymbol{v}}=0,\ldots$ has unique solution $x=0,$ then the solution $x(t)$ of the descriptor system given by (1) and (2) satisfies $x(\infty)=\lim_{t\to\infty}x(t)=0$ for all initial conditions $x\left(0\right)=x_0.$

Proof. We have to prove only that the expressions $\ddot{v}=0,\ldots$ are actually algebraic equations in x. Consider the extended set of equations given by (1) and (2), and $\dot{\boldsymbol{v}}=\boldsymbol{\varphi}(x)=0$ too. By the differentiation of this equation in the variable $t,$ we obtain the equation $\ddot{\boldsymbol{v}}=0.$ To find $\ddot{\boldsymbol{v}}$, as a function of x_1 and $x_2,$ we write at first

$$\ddot{v}=\frac{\partial\boldsymbol{\varphi}}{\partial x_1}\dot{x}_1+\frac{\partial\boldsymbol{\varphi}}{\partial x_2}\dot{x}_2\,, \tag{16}$$

Since $\dot{x}_2$ is not known, we differentiate in t the equation $\boldsymbol{h}(x)=0$ and obtain

$\frac{\partial \boldsymbol{h}}{\partial x_1}\dot{x}_1+\frac{\partial \boldsymbol{h}}{\partial x_2}\dot{x}_2=0$, from where, by using Proposition 1, we obtain

$$\dot{x}_2=-\left(\frac{\partial \boldsymbol{h}}{\partial x_2}\right)^{-1}\frac{\partial \boldsymbol{h}}{\partial x_1}\boldsymbol{f}\,.$$

Then by replacing this identity into (16), we obtain

$$\ddot{\boldsymbol{v}}=\left[\frac{\partial \boldsymbol{\varphi}}{\partial x_1}-\frac{\partial \boldsymbol{\varphi}}{\partial x_2}\left(\frac{\partial \boldsymbol{h}}{\partial x_2}\right)^{-1}\frac{\partial \boldsymbol{h}}{\partial x_1}\right]\boldsymbol{f}=0\,.$$

The higher order time-derivatives of $\boldsymbol{v}$, as function of x_1 and x_2, can be found in an obvious analogous way, which completes the proof. ■

Remark 5. If (1) and (2) is a given linear descriptor system (8), then Corollary 1 corresponds to the case when the pair $(A-sE,C)$ is finite mode observable, instead of solely finite mode detectable (like in Example 1).

In the next corollary, we consider that the vector $\boldsymbol{h}$ and x_2 in the system (1) and (2) are absent, i.e. we consider the autonomous system

$$\dot{x}=\boldsymbol{f}(x),\ x\in\mathbf{N}\subseteq\mathbf{R}^n\,, \tag{17}$$

which satisfies $\boldsymbol{f}(0)=0$ and $\boldsymbol{f}$ has all-order partial derivatives.

The notion of locally weak observability for nonlinear systems is defined on page 733 of [36], and Theorem 3.1 of that paper gives the necessary and sufficient conditions. Here we adapt these results on the simpler autonomous (without control) system (17) the output of which is $y=\boldsymbol{\varphi}(x)$. The operator L_f is defined on scalar functions $\boldsymbol{\varphi}(x)$ as $L_f(\boldsymbol{\varphi})=(\partial\boldsymbol{\varphi}/\partial x)\boldsymbol{f}$. Consider all possible scalar functions $L_f(\cdots L_f(\cdots L_f(\boldsymbol{\varphi})\cdots)\cdots)=:L_f^k(\boldsymbol{\varphi})$, where k is the number of times the symbol $\boldsymbol{f}$ appears. According to Theorem 3.1 of [36], the system is locally weakly observable at some $x\in\mathbf{N}$ if and only if the row-vectors $(\partial/\partial x)L_f^k(\boldsymbol{\varphi}),\ k=0,1,\ldots$ have full rank n at that x. This condition is related to the condition (iii) of the next corollary.

***Corollary 2**:* Consider the autonomous system (17), having a unique solution without a finite escape time for all initial values $x_0\in\mathbf{N}$, and suppose that there exist a function $\boldsymbol{v}(x)$ satisfying the conditions:

(i) $\boldsymbol{v}(x)\geq 0$ for all $x\in\mathbf{N}$, and $\boldsymbol{v}(0)=0$,

(ii) $\boldsymbol{\varphi}(x) := \dfrac{\partial \boldsymbol{v}}{\partial x}\boldsymbol{f}(x) = \dot{\boldsymbol{v}} \le 0$ for all $x \in \mathbf{N}$,

(iii) The unique solution of all algebraic equations $L_f^k(\boldsymbol{\varphi}) = 0, k = 0,1,\ldots$ is $x = 0$.

Then the solution $x(t)$ of the system (17) satisfies $x(\infty) = \lim_{t\to\infty} x(t) = 0$ for all initial conditions $x(0) = x_0$.

Proof. It is a direct consequence of Corollary 1. +

2.2 Feedback Stabilizability of Nonlinear Descriptor Systems

Let us consider the following affine-in-control nonlinear descriptor system:

$$\dot{x}_1 = \boldsymbol{f}(x_1, x_2) + \boldsymbol{G}(x_1, x_2)u\,, \tag{18}$$

$$0 = \boldsymbol{h}(x_1, x_2) + \boldsymbol{E}(x_1, x_2)u \tag{19}$$

where $x_1 \in \mathbf{N}_1 \subseteq \mathbf{R}^{n_1}$, $x_2 \in \mathbf{N}_1 \subseteq \mathbf{R}^{n_2}$, $x = [x_1\ x_2]^T \in \mathbf{N} \subseteq \mathbf{R}^n$, $u = [u_1 \cdots u_m]^T$, $u_1,\ldots,u_m$ are scalars, $\boldsymbol{G} = [\boldsymbol{g}_1,\ldots,\boldsymbol{g}_m]$, $\boldsymbol{E} = [\boldsymbol{e}_1,\ldots,\boldsymbol{e}_m]$, and $\boldsymbol{g}_1,\ldots,\boldsymbol{g}_m$, $\boldsymbol{e}_1,\ldots,\boldsymbol{e}_m$ are column-vectors.

Theorem 2: Let there exist a function $\boldsymbol{v}(x_1)$ such that

(i) $\boldsymbol{v}(x_1) \ge 0$ for all $x_1 \in \mathbf{N}_1$, and $\boldsymbol{v}(0) = 0$,

(ii) $\boldsymbol{\varphi}(x_1, x_2) := \dfrac{\partial \boldsymbol{v}}{\partial x_1}\boldsymbol{f}(x_1, x_2) \le 0$ for all $x \in \mathbf{N}$ satisfying (2).

Introduce the row-vector function $\boldsymbol{\psi}(x_1, x_2)$ by

$$\boldsymbol{\psi}(x_1, x_2) = \frac{\partial \boldsymbol{v}}{\partial x_1}\boldsymbol{G}(x_1, x_2)\,.$$

We apply the control

$$u = \boldsymbol{u}(x_1, x_2) = -\boldsymbol{Q}(x_1, x_2)\,\boldsymbol{\psi}(x_1, x_2)^T\,, \tag{20}$$

where $\boldsymbol{Q}(x_1, x_2)$ is an arbitrary symmetric positive definite matrix function in $\mathbf{N}$.

(iii) The solution $x(t)$ of the descriptor systems given by

$$\dot{x}_1 = \boldsymbol{f}(x_1, x_2), \tag{21}$$

$$\boldsymbol{h}(x_1, x_2) = 0\,, \quad \boldsymbol{\varphi}(x_1, x_2) = 0\,, \quad \boldsymbol{\psi}(x_1, x_2) = 0, \tag{22}$$

satisfies $x(\infty) = \lim_{t\to\infty} x(t) = 0$ for all initial conditions $x(0) = x_0$,

Then, under Assumptions 1 and 2 for the closed-loop descriptor system given by (18), (19) and (20), the solution $x(t)$ of the closed-loop descriptor system satisfies $x(\infty) = \lim_{t\to\infty} x(t) = 0$ for all initial condition $x(0) = x_0$.

Proof. In fact, this theorem is a consequence of Theorem 1. Indeed, having in mind the inequality

$$\dot{\boldsymbol{v}} = \frac{\partial \boldsymbol{v}}{\partial x_1}\boldsymbol{f} + \frac{\partial \boldsymbol{v}}{\partial x_1}\boldsymbol{G}\boldsymbol{u} = \frac{\partial \boldsymbol{v}}{\partial x_1}\boldsymbol{f} - \frac{\partial \boldsymbol{v}}{\partial x_1}\boldsymbol{G}\boldsymbol{Q}\left(\frac{\partial \boldsymbol{v}}{\partial x_1}\boldsymbol{G}\right)^T \le 0,$$

we can deduce that the identity $\dot{\boldsymbol{v}} = 0$ is equivalent with the set of identities

$$\frac{\partial \boldsymbol{v}}{\partial x_1}\boldsymbol{f} = 0 \text{ and } \frac{\partial \boldsymbol{v}}{\partial x_1}\boldsymbol{g}_i = 0,\ i = 1,2,\ldots,m, \tag{23}$$

and consequently $\psi(x_1, x_2) = 0$ along the trajectories of the closed-loop system. ■

Remark 5. The matrix $\boldsymbol{Q}(x_1, x_2)$ has been introduced in order to enable achieving a proper balance between the usually opposite tasks:

(i) Reducing the magnitude of the control; and

(ii) Obtaining an acceptable distance to instability boundary of the closed-loop system, which in this paper for nonlinear descriptor systems is not defined rigorously; it is conditionally assumed based on Lurye's theory [3].

(Recall that for stable linear autonomous systems, $\dot{x} = Ax$, the distance to instability is the smallest distance to the imaginary axis among all eigenvalues of the matrix A).

Remark 6. It is shown in [40] that in the case of linear descriptor system, using a preliminary feedback, we can obtain an impulse-free descriptor system, which is a property of a part of Assumption 2. Similar pre-feedback could be applied on the nonlinear descriptor system (18), (19).

As in Corollaries 1 and 2, here we find sufficient conditions which guarantee that Condition (iii) of Theorem 2 holds without integrating nonlinear differential equations and without solving nonlinear algebraic systems. Introduce the Jacobi brackets $[\boldsymbol{f}, \boldsymbol{g}_i]$ between the vector functions $\boldsymbol{f}$ and $\boldsymbol{g}_i$, i.e. vector fields, defined as:

$[\boldsymbol{f}, \boldsymbol{g}_i] = \frac{\partial \boldsymbol{g}_i}{\partial x_1}\boldsymbol{f} - \frac{\partial \boldsymbol{f}}{\partial x_1}\boldsymbol{g}_i$, and then define inductively the following operator ad: $\mathrm{ad}_f^0 \boldsymbol{g}_i = \boldsymbol{g}_i$, $\mathrm{ad}_f^{k+1}\boldsymbol{g}_i = [\boldsymbol{f}, \mathrm{ad}_f^k \boldsymbol{g}_i]$, $k = 0,1,2,\ldots$ Further, let us denote by $\mathrm{L}_{x_1,x_2}(\boldsymbol{f}, \boldsymbol{g}_1, \ldots \boldsymbol{g}_m)$ the set of vector functions $\boldsymbol{f}$ and $\mathrm{ad}_f^k \boldsymbol{g}_i$, $i = 1,\ldots,m$, $k = 0,1,\ldots$

***Corollary 3**:* Let there exist a function $\boldsymbol{v}(x_1)$ such that

(i) $\boldsymbol{v}(x_1) \geq 0$ for all $x_1 \in \mathbf{N}_1$, $\boldsymbol{v}(0) = 0$,

(ii) $\boldsymbol{\varphi}(x_1, x_2) := \dfrac{\partial \boldsymbol{v}}{\partial x_1} \boldsymbol{f}\left(x_1, x_2\right) = 0$ for all $x \in \mathbf{N}$ satisfying (2).

(iii) $\operatorname{rank}(\mathrm{L}_{x_1, x_2}(\boldsymbol{f}, \boldsymbol{g}_1, \ldots \boldsymbol{g}_m)) = n_1$, for all nonzero $x \in \mathbf{N}$ satisfying (22),

(iv) the algebraic equations given by $\dfrac{\partial \boldsymbol{v}}{\partial x_1} = 0$ and (22) have unique solution $x_1 = 0,\ x_2 = 0.$

With application of the chosen control (20), and under Assumptions 1 and 2 for the closed-loop descriptor system described by means of (18), (19) and (20), the solution $x(t)$ of closed-loop descriptor system satisfies $x(\infty) = \lim\limits_{t \to \infty} x(t) = 0$ for all initial conditions $x(0) = x_0$.

Proof. A consequence of the identities (23) and $\dot{x}_1 = \boldsymbol{f}(x_1, x_2)$ is the following identity

$$0 = \frac{d}{dt}\left(\frac{\partial \boldsymbol{v}(x_1(t))}{\partial x_1} \boldsymbol{g}_i(x_1(t), x_2(t)) \right) = \frac{\partial \boldsymbol{v}}{\partial x_1} \frac{\partial \boldsymbol{g}_i}{\partial x_1} \boldsymbol{f} + \boldsymbol{g}_i^{\mathrm{T}} \frac{\partial^2 \boldsymbol{v}}{\partial x_1^2} \boldsymbol{f}$$

$$= \frac{\partial \boldsymbol{v}}{\partial x_1}\left([\boldsymbol{f}, \boldsymbol{g}_i] + \frac{\partial \boldsymbol{f}}{\partial x_1} \boldsymbol{g}_i \right) + \boldsymbol{f}^{\mathrm{T}} \frac{\partial^2 \boldsymbol{v}}{\partial x_1^2} \boldsymbol{g}_i = \frac{\partial \boldsymbol{v}}{\partial x_1} [\boldsymbol{f}, \boldsymbol{g}_i] + \left(\frac{\partial \boldsymbol{v}}{\partial x_1} \frac{\partial \boldsymbol{f}}{\partial x_1} + \boldsymbol{f}^{\mathrm{T}} \frac{\partial^2 \boldsymbol{v}}{\partial x_1^2} \right) \boldsymbol{g}_i$$

$$= \frac{\partial \boldsymbol{v}}{\partial x_1} [\boldsymbol{f}, \boldsymbol{g}_i] + \frac{\partial}{\partial x_1}\left(\frac{\partial \boldsymbol{v}}{\partial x_1} \boldsymbol{f} \right) \boldsymbol{g}_i = \frac{\partial \boldsymbol{v}}{\partial x_1} [\boldsymbol{f}, \boldsymbol{g}_i]$$

where the property that matrix $\dfrac{\partial^2 \boldsymbol{v}}{\partial x_1^2}$ is symmetric is used, which is true due to the equality of mixed second-order partial derivatives. By means of mathematical induction, we obtain the identity $\dfrac{\partial \boldsymbol{v}}{\partial x_1} \operatorname{ad}_f^k \boldsymbol{g}_i = 0$, $i = 1, \ldots, m$, $k = 0, 1, \ldots$.

Then by the condition (iii) of Corollary 3 and by $\dfrac{\partial \boldsymbol{v}}{\partial x_1} \mathrm{L}_{x_1, x_2}(\boldsymbol{f}, \boldsymbol{g}_1, \ldots \boldsymbol{g}_m) = 0,$ we obtain $\dfrac{\partial \boldsymbol{v}}{\partial x_1} = 0,$ for all $x \in \mathbf{N}$ except $x = 0$. Furthermore due to condition (iv), we have $x_1 = 0$ and $x_2 = 0$. +

In the subsequent corollary, we consider that the equation (19) is void and consequently the vector x_2 is void too. That is, we consider the affine-in-control system

$$\dot{x} = \boldsymbol{f}(x) + \boldsymbol{G}(x)u\,,\ x \in \mathbf{N} \subseteq \mathbf{R}^n\,,\ u \in \mathbf{R}^m\,, \tag{24}$$

which satisfies $\boldsymbol{f}(0) = 0$ and the functions $\boldsymbol{f}$ and $\boldsymbol{G}$ have partial derivatives of all orders. In this case, the definition of set $\mathrm{L}_x(\boldsymbol{f}, \boldsymbol{g}_1, \ldots, \boldsymbol{g}_m)$ is obvious. By Theorem 2.2 of [36], if rank of $\mathrm{L}_x(\boldsymbol{f}, \boldsymbol{g}_1, \ldots, \boldsymbol{g}_m)$ is full at some $x \in \mathbf{N} \subseteq \mathbf{R}^n$ (equal to n), then the system (24) is locally weakly controllable at x.

Corollary 4: Let there exist a function $\boldsymbol{v}(x)$ such that

(i) $\boldsymbol{v}(x) \geq 0$ for all $x \in \mathbf{N}$, and $\boldsymbol{v}(0) = 0$,

(ii) $\boldsymbol{\varphi}(x) := \dfrac{\partial \boldsymbol{v}}{\partial x}\boldsymbol{f}(x) = 0$ for all $x \in \mathbf{N}$.

(iii) $rank(\mathrm{L}_x(\boldsymbol{f}, \boldsymbol{g}_1, \ldots, \boldsymbol{g}_m)) = n$ for all nonzero $x \in \mathbf{N}$ satisfying $\boldsymbol{\varphi}(x) = 0$ and $\psi(x) = 0$,

(iv) The unique solution of the algebraic equations given by $\dfrac{\partial \boldsymbol{v}}{\partial x} = 0$, $\boldsymbol{\varphi}(x) = 0$ and $\boldsymbol{\psi}(x) = 0$, is $x = 0$.

We apply the following control law

$$\boldsymbol{u}(x) = -\boldsymbol{Q}(x)\left(\frac{\partial \boldsymbol{v}}{\partial x}\boldsymbol{G}\right)^T, \tag{25}$$

where $\boldsymbol{Q}(x)$ is an arbitrary symmetric positive definite matrix function in $\mathbf{N}$. If the closed loop system of (24) and (25) has a unique solution without finite escape times, then the solution $x(t)$ of the closed-loop system satisfies $x(\infty) = \lim_{t\to\infty} x(t) = 0$ for all initial conditions $x(0) = x_0$.

Proof. It is a direct consequence of Corollary 3. ■

3 Application to Quadcopter Stabilization Problem

Firstly, an analysis of quadcopters flight dynamics is presented from the viewpoint of control. Thereafter the respective results of the simulation experiments and relevant findings are discussed.

3.1 Feedback Stabilizability of Nonlinear Descriptor Systems

The nonlinear dynamic model of the quadcopter consists the following set of differential equations [39]:

$$\left.\begin{aligned} &\dot{x} = v_x, \quad \dot{y} = v_y, \quad \dot{z} = v_z, && \dot{\phi} = \omega_\phi, \quad \dot{\theta} = \omega_\theta, \quad \dot{\psi} = \omega_\psi, \\ &\dot{v}_x = m^{-1}[\cos\phi \cdot \sin\theta \cdot \cos\psi + \sin\phi \cdot \sin\psi] \cdot U_1, && \dot{p} = J_{xx}^{-1}(J_{yy} - J_{zz})qr + J_{xx}^{-1} \cdot U_2, \\ &\dot{v}_y = m^{-1}[\cos\phi \cdot \sin\theta \cdot \sin\psi - \sin\phi \cdot \cos\psi] \cdot U_1, && \dot{q} = J_{yy}^{-1}(J_{zz} - J_{xx})pr + J_{yy}^{-1} \cdot U_3, \\ &\dot{v}_z = -g + m^{-1}[\cos\phi \cdot \cos\theta] \cdot U_1, && \dot{r} = J_{zz}^{-1}(J_{xx} - J_{yy})pq + J_{zz}^{-1} \cdot U_4. \end{aligned}\right\} \tag{26}$$

In here, U_1, U_2, U_3, U_4 are transformed angular velocities of the four propellers, variables x, y, z and ϕ, θ, ψ represent linear and angular displacements and their derivatives v_x, v_y, v_z , respectively $\omega_\phi, \omega_\theta, \omega_\psi$, are all with respect to the Earth's coordinate frame. On the other hand, p, q, r denote angular rates with respect to the frame of flying body. The parameters m, g denote total mass and gravitational acceleration in the negative z-axis, and J_{xx}, J_{yy}, J_{zz} are the moments of inertia with respect to $x - y - z$ axes. In addition, the following three algebraic equations

$$\begin{aligned} &\omega_\phi = p + s_\phi t_\theta \cdot q + c_\phi t_\theta \cdot r, \\ &\omega_\theta = c_\phi \cdot q - s_\phi \cdot r, \\ &\omega_\psi = s_\phi / c_\theta \cdot q + c_\phi / c_\theta \cdot r, \end{aligned} \tag{27}$$

where $c_{(.)}$, $s_{(.)}$ and $t_{(.)}$ is a short notation for cos-, sin- and tan- functions, respectively, complete the representation model.

In general, the equations (26) and (27) together describe the nonlinear descriptor system for quadcopters. Actually, the differential equation (26) corresponds to the differential equation (18) while the algebraic equations (27) correspond to the algebraic equation (19).

Indeed, it is of the great importance how to select or construct a particular Lyapunov-like function for this particular problem. In order to find Lyapunov-like function for the system without control, i.e. for $\dot{x}_1 = \boldsymbol{f}(x_1, x_2)$, consider that all inputs in (26) are zero, that is. $U_1 = U_2 = U_3 = U_4 = 0$. Thus, we obtain:

$$\left.\begin{aligned} &\dot{x} = v_x, \quad \dot{v}_x = 0, \quad \dot{\phi} = \omega_\phi, \quad \dot{p} = J_{xx}^{-1}\left(J_{yy} - J_{zz}\right)qr, \\ &\dot{y} = v_y, \quad \dot{v}_y = 0, \quad \dot{\theta} = \omega_\theta, \quad \dot{q} = J_{yy}^{-1}\left(J_{zz} - J_{xx}\right)pr, \\ &\dot{z} = v_z, \quad \dot{v}_z = -g, \quad \dot{\psi} = \omega_\psi, \quad \dot{r} = J_{zz}^{-1}\left(J_{xx} - J_{yy}\right)pq. \end{aligned}\right\} \tag{28}$$

It is well-known that the Lyapunov stability theory is in fact energy-based methodology. The quadcopter is a physical system and furthermore, it is an energy

conservative system [13]. In other words, the sum of the kinetic and potential energy does not change in time. Therefore, the Lyapunov-like function, $\boldsymbol{v}$ in our case, is defined as $\boldsymbol{v} = \alpha \boldsymbol{e}_t + \beta \boldsymbol{e}_r$ with some dimensionless tuning coefficients α and β. Furthermore, due to the physics of quadcopter, formula $\boldsymbol{e}_t = 0.5m(v_x^2 + v_y^2 + v_z^2 + 2gz)$ describes the translational energy of motion while formula $\boldsymbol{e}_r = 0.5(J_{xx}p^2 + J_{yy}q^2 + J_{zz}r^2)$ describes the rotational energy. Therefore

$$\boldsymbol{v} = 0.5\alpha m(v_x^2 + v_y^2 + v_z^2 + 2gz) + 0.5\beta(J_{xx}p^2 + J_{yy}q^2 + J_{zz}r^2) \tag{29}$$

does represent the total energy in the considered plant system. In turn, for $\dot{\boldsymbol{v}}$ we have:

$$\dot{\boldsymbol{v}} = \alpha m(v_x\dot{v}_x + v_y\dot{v}_y + v_z\dot{v}_z + g\dot{z}) + \beta(J_{xx}p\dot{p} + J_{yy}q\dot{q} + J_{zz}r\dot{r}) \ . \tag{30}$$

Then by substituting equation (28), one can obtain $\dot{\boldsymbol{v}} = 0$. Consequently, equations (29) and (30) satisfy conditions (i), (ii) of Theorem 2 or else the Corollary 3. For the quadcopter descriptor representation (26) and (27), the selected Lyapunov-like function is shown to be useful for obtaining the needed control vector. Formula (20) along with $Q_1(x_1, x_2) = I_4$ gives the following stabilizing control set u_1, u_2, u_3, u_4:

$$\begin{aligned}
u_1 &= -\alpha[v_x(c_\phi s_\theta c_\psi + s_\phi s_\psi) + v_y(c_\phi s_\theta s_\psi - s_\phi c_\psi) + v_z(c_\phi c_\theta)] \\
u_2 &= -\beta p = -\beta(\omega_\phi - \omega_\psi s_\theta) \\
u_3 &= -\beta q = -\beta(\omega_\theta c_\phi - \omega_\psi s_\phi c_\theta) \\
u_4 &= -\beta r = -\beta(\omega_\psi c_\phi c_\theta - \omega_\theta s_\phi)
\end{aligned} \tag{31}$$

The implementation of feedback nonlinear stabilizing control, which is actually an inner loop of quadcopter stabilization, has been achieved by attaching u_i to the tracking control u_{tci}.

$$U_i = \gamma \cdot u_{tci} + u_i \tag{32}$$

where: $i \in \{1, \cdots, 4\}$, γ is a dimensionless tuning parameter, and U_i represent the actually applied control signals to quadcopter's nonlinear descriptor system. The intended effect of the inner and outer loop is to provide for faster stabilization and slower trajectory tracking, respectively.

3.2 Simulation Experiments of the Quadcopter Stabilization

The theory of the paper has been tested on quadcopter stabilization, under the task of reaching the desired point in space $[x, y, z]^T = [5, 5, 10]^T$ while keeping the quadcopter head (yaw angle) fixed, i.e. $\psi = 0$. The initial posture is taken

$[0, 0, 0]^T$ and $\psi = 0$. The comparison on the quadcopter stabilization is conducted on four different simulations. The control magnitude between the tracking control and stabilizing control in (32) has been achieved by tuning parameters α, β, γ presented on Table 1.

Table 1
Control magnitude tuning parameters

Simulation number	α	β	γ
1	0	0	1
2	0.08	0.01	1
3	0.42	0.02	0.9
4	0.83	0.03	0.8

The first simulation ('1') elaborates the stabilizing achieved only from the tracking control. Then in the following simulations, we gradually decrease the control magnitude of the tracking control (i.e. the parameter γ) and simultaneously increase control magnitude of the stabilizing feedback control (31) (i.e. the parameters α and β).

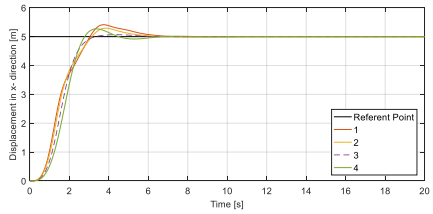

Figure 2
Linear displacement in the x-axis

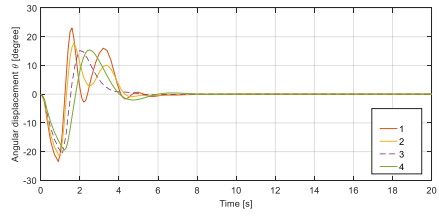

Figure 3
Angular displacement ϕ

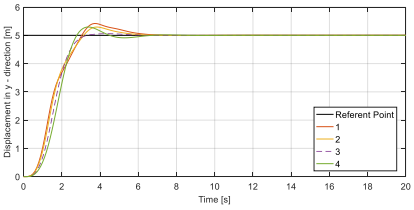

Figure 4
Linear Displacement in the y-axis

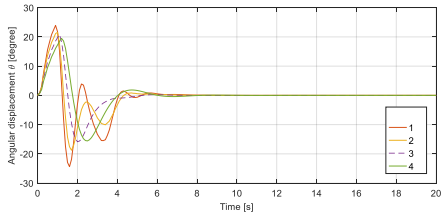

Figure 5
Angular displacement θ

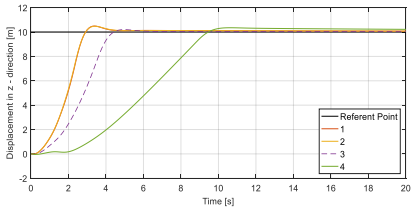

Figure 6
Linear Displacement in the z-axis

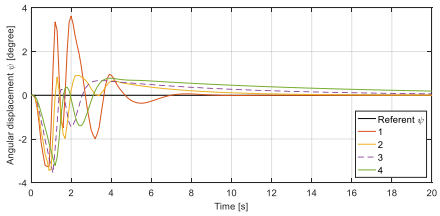

Figure 7
Angular displacement ψ

In comparison with other simulations, in particular with simulation number 1 (pure tracking control), simulation number 3 results on achieving a better tracking of quadcopter in x, y direction, while the height control (z-direction) it increases the rising time, but the settling time remains almost the same. By analyzing Figures 3, 5 and 7, the comparison between a pure tracking control stabilization and the mixed stabilization control (the simulation number 3) shows that the latter one improves the stabilization of the quadcopter by reducing orientation chattering.

Conclusions

In this paper, in addition to designing the nonlinear stabilizing control based on Lyapunov-like stability for nonlinear descriptor system, a new approach for representing the quadcopter, as a nonlinear descriptor system, has been elaborated. It is presented and demonstrated through numerical simulation, the application of the new approach on quadcopter stabilization.

The presented numerical results show that the stabilization of the quadcopter has been improved by introducing a mixed stabilization control (tracking control + stabilizing control derived from Lyapunov-like stability conditions). By decreasing the control magnitude of the tracking control and simultaneously increasing the control magnitude of the stabilization control, a larger converging time appears, which appears to be the only drawback of this new methodology.

Future theoretical extension of the presented results is foreseen, for the further enhancement of the system efficiency as argued in [37]. The other direction of future research will be focused on the improvement of the stabilization of the quadcopter towards a faster convergence and on the application toward other flying objects [38]. We would also like to examine the actual implementation of the stabilization control in a “real-world-scale” quadcopter. This is an open challenge, and it depends on future investment.

References

[1] B. Brogliato, R. Lozano, B. Maschke, O. Egeland: Dissipative Systems Analysis and Control Theory and Application, Springer, London, UK, 2007

[2] P. D. Franco, G. Scarciotti, A. Astolfi: A note on the stability of nonlinear differential-algebraic systems, IFAC PapersOnLine, Vol. 50(1), 2017, pp. 7421-7426

[3] A. I. Lurye: Certain Nonlinear Problems in the Theory of Automatic Control (in Russian, Nekatorie nelineynie zadachi teorii avtomaticheskogo regulirovaniya). Moskva, RU-USSR: Gostehizdat, 1951

[4] J. P. La Salle, S. Lefschetz: Stability by Liapunov's Direct Method with Applications. New York, NY - USA: Academic Press, 1961

[5] T. Watada, M. Ikeda, Y. Ohta, D. D. Siljak: Parametric absolute stability of multivariable Lurye systems, Automatica, Vol. 36, 2000, pp. 1365-1372

[6] T. Watada, M. Ikeda: Absolute stability criteria for multivariable Lurye systems with asymmetric nonlinearities, Proceedings of the 10th IFAC/IFORS/IMACS/IFIP Symposium on Large Scale Systems Theory and App*,* Oxford, UK: Pegamon Elsevier Science, 2004, Vol. 2, pp. 475-481

[7] T. Watada, M. Ikeda, E. Uezato: Stability theory for descriptor systems with non-smooth nonlinearities, Proceeding of the 17th Int. Symposium on Mathematical Theory of Networks and Systems, 2006, pp. 1626-1631

[8] T. Watada, M. Ikeda, E. Uezato: Absolute stability of multivariable lurye-type descriptor systems, Proceeding of the 17th IFAC World Congress, Seoul, R. Korea, July 2008, pp. 6021-6026

[9] C. I. Byrnes, A. Isidori, J. C. Willems: Passivity, feedback equivalence, and the global stabilization of minimum phase nonlinear systems, IEEE Transaction on Automatic Control, Vol. 36(11), 1991, pp. 1228-1240

[10] A. Fradkov: Passification of non-square linear systems and feedback Yakubovich Kalman-Popov lemma, European Journal of Control, Vol. 9(6), 2003, pp. 577-586

[11] A. Saberi, P. V. Kokotovic, H. J. Sussmann: Global stabilization of partially linear composite systems, SIAM Journal of Control and Optimization, Vol. 28(6), 1990, pp. 1491-1503

[12] C. Yang, J. Sun, Q. Zhang, X. Ma: Lyapunov Stability and Strong Passivity Analysis for Nonlinear Descriptor Systems, IEEE Transactions on Circuits and Systems, Vol. 60(4), 2013, pp. 1003-1012

[13] J. D. Stefanovski: Infinite-dimensional conservative systems and a conservativity condition for the Saint-Venant equations, International Journal of Control, Vol. 73(13), 2000, pp. 1224-1234

[14] J. C. Willems: Dissipative dynamical systems, Part I: General Theory*,* Archive of Rational Mechanics Analysis, Vol. 45(5), 1972, pp. 321-352

[15] J. C. Willems: Dissipative dynamical systems, Part II: Linear systems with quadratic supply rates, Archive of Rational Mechanics Analysis, Vol. 45(5), 1972, pp. 352-393

[16] D. J. Hill, P. J. Moylan: Dissipative dynamical systems: Basic input output and state properties, Journal of the Franklin Institute, Vol. 309(5), 1980, pp. 327-357

[17] P. C. Muller: Modelling and control of mechatronic systems by the descriptor approach, Journal of Theoretical and Applied Mechanics, Vol. 43(3), 2005, pp. 593-607

[18] A. Iggidr, B. Kalitine, R. Outbib: Semidefinite Lyapunov functions: Stability and stabilization, Math. of Cont., Sig., and Sys., Vol. 9(2), 1996, pp. 95-106

[19] M. Larsen, M. Jankovic, P. V. Kokotovic: Coordinated passivation designs, Automatica, Vol. 39(2), 2003, pp. 335-341

[20] H. K. Khalil: Nonlinear Systems, Prentice Hall, Upper Saddle River, NJ, 2002, Ch. 6 Passivity

[21] Y. Yin, J. Stefanovski, G. Dimirovski, J. Zhao: Quadratic stability results for switched singular descriptor systems, Proceedings of the 9th European Control Conference ECC07, Island of Kos, Greece, July 2007, pp. 696-701

[22] L. Y. Sun, J. Zhao, G. M. Dimirovski: Adaptive coordinated passivation control for generator excitation and thyristor-controlled series compensation system, Control Engineering Practice, Vol. 17(7), 2009, pp. 1295-1312

[23] J. Zhao, D. J. Hill: Dissipativity theory for switched systems, IEEE Transactions on Automatic Control, Vol. 53(4), 2008, pp. 941-953

[24] Y. Liu, G. S. Stojanovski, M. J. Stankovski, G. M. Dimirovski, J. Zhao: Feedback passivation of switched nonlinear systems using storage-like functions, Int. Journal of Con. Auto. and Sys., Vol. 9(5), 2011, pp. 980-986

[25] D. Ma, G. M. Dimirovski: Passivity-based Switching Rule and Control Law Co-Design of Networked Switched Systems with Feedback Delays, in: G. M. Dimirovski, Editor, Complex Systems: Studies in Systems, Decision and Control, Cham, Springer, 2016, Vol. 55, pp. 249-266

[26] O. Araar, N. Aouf: Full linear control of a quadrotor UAV, LQ vs H_∞, Proceedings of the UKACC International Conference on Control, Loughborough, UK, July 2014, pp. 133-138

[27] P. Wang, Z. Man, Z. Cao, J. Zheng, Y. Zhao: Dynamics modelling and linear control of quadcopter, Proceedings of the 2016 International Conference on Advanced Mechatronic Systems (ICAMechS), Melbourne, VIC, Australia, November 2016, pp. 498-503

[28] S. Deskovski, V. Sazdovski, Z. Gacovski: Guidance Laws and Navigation Systems for Quadrotor UAV: Theoretical and Practical Findings, in: *G. M. Dimirovski, Editor, Complex Systems: Studies in Systems, Decision and Control,* Cham, Springer, 2016, Vol. 55, pp. 381-390

[29] Q. Quan: Introduction to Multicopter Design and Control. Singapore, SG: Springer Singapore, 2017

[30] S. K. Phang, S. Lai, F. Wang, M. Lan, B. M. Chen: Systems design and implementation with jerk-optimized trajectory generation for UAV calligraphy, Mechatronics, Vol. 30, 2015, pp. 65-75

[31] D. Bunjaku, J. D. Stefanovski, G. M. Dimirovski: Regularity conditions for control problem with descriptor systems, Proceedings of the 14th IEEE International Conference on Control & Automation (ICCA), Anchorage, AK-USA, June 2018, pp. 130-135

[32] S. L. Dai, J. Zhao, G. M. Dimirovski: A descriptor system approach to robust H_∞ control for linear systems with time-varying uncertainties, Int. Journal of Systems Science, Vol. 40(12), 2009, pp. 1293-1306

[33] H. J. Sussmann, P. V. Kokotovic: The peaking phenomenon and the global stabilization of nonlinear systems, IEEE Transactions on Automatic Control, Vol. 36(4), 1991, pp. 424-440

[34] K. Takaba, N. Morihira, T. Katayama: A generalized Lyapunov theorem for descriptor system, Sys. and Con. Letters, Vol. 24(1), 1995, pp. 49-51

[35] J. Y. Ishihara, M. H. Terra: Impulse controllability and observability of rectangular descriptor systems, IEEE Transactions on Automatic Control, Vol. 46(6), 2001, pp. 991-994

[36] R. Hermann, A. J. Krener: Nonlinear controllability and observability, IEEE Trans. on Automatic Control, Vol. AC-22(5), 1977, pp. 728-740

[37] P. Kokotovic, M. Arcak: Constructive nonlinear control: A historical perspective, Automatica, Vol. 37(5), 2001, pp. 637-662

[38] B. L. Stevens, F. L. Lewis, E. N. Johnson: Aircraft control and simulation, Third Edition Dynamics, Controls Design, and Autonomous Systems, John Wiley & Sons, Inc., Hoboken, New Jersey, 2016

[39] D. Bunjaku, G. Nadzinski, M. Stankovski, J. D. Stefanovski: Dynamic Modeling and Flight Control Design for Multicopter, International Review of Aerospace Engineering, Vol. 11(5), 2018, pp. 224-235

[40] D. Bunjaku, J. D. Stefanovski, G. M. Dimirovski, D. Juričić: New Approach on Solving Control Problems with Descriptor Systems, Journal of The Franklin Institute, Vol. 356(6), 2019, pp. 3270-3289

[41] G. Lu, D.W. Ho and L. Zhou: A note on the existence of a solution and stability for Lipschitz discrete-time descriptor systems, Automatica, Vol. 47(7), 2011, pp. 1525-1529

Feature Space Reduction, using PCA in the Algorithm for Epilepsy Detection, using an Adaptive Neuro-Fuzzy Inference System and Comparative Analysis

Marjan Stoimchev, Vesna Ojleska Latkoska

Faculty of Electrical Engineering and Information Technologies, "Ss. Cyril and Methodius" University in Skopje, 1000 Skopje, Republic of Macedonia, ksiar3122013@feit.ukim.edu.mk, vojleska@feit.ukim.edu.mk

Abstract: This study presents an upgrade to our previously published algorithm for the detection of Epilepsy. The upgrade in the old algorithm, which was based on wavelet transform (WT) for feature extraction, and Adaptive Neuro-Fuzzy Inference System (ANFIS) for classification, is made by using Principal Component Analysis (PCA) in order to reduce the number of features used, for the training the ANFIS network. In order to make a comparison of the old and the upgraded algorithm with PCA, i.e. evaluating both algorithms, in terms of training performance and classification accuracies, comparative analysis of the both algorithms was made, when using different data splitting methods, and different input space partitioning methods. It was concluded that the upgraded algorithm exhibits a satisfactory performance, and in some cases, performs better than the old algorithm, even though the number of features is significantly reduced (from 20 to 7), which plays a crucial role in making the new algorithm more resistant to overfitting.

Keywords: Adaptive Neuro-Fuzzy Inference System (ANFIS); wavelet transform; fuzzy logic; Finite Impulse Response (FIR) filter; electroencephalogram (EEG); comparative analysis; normalization; input space partitioning; Principal Component Analysis (PCA)

1 Introduction

Epilepsy is chronic brain disorder, characterized by seizures, which can affect any person, at any age. It is characterized by recurrent convulsions over a time-period. Clinical diagnosis of epilepsy requires detailed history and neurological examinations [1]. There are many techniques to investigate the recurrent epileptic convulsions (namely, Computer Tomography-CT, Magnetic Resonance Imaging-MRI and Electroencephalogram-EEG). As it is stated in [1], the most common effective diagnostic method for the detection of epilepsy is the analysis of EEG signals, which can be based on different types of approaches [14] [26] [27].

Although it is possible for experienced neurophysiologist to detect the epilepsy by visually scanning of the EEG signals, for a more objective analysis and reproducible results, it is always advantageous to detect these activities from the EEG signals through some computer methods by extracting relevant features from the signals [1] [26] [27]. In order to solve this, there are many proposed methodologies. In general, all of the techniques consist of several steps, i.e. from data preprocessing, as the first step, feature extraction as a second step and to classification, as a third step.

In the first step, EEG signal de-noising is done, and it can be based using conventional filtering methods [8] [9], or filtering through wavelet analysis [11], [25]. For the second step (feature extraction), there are many, different methods (based on frequency domain analysis, or time domain analysis, or both), whereas the results of the studies in the literature have demonstrated that the WT is the most promising method to extract relevant features from the EEG signals [26], [27] [13]. For the final step there are also different ways for classifying the EEG signals [26], (feature extraction using genetic algorithms [28], the wavelet-based support vector machine (SVM) classifier [29], wavelet-based feed forward artificial neural network-FFANN [23] [24], fuzzy rule-based detection [30], Adaptive Neuro-Fuzzy Inference System (ANFIS) [13] [14] [7] [2], and many others).

In our previous study [2] and [3] an algorithm for classification of EEG signals was proposed, that combines Finite Impulse Response (FIR) filtering for artefact removal [8] [9] [7], WT for feature extraction [12] [13] [14] [26] [27], and ANFIS for classification [12] [13] [14]. ANFIS model learns how to classify the EEG signal, through the standard hybrid learning algorithm, whereas a special form of ANFIS model was used, which depending on the number of inputs, splits the model into appropriate number of substructures (sub-ANFIS models).

This study is a continuation of the study reported in [2] and [3], whereas in order to reduce the number of features in the old algorithm ([2] and [3]) an upgrade to the algorithm was made, introducing PCA. The researchers in [4] [5] [6] have also applied PCA to classify the epileptic EEG signals, using this time domain method to reduce the large number of data and select the most important components as feature vectors. The main difference of this papers with our study is that researchers in [4] used SVM based classification on EEG signals, whereas the researchers in [5] used EEG signal decomposition with the Wavelet Packet Decomposition (WPD) method, and the classification was obtained with the Gaussian Mixture Model (GMM) classifier and lastly, researchers in [6] have tested several classifiers, namely the K-Nearest Neighbor (KNN), SVM, the naive bayes (NB) classifier and the LDA method.

As the proposed algorithm in [2] [3] had a good performance in comparison to the several similar algorithms from different researchers [23] [24] [7] [14], in this study a comparison analysis of the old [2] [3]) and the upgraded algorithm was

made, i.e. evaluating the both algorithms in terms of training performance and classification accuracies. The comparative analysis of the both algorithms was made using different data splitting methods, and different input space partitioning methods. Firstly, an initial simulation comparison analysis of the both algorithms over the grid partitioning method [15] was made, by dividing the dataset into various ways (using 70%-30% and 50%-50% ratio of the training and testing dataset, and using K-Fold cross validation technique) [19]. The second comparative analysis was made by analyzing the old and the upgraded algorithm, through different input space partitioning methods (grid partitioning versus fuzzy c-means clustering, versus subtractive clustering) [15] [16] [20]. It was concluded that the new algorithm has satisfactory performance, and in some cases performs even better than the old algorithm. Nevertheless, due to the reduced number of features (from 20 to 7), used for training the ANFIS network, the upgraded algorithm is much more resistant to overfitting.

This paper is organized as follows. In Section 2 the upgraded algorithm for epilepsy detection using PCA is presented. In Section 3 a comparative analysis for the influence of the training and testing data was made, both for the old and the upgraded algorithm, whereas in Section 4 the comparative analysis of the both algorithms using different types of input space partitioning methods was made. Finally, the study is summarized giving the necessary conclusions.

2 Upgrade of the Algorithm for Epilepsy Detection with Fuzzy-Neural Network using PCA

This work is a continuation of our previous work, published in [2] and [3], where the algorithm for detection of epilepsy with fuzzy-neural networks was presented. Here, except giving the short insight in the basic algorithm, presented in [2], and [3], an upgrade of the algorithm is introduced, using PCA method, in order to make further reduction of the used features. For the purpose of comparison on how different factors influence the system performance (both, when the old and the upgraded algorithm with PCA is used) bellow the old algorithm [2] [3], and the upgraded one are presented.

The algorithm for epilepsy detection with fuzzy-neural networks for classification of EEG signals [2] and [3], consists of three main steps (Figure 1-a)):

1) Filtering of the EEG signals, with FIR filter
2) Feature extraction and dimensionality reduction, with discrete wavelet transform (DWT)
3) Classification, using ANFIS

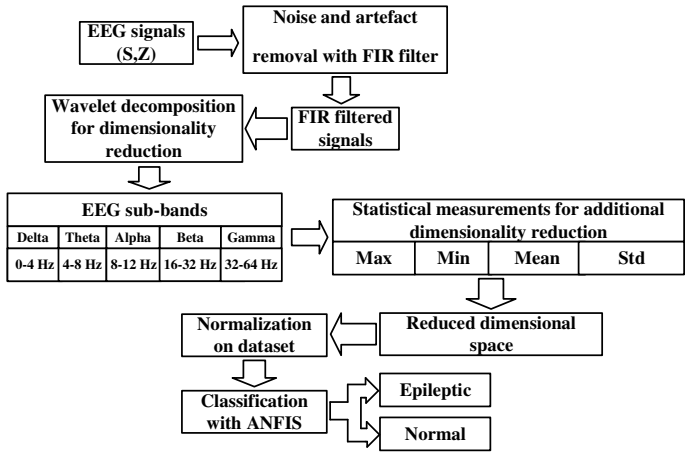

a)

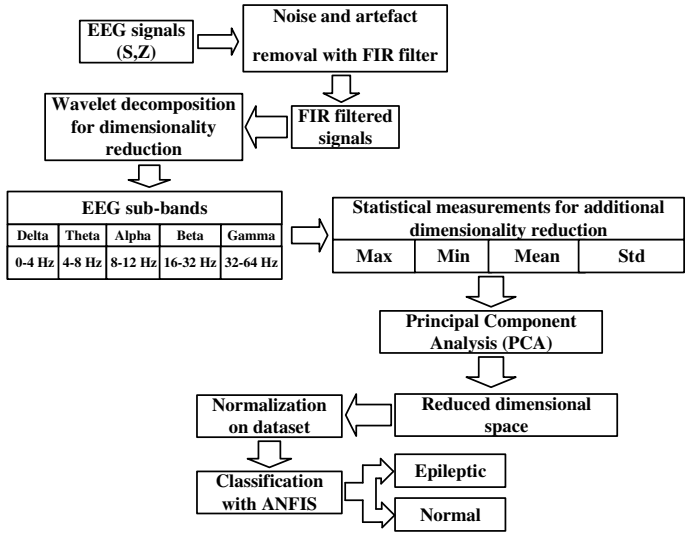

b)

Figure 1

a) Data flow for the algorithm in [2], and [3], and b) Data flow for the upgraded algorithm, using PCA

whereas the upgraded algorithm in this study consists of one additional step, which implies the four following steps (Figure 1-b) and Figure 2):

1) Filtering of the EEG signals, with FIR filter
2) Feature extraction and dimensionality reduction, with DWT
3) Using PCA, for additional dimensionality reduction
4) Classification, using ANFIS

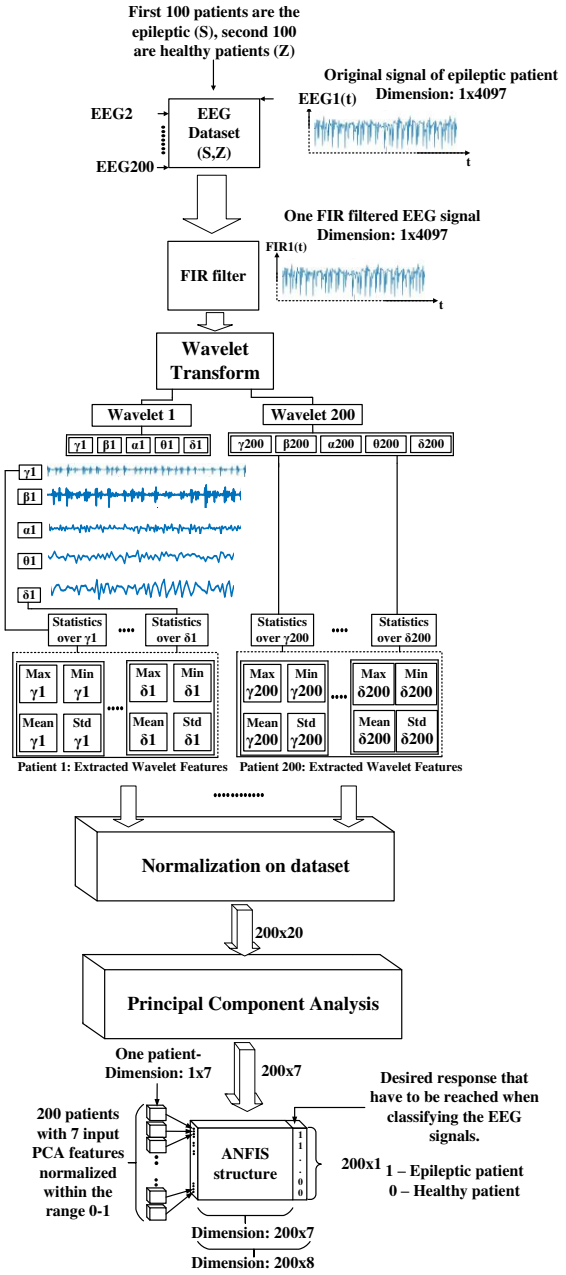

Figure 2
Detailed analysis for the overall upgraded algorithm from Figure 1-b)

Below we present a brief introduction for the used methodologies in the upgraded algorithm.

2.1 Input Data and De-noising of the EEG Signals

One of the major difficulties in analysis of EEG signals is the presence of artefacts [2] [7]. This disturbance represents serious obstructing factor that prohibits further processing to identify useful diagnostic features [2] [7].

In our case, as a first step in the upgraded algorithm (also in the old one, presented in [2] [3]), the band-pass FIR filter with the Hamming windowing method [8] [9] is used. The FIR filter is defined by two cutoff frequencies (in case of band-pass filtering), stopband attenuations and passband attenuation. The overall band of frequencies is defined by the Nyquist frequency, i.e. Fs/2 [8]. In our case, we used 1 Hz and 60 Hz, respectively. Below 1 Hz are the artefacts that are coming from the human body, and above 60 Hz is the power line noise [11].

The EEG data in this study was taken from the database of the university hospital in Bonn, Germany [10]. It consists of EEG signals that are recorded from three different events, namely, healthy subjects, epileptic subjects during seizure-free intervals (known as Interictal States) and epileptic subjects during a seizure (Ictal States).

The overall data consists of five subsets namely, O, Z, F, N and S. Set O and Z were obtained from healthy subjects with eyes open and closed respectively, sets F (epileptogenic zone) and N (hippocampal formation of the opposite hemisphere of the brain) were obtained during Interictal States in different zones of the brain and set S was taken from subjects during ictal state. Each subset contains 100 segments along with 4097 samples with sampling frequency of 173.61 Hz, each with duration of 23.6 seconds. We restrict ourselves to subsets S and Z, where the subset S denotes for epileptic subjects during epilepsy, whereas subset Z denotes for healthy subjects with eyes open. The dimension of our dataset is 200 segments by 4097 samples [10].

2.2 The use of Discrete Wavelet Transform for Feature Extraction

As a second step in the upgraded algorithm (also in the old one, presented in [2] [3], the DWT is used, which analyses the signal at different frequency bands, with different resolutions, in terms of approximation and detail coefficients [12] [27].

The DWT is used for feature extraction [13] [14] where each EEG signal is decomposed into 4 levels, resulting in 4 detail coefficients and one final approximation coefficient. They are related to the EEG sub-bands, namely, α, β, γ, δ and θ [14]. After the DWT procedure, the dimension of the initial dataset was reduced. In [2], the wavelet coefficients were calculated using Daubechies wavelets of order 2 (db2) in MATLAB [17], whereas in [3] a comparative analysis of the influence of different wavelet families to the overall performance of the

system was made. As in [3], we concluded that Daubechies wavelets of order 2 (db2) gave the most satisfactory results, for all the analysis in this study db2 wavelets are used.

For further dimensionality reduction, statistics over the extracted wavelet coefficients is made, namely, maximum, minimum, mean value and standard deviation of the wavelet coefficients [14]. We present the initial dataset into a more compact representation, i.e. a dataset with dimensions of 200x20 (4 statistical measurements x number of extracted coefficients = 20 features for each EEG segment).

2.3 Further Dimensionality Reduction of the Feature Space by using the Principal Component Analysis (PCA) Method

As a third step in the upgraded algorithm (which was not present in the algorithms in [2] [3], PCA is used, which out of the given set of features selects the most important ones, in what way, further dimensionality reduction is performed. The researchers in [4] [5] [6] also applied the PCA to classify the epileptic EEG signals.

In general, PCA is a time domain method which is used to reduce the large number of data and select the most important components as feature vectors. Since patterns in data can be hard to find in data of high dimensions, where the luxury of graphical representation is not available, PCA is a powerful tool for analyzing data. The objective is to represent data in a space that best expresses the variation in a sum-squared error sense.

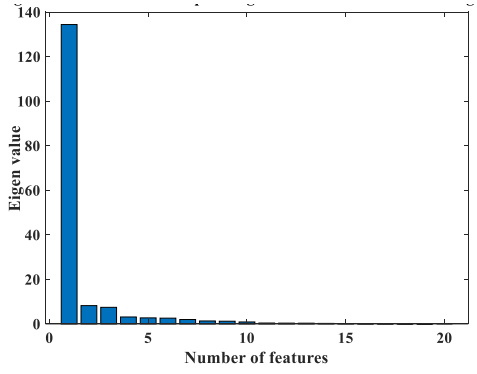

Figure 3
Eigen values for the corresponding features sorted in descending order

First, the d-dimensional mean vector μ and $d \times d$ covariance matrix is computed for the full data set. Next, the eigenvectors and eigenvalues are computed, and sorted according to decreasing eigenvalue. Subsequently, the largest k such eigenvectors are chosen [4].

In this extended version of the algorithm, the PCA method comes after the dimensionally reduced space from the DWT. The PCA replaces original features with new features, called principal components, which are orthogonal and have eigenvectors with adequate eigenvalues. Eigenvalues for the given 20 features are shown in decreasing order on Figure 3.

In order to decide which eigenvector(s) can be dropped without losing too much information from the construction of lower-dimensional subspace, inspection of the corresponding eigenvalues is made. The eigenvectors with the lowest eigenvalues bear the least information about the distribution of the data, and those are the ones that can be dropped. The common approach is to rank the eigenvalues from highest to lowest in order to choose the top k eigenvectors (as it is shown on Figure 3). In order to choose adequate number of principal components, a useful measure, a so-called explained variance, is used. The total variance is the sum of variances of all individual principal components, so the fraction of variance explained by a principal component is the ratio between the variance of the principal component and the total variance, as shown on Figure 4. The explained variance is a measure of how much information (variance) can be attributed to each of the principal components. It is clear that the first principal component explains the largest amount of variance (67.66%) compared to other principal components. Together, the first seven principal components contain 96.40% of the information. According to this, the first 7 principal components as features are used, implying reduced dataset of 200 instances by 7 features. Subsequently, those 7 feature vectors are used as an inputs to the ANFIS model [13] [14].

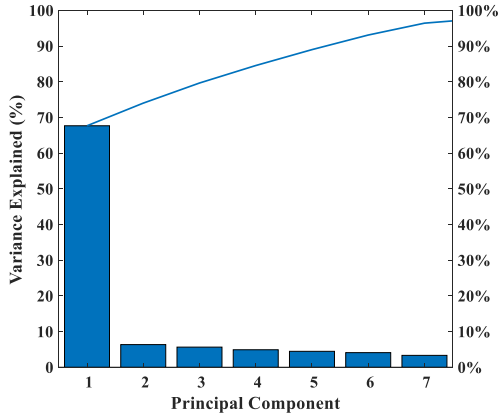

Figure 4
Variance explained for each principal component

It has to be emphasized that before the PCA, all the columns of the dataset have to be normalized within the range from 0 to 1 (Figure 2), in order to achieve stable convergence on the weighted factors of the lately used neural network training [18]. Min-max normalization is used, i.e. we are normalizing the feature column

vectors in the range from 0 to 1, [18] [22]. This method is also called "feature scaling", and represents a preprocessing technique [22].

2.4 Adaptive Neuro-Fuzzy Inference System (ANFIS)

ANFIS is an Adaptive Neural Network (ANN) that is based on a fusion of ideas from fuzzy control and neural networks and possesses the advantages of both [15]. ANFIS is used as a fourth step in the upgraded algorithm (the third step in the old algorithm presented in [2] [3]), in order to make the final classification of the EEG patients.

The ANFIS classifier is trained with the hybrid learning algorithm [12] [14] [15]. In the old algorithm [2] [3], the 20 features were used as input patterns which represented the EEG signals, and output vector as the 21st column (epileptic patients were labelled with ones, and the healthy patients were labelled with zeros) which represented the desired response. In this paper only 7 features as an input in the ANFIS classifier are used, and the output vector as the 8th column (epileptic and healthy patients are also labelled with ones and zeros, respectively).

In the previous study [2], the ANFIS model used the grid partitioning method [15] for input space partitioning, where we presented a way of manipulating 20 inputs (with 3 MFs each) by partitioning the ANFIS model on sub-ANFIS models, as shown in Figure 6-a), surpassing the major obstacle of the "curse of dimensionality" [15]. In the upgraded algorithm simulations with grid partitioning method were also performed, but now only 7 inputs have to be manipulated (Figure 6-c)).

3 Comparative Analysis for the Influence of the Training and Testing Data, for the previous and the Upgraded Algorithm

In [3] different approaches on dividing the dataset were presented, i.e. how the size of the training and testing data influence the accuracy. In order to make a comparison on the performance of the old algorithm (that uses 20 features) and the upgraded algorithm with PCA (that uses 7 features) bellow 3 splitting methods were compared (divided dataset into 70%-30% and 50%-50% ratio, as well as, using the splitting method based on cross validation [19]). This initial comparative analysis is obtained using grid partitioning method, and use of Gauss MFs [17], as this type of MFs gave best results in our previous study [3].

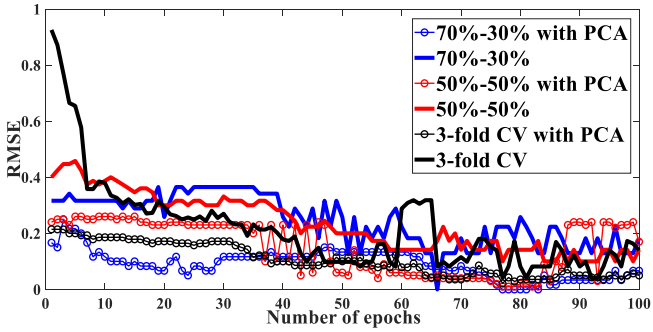

Figure 5

Comparison of the test set RMSEs over the three data split methods, using grid partitioning, for the old and the upgraded algorithm

When using the conventional splitting methods (70%-30%, or 50%-50% ratio of training and testing data, respectively) the data is simply divided into 2 appropriate sets. On the other hand, the K-Fold cross validation uses different approach.

With K-Fold cross validation, the available data is partitioned into K separate sets of approximately equal size [19]. The procedure involves K learning iterations, where for every iteration K-1 subsets are used for training, and the remaining set is used as the testing data. Every iteration leaves out a different subset, which means that each subset is used as test subset only once. In the end, all accuracies obtained from each iteration (testing fold) are averaged in order to obtain a reliable estimate of the model performance [19]. In our case 3-Fold cross validation is used.

Figure 5 presents the test set Root Mean Square Errors (RMSEs) when using the grid partitioning method during 100 epoch period, by applying the three different data split methods (70%-30%; 50%-50%; 3-Fold), for the old and the upgraded algorithm.

As can be seen from Figure 5, the lowest RMSEs are obtained in different number of epochs during the three partitioning methods. Nevertheless, it is evident that for the all three splitting methods, when the upgraded algorithm is used, RMSE values are lower than the RMSE values in the old algorithm. This implies that the use of PCA has a positive influence on the overall algorithm, when grid partitioning is used.

4 Influence of the Different Types of Input Space Partitioning

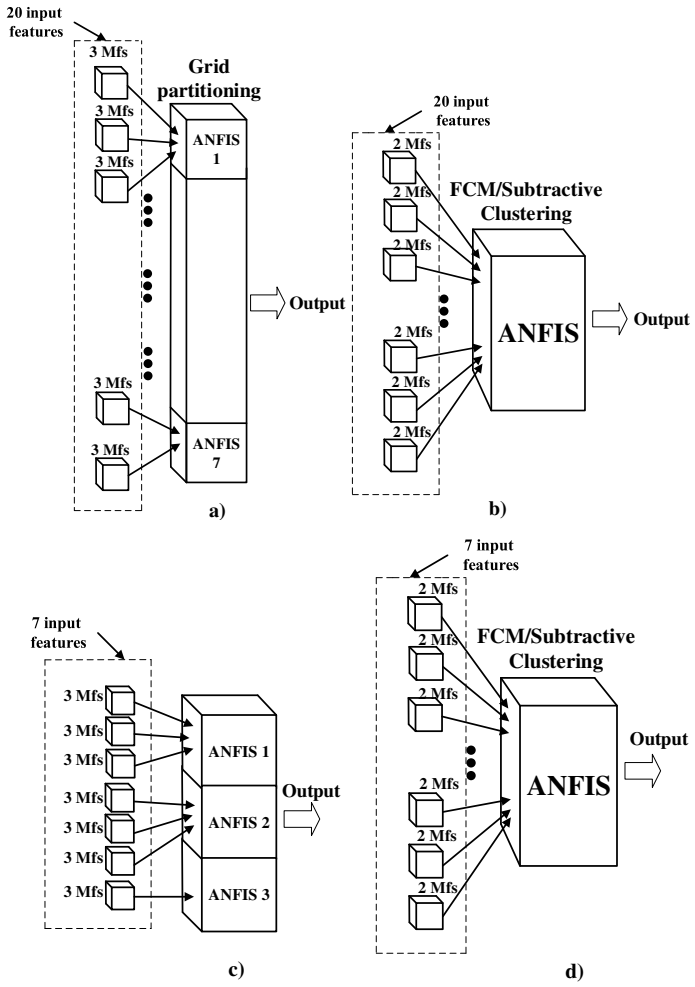

Figure 6

The structure of the model generated using different input space partitioning methods: a) Grid partitioning when the old algorithm with 20 input features is used ([2][3]), b) FCM/Subtractive clustering when the old algorithm with 20 input features is used ([2][3], c) Grid partitioning when the upgraded algorithm with PCA and 7 input features is used; d) FCM/Subtractive clustering when the upgraded algorithm with PCA and 7 input features is used

This section presents different methods of input space partitioning in the ANFIS model and the overall overview is given in Figure 6. In the previous study, proposed in [2], only the grid partitioning method as shown in Figure 6-a) is used,

where in order to reduce the number of rules, sub-ANFIS models are formed. As it is clear from Figure 6-a), sub-ANFIS models from 1 to 6 accept 3 inputs and the last sub-ANFIS model accepts 2 inputs. In the study in [3], two new approaches for input space partitioning, namely, fuzzy c-means (FCM) clustering and subtractive clustering [15] were used. The resulting ANFIS structure in that case is shown on Figure 6-b), where all the 20 inputs are passed at once, i.e. the number of rules is equal to the number of clusters, thus we do not face the problem called "curse of dimensionality" as presented in [2]. In this paper further reduction of the number of features (from 20 down to 7 features using PCA) was made, whereas the ANFIS input/output structure, when grid partitioning and FCM/Subtractive clustering are used is given on Figure6-c) and Figure 6-d), respectively.

FCM is a data clustering algorithm in which each data point belongs to a cluster to a degree specified by a membership grade (i.e. given data point can belong to several groups with the degree of membership between 0 and 1). The cluster centers are manually specified, where the performance depends on the initial cluster centers [15] [20].

Subtractive clustering, on the other hand, considers each data point as a potential cluster center, where the measure of potential is based on the distance of the data point from other data points (a data point located in a mound of different data points has a greater chance of being a cluster center) [15] [16].

Adequately to Figure 5, Figure 7 and Figure 8, present the test set RMSEs for FCM clustering and Subtractive clustering, respectively, using different data split methods, when both the old and the upgraded algorithm are used. 2 clusters for FCM clustering are used, and 0.8 radius of coverage (influence) for the subtractive clustering (for more information of the parameters in these clustering algorithms see [15] [17]). In both cases Gauss MFs [17] are used, and db2 wavelets, as this parameters gave best results in our previous study [3]. As we can see form Figure 7 and Figure 8, same as for the grid partitioning method (Figure 5), satisfying results are obtained when trained between 40 and 60 epochs approximately (old algorithm performs better at about 40 epochs, but the upgraded one needs more epochs for training, which is expected as in the upgraded algorithm we use less data compared to the old algorithm).

In the case of FCM clustering (Figure 7), different results are obtained, when the old and the upgraded algorithm are used, for the three splitting methods. At the beginning, for all the three splitting methods the upgraded algorithm shows worse behavior, but as the number of epochs increases this algorithm seams to stabilize after 60 epochs and does not show overfitting afterwards [21], as is the case with the old algorithm (for 50%-50% splitting method).

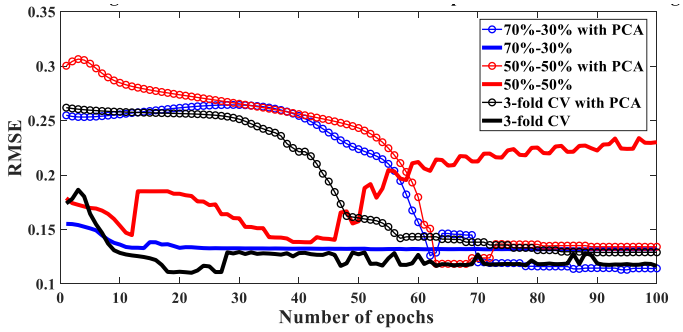

Figure 7

RMSE values for FCM clustering for different data split methods

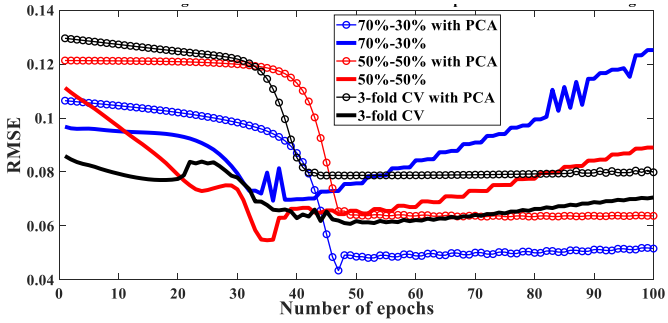

Figure 8

RMSE values for Subtractive clustering for different data split methods

In the case of subtractive clustering (Figure 8), we also get different results when the old and the upgraded algorithm are used, for the three splitting methods. Nevertheless, it is evident that for this type of input space partitioning, the upgraded algorithm with PCA shows better results, as after about 45 epochs it is stable for all the three types of splitting, and it does not overfit, as is the case with the old algorithm.

In order to conclude the comparisons, in Table 1 and Table 2 test set accuracies of the old and the upgraded algorithm are presented for the three different data splitting methods, using the three different input space partitioning methods.

Firstly, we choose to make comparative analysis using 40 training epochs (Table 1), as for some of the cases, the first algorithm overfits after 40 epochs (Figure 5, Figure 7, and Figure 8). On the other hand, as the upgraded algorithm in some of the cases needs more than 40 epochs for training, we choose to make comparative analysis of the both algorithms using 60 epochs for training (Table 2).

Table 1
Accuracies Obtained for Grid Partitioning, FCM and Subtractive clustering, for the old and the upgraded algorithm, when 40 epochs for training are used

Grid partitioning				**70-30%**	**50-50%**	**3-Fold**
Filter	**Wavelet**	**MFs type**	**Old versus upgraded algorithm**			
FIR	db2	Gauss MFs	Old algorithm from [2], and [3]	95	87	95.51
			Upgraded algorithm with PCA	97.33	89	96.03
Fuzzy c-means clustering (number of clusters = 2)				**70-30%**	**50-50%**	**3-Fold**
Filter	**Wavelet**	**MFs type**	**Old versus upgraded algorithm**			
FIR	db2	Gauss MFs	Old algorithm from [2], and [3]	98.25	95.41	96.39
			Upgraded algorithm with PCA	83.43	82.21	85.33
Subtractive clustering (radius of coverage – influence = 0.8)				**70-30%**	**50-50%**	**3-Fold**
Filter	**Wavelet**	**MFs type**	**Old versus upgraded algorithm**			
FIR	**db2**	Gauss MFs	Old algorithm from [2], and [3]	98.07	99.45	99.59
			Upgraded algorithm with PCA	97.21	93.33	98.22

Table 2
Accuracies Obtained for Grid Partitioning, FCM and Subtractive clustering, for the old and the upgraded algorithm, when 60 epochs for training are used

Grid partitioning				**70-30%**	**50-50%**	**3-Fold**
Filter	**Wavelet**	**MFs type**	**Old versus upgraded algorithm**			
FIR	db2	Gauss MFs	Old algorithm from [2], and [3]	98.33	97	92.96
			Upgraded algorithm with PCA	96.67	98	96.53
Fuzzy c-means clustering (number of clusters = 2)				**70-30%**	**50-50%**	**3-Fold**
Filter	**Wavelet**	**MFs type**	**Old versus upgraded algorithm**			
FIR	db2	Gauss MFs	Old algorithm from [2], and [3]	99.74	90	98.98
			Upgraded algorithm with PCA	98.85	97.93	95.33

Subtractive clustering (radius of coverage – influence = 0.8)				**70-30%**	**50-50%**	**3-Fold**
Filter	**Wavelet**	**MFs type**	**Old versus upgraded algorithm**			
FIR	**db2**	Gauss MFs	Old algorithm from [2], and [3]	92.21	93.33	97.43
			Upgraded algorithm with PCA	99.5	98.63	97.94

Form Table 1 it is evident that the upgraded algorithm in most of the cases have worse performance than the old algorithm, but this is expected, as according to Figure 5, Figure 7, and Figure 8, the upgraded algorithm needs more than 40 epochs for training. On the other hand, the test set accuracies for both algorithms, trained with 60 epochs, show better performance in most of the cases for the upgraded algorithm.

It general, it is evident that the upgraded algorithm has satisfactory performance, and in some cases performs even better than the old algorithm, although the number of features is significantly reduced (from 20 to 7), which also plays a crucial role in making the new algorithm more resistant to overfitting.

As in our previous study [2] [3], the papers are concluded giving comparison of different relevant works, that have also used the Bonn database [10], here we expand that comparison. The results are shown in Table 2.

We have to note that the authors in [14], also use WT and ANFIS, but our approach differs as we use FIR filtering, as well as normalization. Our approach gives similar, or even better results, they have a 98.63% test accuracy of the test set Z (healthy), and a 98.25% test accuracy on the test set S (epileptic) patients. However, they make 5 class classification, which differs from our 2 class classification, for we did not summarize their results in Table 2.

Table 3

Comparison between accuracy in this study and other related studies

Related studies	**Test set Accuracy (%)**
Old algorithm-Grid Partitioning [2]	98.33
Old algorithm-FCM [3]	99.74
Old algorithm-Subtractive clustering [3]	99.59
Upgraded algorithm with PCA - Grid Partitioning	98
Upgraded algorithm with PCA – FCM	95.33
Upgraded algorithm with PCA – Subtractive clustering	99.5
E.Juarez-FFANN *[23]* (WT and NN, using six features. Several filters and wavelets were used, namely,	93.23

Haar, Db2 and Db4, getting 93.23% as the highest accuracy)	
I.Overhodzic-Wavelet+NN *[24]* (Wavelet and NN. DWT with Multiresolution analysis (MRA), based on db4 was used)	94

Conclusions

This paper represents a continuation of our previous work, representing, an extension of the previously presented algorithm, reducing the number of used features, using PCA. In order to show that the upgraded algorithm performs in a similar, or even better method, as related to the old algorithm, several comparative analyses were made, comparing the old and the upgraded algorithm for different data splitting methods (70%-30%, 50%-50%, and 3-Fold cross validation), and the different types of input space partitioning methods (grid partitioning, versus FCM clustering, versus subtractive clustering). As in our previous study, it was concluded that the combination of db2 wavelets, and the Gauss MFs gave satisfactory results, here the comparisons were made using only db2 wavelets and Gauss MFs. The comparisons of the accuracies of the old and the upgraded algorithm for the different data split methods and the different input space partitioning were made both for 40 and 60 epochs, as with the old algorithm, in some of the cases, overfits after 40 epochs and 60 epochs seemed a reasonable sublimate according the RMSE simulation results. It is well known that size reduction methods are preferred, in applications where the number of input parameters in the data set is too large [31]. In this sense, the PCA in the upgraded algorithm plays a key role, i.e. although it sufficiently reduces the data dimension features from 20 to 7, according to the results, the essence of the original data is preserved, but the algorithm has a potential of greatly reducing the computational costs.

References

[1] U. Rajendra Acharya, S. Vinitha Sree, G. Swapna, Roshan Joy Martis, Jasjit S. Suri, "Automated EEG analysis of epilepsy: A review," in Knowledge-based Systems, Vol. 45, pp. 147-165, June 2013

[2] Marjan Stoimchev, Vesna Ojleska Latkoska, "Detection of Epilepsy Using Adaptive Neuro-Fuzzy Inference System," Journal of Electrical Engineering and Information Technologies, in press

[3] Marjan Stoimchev, Vesna Ojleska Latkoska, "Comparative Analysis for the Influence of the Tuning Parameters in the Algorithm for Detection of Epilepsy Based on Fuzzy Neural Networks," in Proceedings of the 14th International Conference - ETAI 2018, Struga, R.Macedonia, September 20-22, 2018

[4] Subasi, A. and Gursoy, M. I.: 'EEG Signal Classification Using PCA, Ica, LDA and Support Vector Machines', *Expert Systems with Applications*, 2010, 37, (12), pp. 8659-8666

[5] Acharya, U. R., Sree, S. V., Alvin, A. P. C., *et al.*: 'Use of Principal Component Analysis for Automatic Classification of Epileptic EEG Activities in Wavelet Framework', *Expert Systems with Applications*, 2012, 39, (10), pp. 9072-9078

[6] Siuly, S. and Li, Y.: 'Designing a Robust Feature Extraction Method Based on Optimum Allocation and Principal Component Analysis for Epileptic EEG Signal Classification', *Computer methods and programs in biomedicine*, 2015, 119, (1), pp. 29-42

[7] D. Najumnissa, T. R Rangaswamy, "Detection and Classification of Epilepsy Seizures using Wavelet feature extraction and Adaptive Neuro-Fuzzy Inverence System," International Journal of Computational Engineering Research, Vol. 2, pp. 755-761, May-June 2013

[8] P. Sinha, Speech Processing in Embedded Systems, Springer Science+Business Media, LLC 2010, pp. 25-32

[9] S. H. Mneney, An Introduction to Digital Signal Processing: A Focus on Implementation, River Publishers, 2008, pp. 153-158

[10] R. G Andrzejak, K. Lehnertz, C. Rieke, F. Mormann, P. David, C. E. Elger, "Indications of nonlinear deterministic and finite dimensional structures in time series of brain electrical activity: http://epileptologie-bonn.de/cms/front_content.php?idcat=193&lang=3

[11] A. Nakate, P. D Bahirgonde, "Feature Extraction of EEG Signals using Wavelet Transform," International Journal of Computer Applications, Vol. 124, No. 2, August 2015

[12] A. Subasi, "Application of adaptive neuro-fuzzy inference system for epileptic seizure detection using wavelet feature extraction," Computers in Biology and Medicine, Vol. 37, Iss. 2, pp. 227-244, December 2005

[13] İ. Güller, E. D. Übeyli, "Application of adaptive neuro-fuzzy inference system for detection of electrocardiographic changes in patients with partial epilepsy using feature extraction," Expert Systems with Applications, Vol. 27, Iss. 3, pp. 323-330, October 2004

[14] İnan Güller, Elif Derya Übeyli, "Adaptive neuro-fuzzy inference system for classification of EEG signals using wavelet coefficients," Journal of Neuroscience Methods, Vol. 148, Iss. 2, pp. 113-121, 30 October 2005

[15] J. S. R Jang, C. T Sun, E. Mizutani, Neuro-Fuzzy and Soft Computing-A Computational Approach to Learning and Machine Intelligence, Prentice Hall Upper Saddle River, 1997

[16] N. Pandey, N. Tiwari, "Predictive Accuracy of Modified Subtractive Clustering Algorithm on Large Dataset," International Journal of Research and Development in Applied Science and Engineering (IJRDASE), Vol. 8, Iss. 2, December 2015

[17] https://www.mathworks.com/products/matlab.html

[18] Z. Mustaffa, Y. Yusof, "A Comparison of Normalization Techniques in Predictiong Dengue Outbreak," Internation Conference on Business and Economics Research," Vol. 1, 2011

[19] Z. Omary, F. Mtenzi, "Machine Learning Approach to Identifying the Dataset Treshold for the Performance Estimators in Supervised Learning," International Journal for Informatics (IJI), Vol. 3, Iss. 3, September 2010

[20] S. S. Ghuman, "Clustering Techniques-A Review," International Journal of Computer Science and Mobile Computing, Vol. 5, Iss. 5, May 2016

[21] P. Domingos, "A Few Useful Things to Know about Machine Learning," Communications ACM, Vol. 55, Iss. 10, pp. 78-87, October 2012

[22] B. K. Singh, K. Verma, A. S. Thoke, "Investigations of Impact of Feature Normalization Techniques on Classifier's Performance in Breast Tumor Classification," International Journal of Computer Applications. Vol. 116, No. 19, April 2015

[23] E. J. Guerra, V. A. Aquino, P. G. Gil, "Epilepsy Seizure Detection in EEG Signals Using Wavelet Transforms and Neural Networks," Computer, Information and Systems Sciences and Engineering (CISSE), December 12-14, 2013

[24] I. Omerhodzic, S. Avdakovic, A. Nuhanovic, K. Dizdarevic, Energy Distrubution of EEG Signals: EEG Signal Wavelet-Neural Network Classifier, https://arxiv.org/abs/1307.7897v1, July, 2013

[25] L. Wang, W. Xue, Y. L., M. Luo, L. Huang, W. Cui, C. Huang, "Automatic Epileptic Seizure Detection in EEG Signals Using Multi-Domain Feature Extraction and Nonlinear Analysis," Entropy, Vol. 19, Iss. 6, 27 May 2017

[26] H. Adeli, Z. Zhou, N. Dadmehr, "Analysis of EEG records in an epileptic patient using wavelet transform," Journal of Neuroscience Methods, Vol. 123, Iss. 1, pp. 69-87, 15 February 2003

[27] H. Adeli, S. G. Dastidar, Automated EEG-Based Diagnosis of Neurological Disorders: Inventing the Future of Neurology, Taylor and Francis Group, 2010

[28] T. Wen, Z. Zhang, Effective and Extensible Feature Extraction Method Using Genetic Algorithm-Based Frequency-Domain Feature Search for Epileptic EEG Multi-classification, https://arxiv.org/abs/1701.06120v1, January, 2017

[29] P. K. Bhatia, A. Sharma, "Epilepsy Seizure Detection Using Wavelet Support Vector Machine Classifier," International Journal of Bio-Science and Bio-Technology, Vol. 8, No. 2, pp. 11-22, 2016

[30] A. F. Rabbi, R. F. Rezai, "A Fuzzy Logic System for Seizure Onset Detection in Intracranial EEG," Computational Intelligence and Neuroscience, Vol. 2012, 4 November 2011

[31] Ahmet Yüksek, Halil Arslan, Oguz Kaynar, Emre Delibaş, "Comparison of the Effects of Different Dimensional Reduction Algorithms on the Training Performance of Anfis (Adaptive Neuro-Fuzzy Inference System) Model," Cumhuriyet Science Journal, Vol. 38-4, pp. 716-730, 2017

Option Predictive Clustering Trees for Multi-label Classification

Tomaž Stepišnik, Dragi Kocev, Sašo Džeroski

Jožef Stefan Institute, Jamova 39, 1000 Ljubljana, Slovenia
Jožef Stefan Postgraduate School, Jamova 39, 1000 Ljubljana, Slovenia
{tomaz.stepisnik, dragi.kocev, saso.dzeroski}@ijs.si

Abstract: In this work, we focus on the task of multi-label classification (MLC), where every example is associated with a set of labels. We present an algorithm for learning option predictive clustering trees (OPCTs) for MLC, based on the predictive clustering framework. The algorithm addresses the myopia of the standard tree induction algorithm by considering alternative splits in the internal nodes of the tree and introducing option nodes where appropriate. An option tree can be viewed as a compact representation of an ensemble, as well as, used as a pool of candidates from which a single tree can be extracted. This broadens the space of trees that is searched and reduces the myopia, compared to the standard tree induction. We evaluate the proposed OPCTs on 12 benchmark MLC datasets from different domains. Results show that OPCTs as ensembles can achieve performance similar to the bagging ensembles of PCTs, while the single trees extracted from OPCTs can outperform standard PCTs. We also perform parameter sensitivity analysis and provide avenues for future work.

Keywords: predictive clustering trees; option trees; multi-label classification; myopia

1 Introduction

The most widely studied machine learning task is binary classification where the goal is to predict whether an example belongs to a group/class or not. If the examples can belong to a single class from a given set of m classes ($m > 2$) the task is known as multi-class classification. In this work, we focus on the multi-label classification (MLC) task, where a single example can be assigned several labels (i.e., a subset of a given set of possible labels).

MLC is a well-established predictive modelling task. The methods addressing this task belong in two groups: problem transformation and algorithm adaptation methods [4]. The problem transformation methods transform the multi-label learning problem into one or more single-label classification problems, which a great number of machine learning algorithms are capable of solving.

The problem transformation methods can be further split into three categories: binary relevance, label power-set and pair-wise methods. Binary relevance methods use the one-against-all strategy to convert the problem into several binary classification problems. A closely related method is the classifier chain method and its ensemble extension [9]. Label power-set (LP) methods transform the problem into a single multi-class classification problem, where a separate class is created for every possible subset of original labels. In this way, LP based methods directly take into account the label correlations. Representative methods include HOMER [5] and RAkEL [3]. Pair-wise methods perform pair-wise or round robin classification, with binary classifiers using Q(Q - 1)/2 classifiers covering all pairs of labels [17]. To combine these classifiers, the pairwise classification method uses majority voting.

The algorithm adaptation methods customize existing machine learning algorithms for the task of MLC. There are extensions of the following machine learning algorithms: boosting, k-nearest neighbors, decision trees and neural networks. The extended methods are able to directly handle multi-label data. AdaBoost.MH and AdaBoost.MR [8] are two extensions of AdaBoost for multi-label data. While AdaBoost.MH is designed to minimize Hamming loss, AdaBoost.MR is designed to find a hypothesis which ranks the correct labels at the top. Several variants for multi-label learning (ML-kNN) of the popular *k*-Nearest Neighbors (kNN) lazy learning algorithm have been proposed [1]. Decision tree extension was proposed within the predictive clustering framework [22]. A single predictive clustering tree (PCT) is constructed by using a splitting criterion that considers all of the labels. The PCTs for MLC were also used in an ensemble setting [14]. Neural networks have been adapted for MLC by introducing a new error function that takes multiple labels into account [18].

An extensive experimental comparison [12] of 12 MLC methods on 11 datasets using 16 performance measures showed that ensembles of PCTs are a state-of-the-art method for the MLC task. However, as already pointed out, a common concern with decision tree based models is their myopia, resulting from the greedy induction algorithm used to learn them. For this reason, several alternatives were proposed, such as beam search induction [15] and option trees [19], aimed at reducing the myopia of the trees. Both approaches showed that they can improve the performance of standard decision trees, while [12] also showed that very large option trees achieve the performance of bagging ensembles of decision trees. Conversely, [10] argues that exhaustive searching of the model space often leads to an inferior generalization.

In this work, we extend predictive clustering trees (PCTs) for MLC with option nodes, thus forming option predictive clustering trees (OPCTs). An option tree can be seen as a condensed representation of an ensemble of trees which share a common substructure. For illustration, see Figures 2 and 6. We also examine different techniques for selecting the optimal embedded tree from the OPCT. In this way, we increase the space of trees searched by the algorithm. We evaluate

both OPCTs as ensembles and the best embedded trees extracted from OPCTs on several datasets from different domains. The goal of this paper is to see whether OPCTs as ensembles can achieve the performance of bagging ensembles for the MLC task, and if selecting the best embedded tree can reduce the myopia of the standard decision trees.

The remainder of this paper is organized as follows. Section 2 describes the algorithm for learning OPCTs for MLC. Next, Section 3 outlines the design of the experimental evaluation. Section 4 continues with a discussion of the results. Finally, we conclude and provides possible directions for further work.

2 Option Predictive Clustering Trees

The predictive clustering trees framework views a decision tree as a hierarchy of clusters. The top-node corresponds to one cluster containing all data, which is recursively partitioned into smaller clusters while moving down the tree. The PCT framework is implemented in the CLUS system [23] available at *http://clus.sourceforge.net*.

OPCTs extend the PCT framework by introducing option nodes into the tree building procedure. Option decision trees were first introduced as classification trees by Buntine [19] and then analyzed in more detail by Kohavi and Kunz [13]. Ikonomovska et al. [16] analyzed regression option trees in the context of data streams. We also evaluated OPCTs for the multi-target regression task [11] and hierarchical multi-label classification task [7].

The motivation for the introduction of option trees is to address the myopia of the *top-down induction of decision trees* (TDIDT) algorithm [20]. From the perspective of the predictive clustering framework, a PCT is a non-overlapping hierarchical clustering of the whole input space. Each node (subtree) corresponds to a clustering of a subspace and prediction functions are placed in the leaves, i.e., the lowest clusters in the hierarchy. In contrast, an OPCT allows the construction of an overlapping hierarchical clustering. This means that at each node of the tree several alternative hierarchical clusterings of the subspace can appear instead of a single one. When using TDIDT to construct a predictive clustering tree, all possible splits are evaluated by using a heuristic, and the best split is selected. However, other splits may have very similar heuristic values and the difference between them could be a consequence of noise or sampling that generated the data. In this case, selecting a different split could be optimal. To address this concern, the use of option nodes was proposed [13].

Figure 1 presents the TDIDT algorithm modified for the induction of OPCTs. The function call *FindBestTests(E,O)* returns the *O* best tests according to the heuristic score in descending order (best first). Every test is represented as a triplet *(t,h,P)*,

where t is the actual test function, h is its heuristic value and P is the set of partitions produced by the test.

Procedure OptionPCT
Input: A data set E, parameter ε, maximum number of options O, current tree level l, maximum level for option nodes L
Output: An option predictive clustering tree
$candidates = \text{FindBestTests}(E, O)$
if $|candidates| > 0$ **then**
  if $|candidates| = 1$ **or** $l > L$ **then**
    $(t^*, h^*, \mathscr{P}^*) = candidates[0]$
    for each $E_i \in \mathscr{P}^*$ **do**
      $tree_i = \text{OptionPCT}(E_i, \varepsilon, O, l+1, L)$
    return $\text{node}(t^*, \bigcup_i \{tree_i\})$
  else
    $(t_0^*, h_0^*, \mathscr{P}_0^*) = candidates[0]$
    $nodes = \{\}$
    for each $(t_i^*, h_i^*, \mathscr{P}_i^*) \in candidates$ **do**
      if $\frac{h_i^*}{h_0^*} \geq 1 - \varepsilon$ **then**
        for each $E_j \in \mathscr{P}_i^*$ **do**
          $tree_j = \text{OptionPCT}(E_j, \varepsilon, O, l+1, L)$
        $nodes = nodes \cup \{\text{node}(t^*, \bigcup_j \{tree_j\})\}$
    if $|nodes| > 1$ **then**
      return $\text{option\_node}(nodes)$
    else
      return $nodes[0]$
else
  return $\text{leaf}(\text{Prototype}(E))$

Figure 1
The top down induction algorithm for option PCTs

The main component of the algorithm is the heuristic score used to evaluate the splits. For the MLC task, sets of labels are presented as binary vectors, where every component denotes the presence (1) or absence (0) of one label. For every component the Gini index is calculated, and their average is the final heuristic score. The algorithm introduces an option node into the tree when the best splits have similar heuristic values. Instead of selecting only the best split, we select every split s that satisfies the condition:

$$\frac{Heur(s)}{Heur(s_{best})} \geq 1 - \varepsilon \tag{1}$$

where s_{best} is the best split and ε determines how similar the heuristics must be. E.g., when ε=0.1, we are selecting only splits whose heuristics are within 10% of the best split. Typical values of ε are in the [0, 1] interval. After we have determined the candidate splits, we introduce an option node whose children are split nodes containing the selected splits. When no suitable test is found, a leaf node is created that stores the prototype of examples sorted to that leaf. For the MLC task, the *i*-th component of the prototype is the average value of the *i*-th components of examples in that leaf.

Introducing an option node with a large number of options is not advised [13] as it can lead to the explosion of model sizes. Therefore, we limit the maximum number of options included in a single option node (parameter *O*). To further limit the exponential growth of the tree, we also set the maximum depth in the tree where an option node can be introduced (parameter *L*). This means that on levels deeper than *L*, the tree is built following the standard TDIDT algorithm. This follows our intuition that splits lower in the tree, where clusters are already more homogeneous, are less important than splits higher in the tree.

Once an OPCT is learned, we use it to make predictions. In a regular PCT an example is sorted into a leaf (reached according to the tests in the nodes of the tree) where the prototype stored in that leaf is predicted. Traversing an example through an OPCT is the same for split nodes and leaves. When we encounter an option node, however, we traverse the example down each of the options. This means that in an option node an example is sorted to multiple leaves, where multiple predictions are produced. To obtain a single prediction in an option node, we aggregate the obtained predictions. For the MLC task, the aggregation is simple component-wise averaging of the vectors, as it is done in PCT ensembles. The resulting vector gives us pseudo-probabilities of every label, to which a threshold can be applied to select the actual labels.

An option tree is usually observed as a single tree, however, it can also be interpreted as a compact representation of an ensemble. We can extract *embedded trees* out of an option tree by replacing every option node with one of its options (Figure 2). A given OPCT is also an extension of the PCT learned on the same data. By definition, whenever we introduce an option node, the best split is one of the options included. Consequently, the PCT is an embedded tree in the OPCT, resulting from replacing all option nodes with the best option.

In addition to using an option tree as an ensemble of embedded trees, we can also extract a single embedded PCT out of it. This increases the space of trees searched by the TDIDT algorithm and directly addresses its myopia. The simplest way to select a single embedded PCT is to use the error on the training dataset as the selection criterion. This is an attractive option since it requires very little extra work and no extra data, but can lead to overfitting.

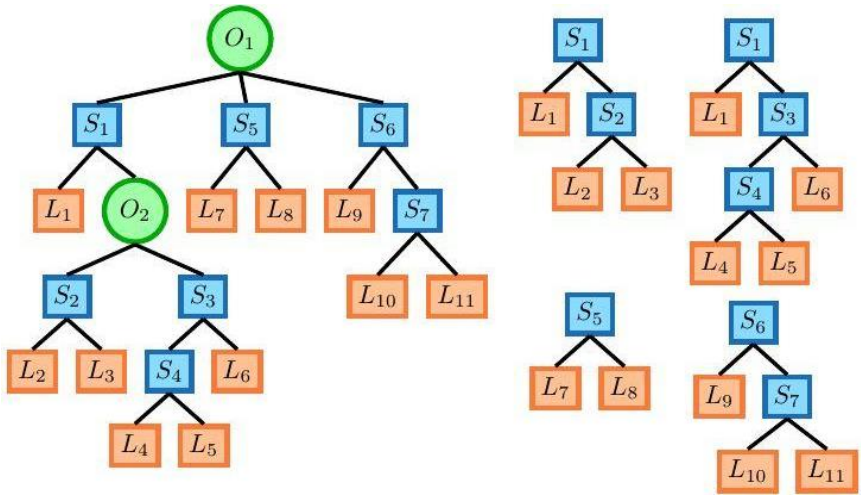

Figure 2

An option tree (left) and the ensemble of its embedded trees (right). O_i are option nodes, S_j split nodes and L_k leaf nodes.

Another option is to use a part of the training data as a separated validation set, which would not be used for the initial learning of the OPCT, but would be utilized to determine which of the embedded trees has the best predictive performance. We can also use expert knowledge to select the embedded tree. Providing a domain expert with an option tree gives them a lot of choices with regards to the model. This approach also has the advantage that the domain expert need not be available for interaction when the model is learned, but can assess the OPCT and chose the preferred options later on.

3 Experimental Design

The experimental evaluation was performed on 12 datasets from biology, text classification and multimedia domains. They are described in Table 1. All datasets except *CAL500* were retrieved pre-divided into training and testing sets and we used them in their original format to facilitate easier comparison of the results. The *CAL500* dataset was randomly split on training and test sets. All 12 datasets can be found at *http://mulan.sourceforge.net/datasets-mlc.html*.

There are many measures of performance used for the MLC task [12]. In our comparison we focus on Area Under the Average Precision-Recall Curve ($\overline{AUPRC}$) [2]. It combines the pseudo-probabilities of all the different labels as if they belonged to a single binary classification problem, and calculates the area under the precision-recall curve from them. A nice feature of $\overline{AUPRC}$ is that it is

a threshold independent measure, so we do not have to worry about setting the threshold at which the labels are predicted in the leaves (as explained in Section 2). In the appendix we include the results for two additional performance measures (Ranking Loss and One Error [12]), from which similar conclusions can be made.

Table 1

Properties of the datasets used in the study: number of examples in the training/testing datasets (Ntr/Nte), number of descriptive attributes (discrete/continuous, *D*/*C*), the total number of labels (*Q*) and label cardinality (l_c)

	Ntr/Nte	*D*/*C*	*Q*	l_c
bibtex	4880/2515	1836/0	159	2.40
birds	322/323	2/258	19	1.01
CAL500	302/200	0/68	174	26.0
corel5k	4500/500	499/0	374	3.52
emotions	391/202	0/72	6	1.87
enron	1123/579	1001/0	53	3.38
flags	129/65	9/10	7	3.39
genbase	463/199	1185/0	27	1.25
medical	645/333	1449/0	45	1.25
scene	1211/1196	0/294	6	1.07
tmc2007-500	21519/7077	500/0	22	2.16
yeast	1500/917	0/103	14	4.24

We used the 12 benchmark datasets to evaluate OPCTs. Firstly, we wanted to see how the OPCTs as ensembles of embedded PCTs compare to the bagging ensembles of PCTs [21]. Specifically, we were interested in the trade-off between the performance and the size of the model. For the size of the model we looked at the total number of leaves in the tree(s). For the bagging ensembles of PCTs, the number of trees in the ensemble is the primary way to control the size of the model. We ran the experiments with 10, 25, 50, 100 and 125 PCTs in the ensemble.

For OPCTs, we can influence the number of option nodes introduced into the tree by using different parameter values. We considered different values for the ε parameter from the set {0.01, 0.05, 0.1, 0.2, 0.3, 0.4, 0.5, 1.0}. When ε=1, option nodes with the best *O* splits are always introduced at the top *L* levels of the tree. We also tried different settings of the *O* and *L* parameters. Specifically, we used pairs (*O, L*) from the set {(10, 2), (5, 3), (3, 4)}. In addition to a better understanding of the performance vs. size trade-off, this also gives us insight into what is more valuable in OPCTs: more options at the top of the tree, or allowing option nodes lower in the tree. The pairs were selected in a way that at the maximum amount of option nodes introduced (e.g., at ε=1), the OPCTs would aggregate a similar amount of predictions compared to bagging ensembles of 100

PCTs. An important thing to note here is that different selections of parameters can still produce the same OPCT, if for a given dataset the same splits satisfy both criteria.

We also compared standard PCTs to the best embedded trees extracted from OPCTs (from here on referred to as BestEmbedded trees). We tried two approaches to extracting the BestEmbedded trees from OPCTs: selecting the embedded tree based on the training set performance, and based on the performance on a separate validation set not used to build the original OPCT. Both PCTs and BestEmbedded trees were post pruned using the training set in the first set of experiments, and using the validation set in the second set. This way, standard PCTs also benefited from the validation set, thus enabling a fair comparison. Note that BestEmbedded trees therefore use the validation set both for embedded tree selection and pruning. BestEmbedded trees were extracted from various OPCTs built with the same parameter settings described in the previous paragraph. This gave us insight into how different parameters influence the performance of the BestEmbedded trees. As a validation set, we randomly selected 20% of examples from the initial training set.

4 Results and Discussion

4.1 Comparison of OPCTs and Bagging Ensembles

Figure 3 shows the trade-off between the performance and size of the model for bagging ensembles of PCTs and OPCTs as ensembles. We can see that increasing the number of options improves the performance of OPCTs. In contrast to adding more trees to an ensemble, this is not guaranteed, since additional options include split nodes with lower heuristic scores. The performance improvement saturates at the largest OPCTs and often reaches the performance of bagging ensembles (on 7 datasets). All models seem to perform equally well on the *genbase* dataset, and much better than single PCTs (results on Figure 4).

Note that the comparison of the sizes of the trees is closely related to the comparison of running times. The most time consuming items when learning a tree are the evaluations of the candidate splits and then splitting the data. This is done in the same way in both PCTs (and ensembles thereof) and OPCTs, therefore, similar number of nodes in the trees indicates similar time needed for their induction.

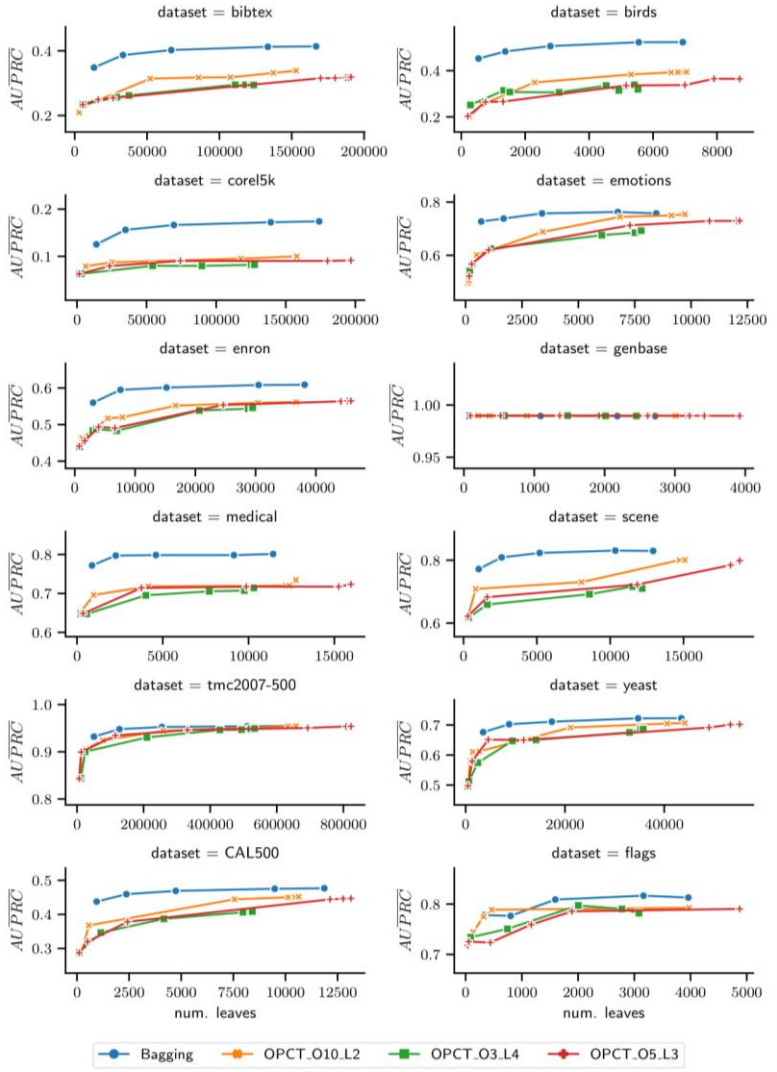

Figure 3

Trade-off between size and performance of bagging ensembles of PCTs and OPCTs. The size of ensembles is influenced by the number of trees, whereas the size of OPCTs is mainly influenced by the number of option nodes introduced into the tree. Note that every graph is on a different scale.

By comparing the results of OPCTs with different settings of parameters O and L, we can see that the pair $(O, L) = (10, 2)$ offers the best performance, followed by $(O, L) = (5, 3)$. This confirms our intuition that option nodes lower in the tree are less useful and do not offer enough improvement in performance to justify the increased model size. This is especially evident on the *bibtex*, *birds*, *emotions* and *scene* datasets.

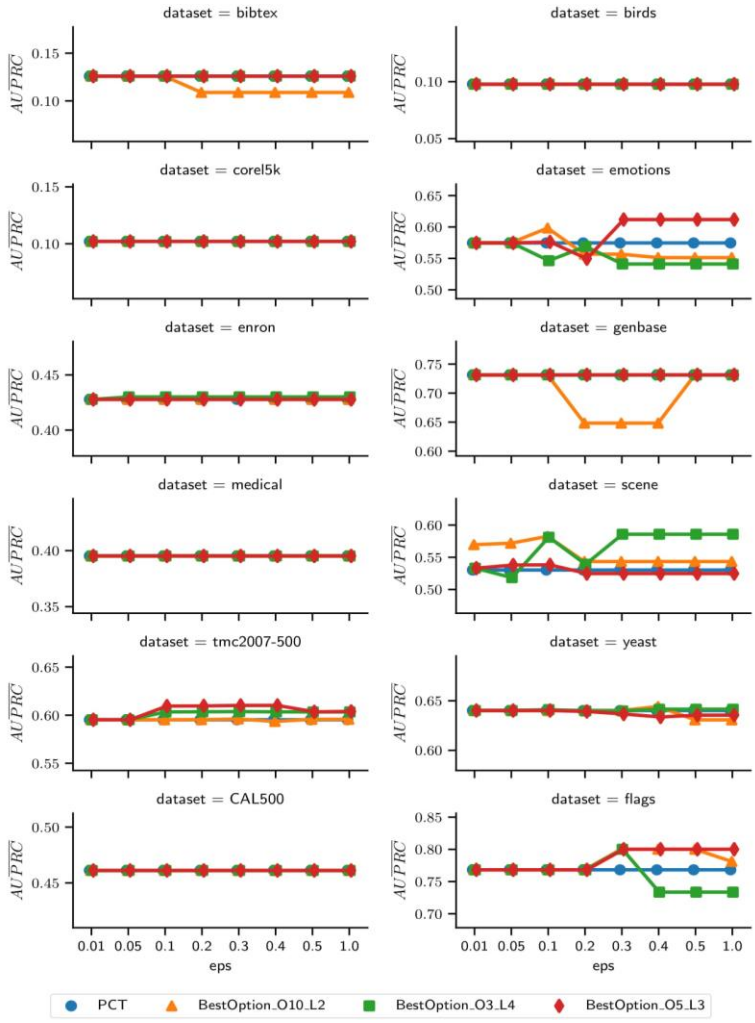

Figure 4

Performance of BestEmbedded trees produced by different parametrizations of OPCTs and selected based on training set performance, compared to the performance of a single PCT. Note that every graph is on a different scale.

4.2 Comparison of BestOptions and Standard PCTs

Figures 4 and 5 show the comparison of standard PCTs and the BestEmbedded trees extracted from OPCTs with different parameters. Figure 4 shows the results for BestEmbedded trees selected based on the training set performance, and Figure 5 based on the validation set performance. First thing we can notice is that

the BestEmbedded trees and PCTs often have very similar or identical performance. There are usually no significant differences in size as well. In fact, often the BestEmbedded tree is the same as the standard PCT, especially when it is selected based on the training set. This is not surprising, since standard PCTs choose splits that perform best on the training set at each step. We can also see that having a separate validation set for pruning can greatly improve the performance of both standard PCTs and BestEmbedded trees (the *bibtex*, *genbase*, *medical* and *tmc2007* datasets).

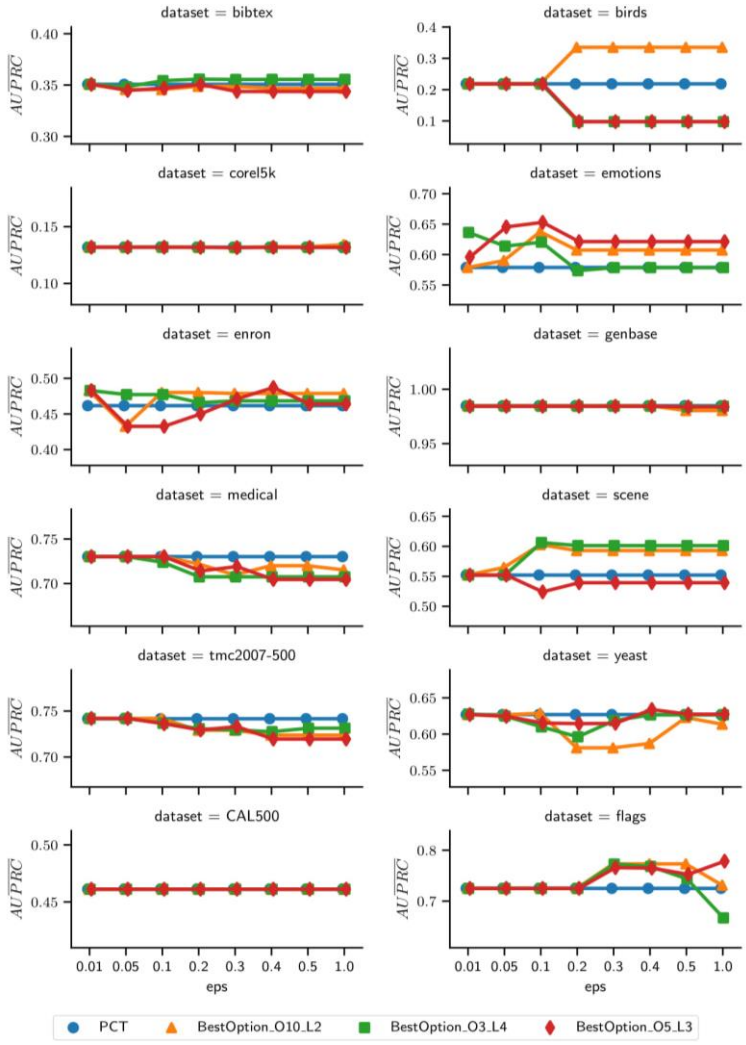

Figure 5
Performance of BestEmbedded trees produced by different parametrizations of OPCTs and selected based on validation set performance, compared to the performance of a single PCT. Note that every graph is on a different scale.

Another thing that the results show is that for extracting BestOptions, option nodes deeper in the tree are still helpful. While the parameter values (O, L) = (10, 2) always provided the best results for OPCTs as ensembles, even parameter values (O, L) = (3, 4) often lead to the best selection of BestEmbedded trees.

With larger OPCTs a larger space of trees is searched when selecting BestEmbedded trees, and that is where there are more differences compared to standard PCTs. Even when selected based on the training set performance, BestEmbedded trees often perform better than standard PCTs (on the *scene*, *tmc2007* and mostly *flags* datasets). But it also frequently happens that the BestEmbedded tree generalizes worse than the standard PCT (the *bibtex*, *emotions*, *genbase* and *flags* datasets).

Using a validation set to select the BestEmbedded tree mostly helps in selecting a tree that generalizes better, when compared to the train set selection. This can be nicely seen on the *bibtex*, *emotions*, *enron*, *scene* and *flags* datasets. However, in some cases it leads to a worse selection relatively to the standard PCT, as seen on the *medical*, *tmc2007* and *yeast* datasets. The cause for this may be oversearching, as described in [10]. By searching the space of trees more exhaustively, we have a higher chance of discovering "fluke" theories that fit the data well, but generalize poorly. As opposed to what is commonly understood as overfitting, these "fluke" theories are not overly complex. For example, when selecting the BestEmbedded tree, the standard PCT is always one of the options. It often happens that the tree with the best performance on the validation set is smaller (represents a simpler theory) than the standard PCT, but it still has a poorer performance on the test set.

4.3 Use Case Demonstration

We demonstrate the usefulness of OPCTs on the *emotions* dataset [6]. The examples in the *emotions* dataset are 30 seconds long music samples extracted from 100 different songs from different genres. The goal is to label the music samples with the emotions present in the music. There are 6 possible labels corresponding to 6 emotional clusters. The music samples are described with 8 rhythmic features and 64 timbre features.

Figure 6 shows an example of an OPCT trained on the *emotions* dataset for illustrative purpose. It was pruned to reduce the tree size to a humanly manageable proportions and contains only one option node with three options.

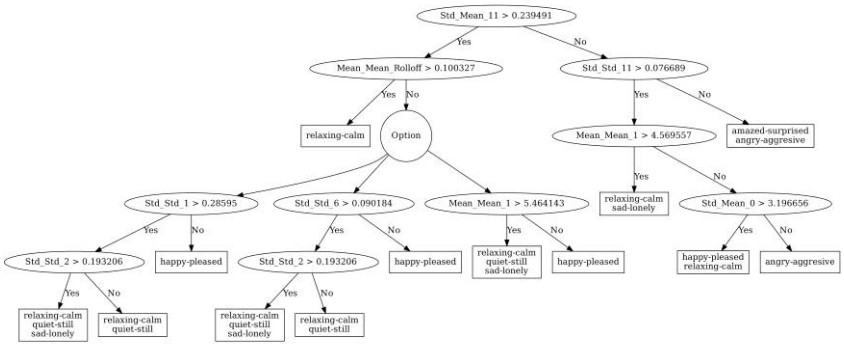

Figure 6

A heavily pruned OPCT constructed on the *emotions* dataset. Option nodes are represented as circles, standard split nodes have oval shape and leaf nodes are shown as boxes containing the labels predicted in that leaf.

Figure 7 shows a PCT trained using the standard top down induction algorithm.

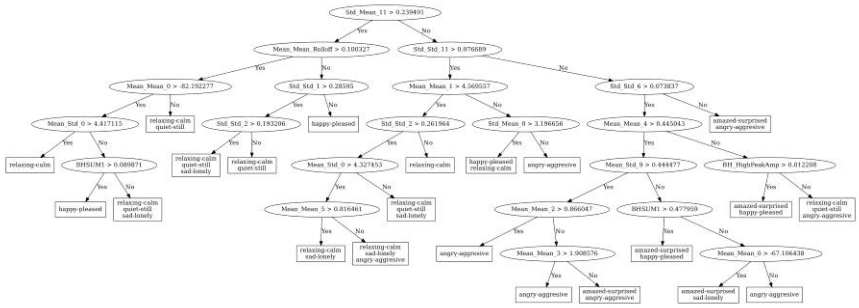

Figure 7

A standard PCT constructed on the *emotions* dataset. Split nodes have oval shapes and leaf nodes are shown as boxes containing the labels predicted in that leaf.

Figure 8 shows the BestEmbedded tree selected from OPCT_O5_L3 with ε=0.2. They were both pruned using the validation set. The standard PCT has 22 leaf nodes and it achieved 0.57 $AU\overline{PRC}$, while the BestEmbedded tree is much smaller with only 9 leaves and has better predictive performance with 0.62 $AU\overline{PRC}$. We can see that they differ already at the root node.

This demonstrates the ability of OPCTs to help us find better performing trees, which can even be smaller than standard trees. Ideally, the BestEmbedded trees can be selected by experts, looking at the OPCT and selecting the options that are consistent with their knowledge.

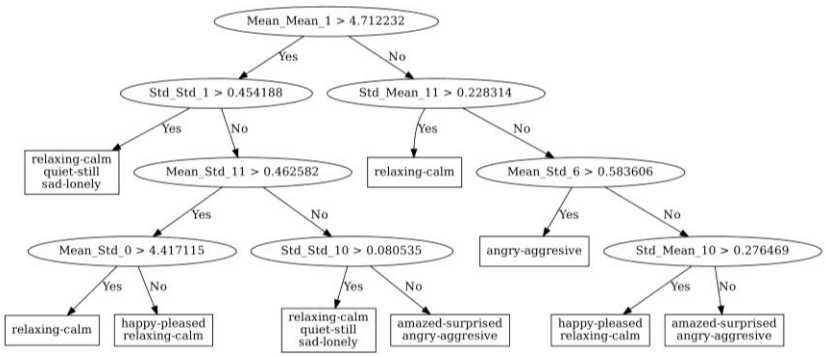

Figure 8
The BestEmbedded tree selected from OPCT_O5_L3 with ε=0.2 constructed on the *emotions* dataset. Standard split nodes have oval shapes and leaf nodes are shown as boxes containing the labels predicted in that leaf.

Conclusions

In this work, we present an algorithm for learning option predictive clustering trees for the task of multi-label classification, where every example is associated with a set of labels. OPCTs are global models that predict the entire label sets simultaneously and belong in the algorithm adaptation group of methods. The main purpose of the proposed algorithm is to reduce the myopia of the standard greedy algorithm for learning PCTs. During tree construction, if multiple tests have heuristic scores similar to that of the best test, an option node is created that contains a set of alternative sub-nodes, called options, i.e., a set of the best performing splits. When predicting the labels of an example, each option produces a prediction, and predictions from different options are then aggregated in the option node. This leads us to consider option trees as condensed representations of an ensemble of trees.

In addition to the pseudo-ensemble aspect of OPCTs, we can also look at them as a set of possible PCTs (embedded trees), and select one of them as the final model. This broadens the search over the space of possible trees and decreases the myopia of the algorithm. There are multiple ways of selecting the best embedded trees. In our experiments, we used the performance on the training set, and the performance on a validation set. Another option is to use expert knowledge to select the best options in the option tree.

We performed an experimental evaluation of the OPCT method and the BestEmbedded trees, and compared them to standard PCTs and bagging ensembles of PCTs. The evaluation was performed on 12 datasets appropriate for the MLC task, and we measured model performance with $AU\overline{PRC}$. The results show that large OPCTs can often reach the performance of tree ensembles, and that BestEmbedded trees can outperform standard trees. Unfortunately, we can also fall in the trap of oversearching and find BestEmbedded trees with worse

predictive performance compared to standard PCTs. We also looked into how different parameters affect the performance of OPCTs and BestEmbedded trees. We found that allowing more option nodes higher in the tree, while limiting them on the lower levels (parameter values $(O, L) = (10, 2)$) works best for OPCTs as ensembles. For BestEmbedded trees, option nodes lower in the tree are still useful and can help find better trees. We demonstrated the potential of OPCTs on a music emotion labelling dataset, where the BestEmbedded tree was much smaller than the standard PCT, yet had a better predictive performance.

There are several paths for further work. We would like to evaluate OPCTs and BestEmbedded trees in a domain where an expert would help select the best splits in the option nodes. Additionally, we plan to investigate the use of OPCTs for feature ranking and selection for MLC datasets.

Acknowledgement

We acknowledge the financial support of the Slovenian Research Agency via the grants P2-0103 and a young researcher grant to TS, as well as the European Commission, through the grants MAESTRA (Learning from Massive, Incompletely annotated, and Structured Data) and HBP (The Human Brain Project), SGA1 and SGA2. SD and DK also acknowledge support by Slovenian Research Agency (via grants J4-7362, L2-7509, N2-0056 and J2-9230), the European Commission (the LANDMARK project). The computational experiments presented here were executed on the computing infrastructure from the Slovenian Grid (SLING) initiative.

References

[1] M. L. Zhang and Z. H. Zhou, "ML-KNN: A lazy learning approach to multi-label learning," *Pattern Recognition,* Vol. 40, pp. 2038-2048, 2007

[2] C. Vens, J. Struyf, L. Schietgat, S. Džeroski and H. Blockeel, "Decision trees for hierarchical multi-label classification," *Machine Learning,* Vol. 73, pp. 185-214, 2008

[3] G. Tsoumakas and I. Vlahavas, "Random k-Labelsets: An Ensemble Method for Multilabel Classification," in *Proc. of the 18th European conference on Machine Learning*, 2007

[4] G. Tsoumakas, I. Katakis and I. Vlahavas, "Mining Multi-label Data," in *Data Mining and Knowledge Discovery Handbook*, Springer Berlin / Heidelberg, 2010, pp. 667-685

[5] G. Tsoumakas, I. Katakis and I. Vlahavas, "Effective and Efficient Multilabel Classification in Domains with Large Number of Labels," in *Proc. of the ECML/PKDD Workshop on Mining Multidimensional Data*, 2008

[6] K. Trochidis, G. Tsoumakas, G. Kalliris and I. Vlahavas, "Multi-label classification of music into emotions," 2008

[7] T. Stepišnik Perdih, A. Osojnik, S. Džeroski and D. Kocev, "Option Predictive Clustering Trees for Hierarchical Multi-label Classification," in *Discovery Science*, 2017

[8] R. E. Schapire and Y. Singer, "BoosTexter: A Boosting-based System for Text Categorization," *Machine Learning,* Vol. 39, No. 2, pp. 135-168, 2000

[9] J. Read, B. Pfahringer, G. Holmes and E. Frank, "Classifier chains for multi-label classification," *Machine Learning,* Vol. 85, pp. 333-359, 2011

[10] J. R. Quinlan and R. M. Cameron-Jones, "Oversearching and Layered Search in Empirical Learning," in *Proceedings of the 14th International Joint Conference on Artificial Intelligence - Volume 2*, San Francisco, CA, USA, 1995

[11] Osojnik, S. Džeroski and D. Kocev, "Option predictive clustering trees for multi-target regression," in *Discovery Science: 19th International Conference (DS 2016)*, 2016

[12] G. Madjarov, D. Kocev, D. Gjorgjevikj and S. Džeroski, "An extensive experimental comparison of methods for multi-label learning," *Pattern Recognition,* Vol. 45, pp. 3084-3104, 2012

[13] R. Kohavi and C. Kunz, "Option Decision Trees with Majority Votes," in *Proceedings of the 14th International Conference on Machine Learning*, San Francisco, CA, USA, 1997

[14] D. Kocev, C. Vens, J. Struyf and S. Džeroski, "Tree ensembles for predicting structured outputs," *Pattern Recognition,* Vol. 46, pp. 817-833, 2013

[15] D. Kocev, J. Struyf and S. Džeroski, "Beam search induction and similarity constraints for predictive clustering trees," in *Proc. of the 5th Intl Workshop on Know. Disc. in Inductive Databases KDID - LNCS 4747*, 2007

[16] E. Ikonomovska, J. Gama, B. Zenko and S. Dzeroski, "Speeding-Up Hoeffding-Based Regression Trees With Options," in *Proceedings of the 28th International Conference on Machine Learning, ICML 2011*, 2011

[17] J. Fürnkranz, "Round robin classification," *Journal of Machine Learning Research,* Vol. 2, pp. 721-747, 2002

[18] K. Crammer and Y. Singer, "A family of additive online algorithms for category ranking," *Journal of Machine Learning Research,* Vol. 3, pp. 1025-1058, 2003

[19] W. Buntine, "Learning classification trees," *Statistics and Computing,* Vol. 2, pp. 63-73, 1992

[20] L. Breiman, J. Friedman, R. A. Olshen and C. J. Stone, Classification and Regression Trees, Chapman & Hall/CRC, 1984

[21] L. Breiman, "Bagging Predictors," *Machine Learning,* Vol. 24, pp. 123-140, 1996

[22] H. Blockeel, L. D. Raedt and J. Ramon, "Top-down induction of clustering trees," in *Proceedings of the 15th International Conference on Machine Learning*, 1998

[23] H. Blockeel and J. Struyf, "Efficient algorithms for decision tree cross-validation," *Journal of Machine Learning Research,* Vol. 3, pp. 621-650, 2002

Appendix – additional results

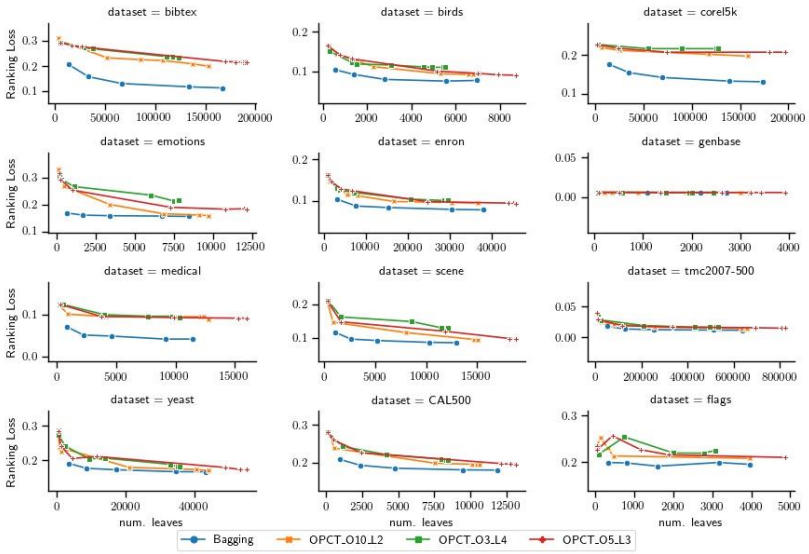

Figure 9

Comparison of bagging and OPCTs using the ranking loss measure. For details see Figure 3.

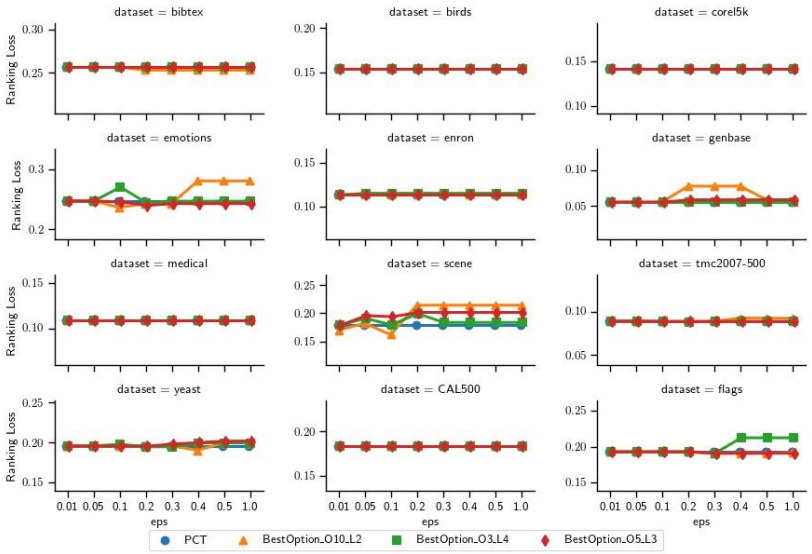

Figure 10
Comparison of PCTs and BestOption trees selected based on the training set performance using the ranking loss measure

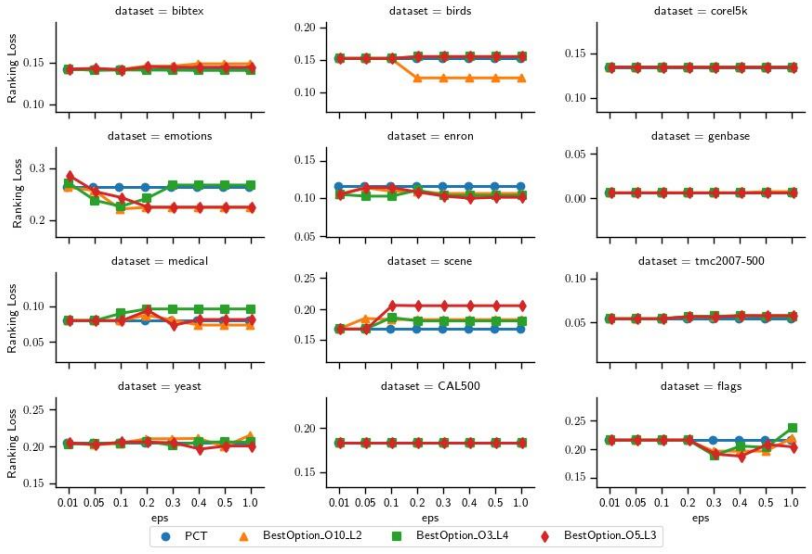

Figure 11
Comparison of PCTs and BestOption trees selected based on the validation set performance using the ranking loss measure

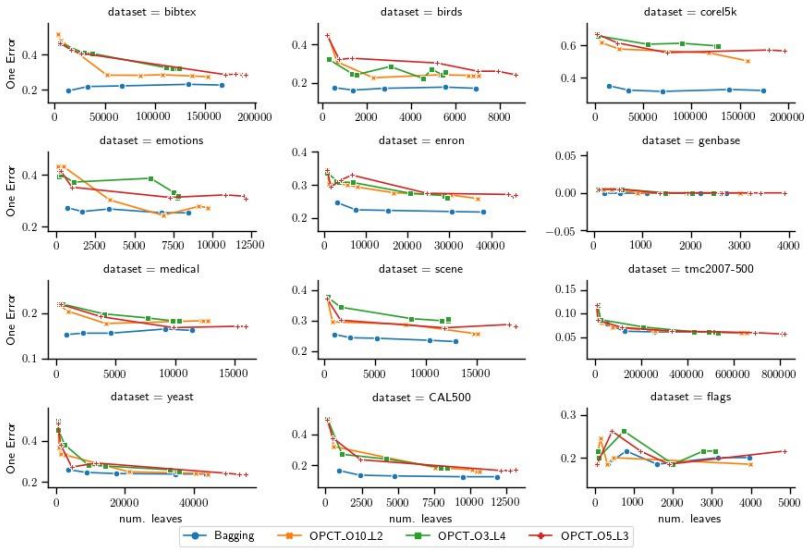

Figure 12

Comparison of bagging ensembles and OPCTs using the one error measure. For details see Figure 3.

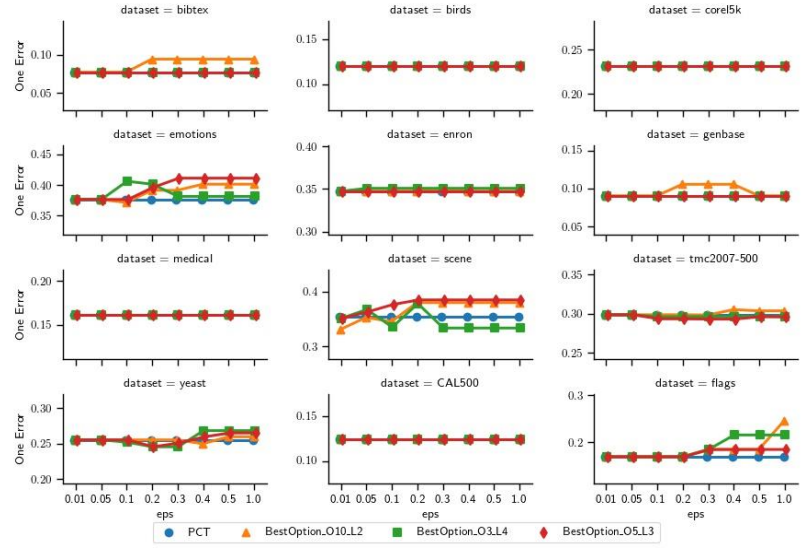

Figure 13

Comparison of PCTs and BestOption trees selected based on the training set performance using the one error measure

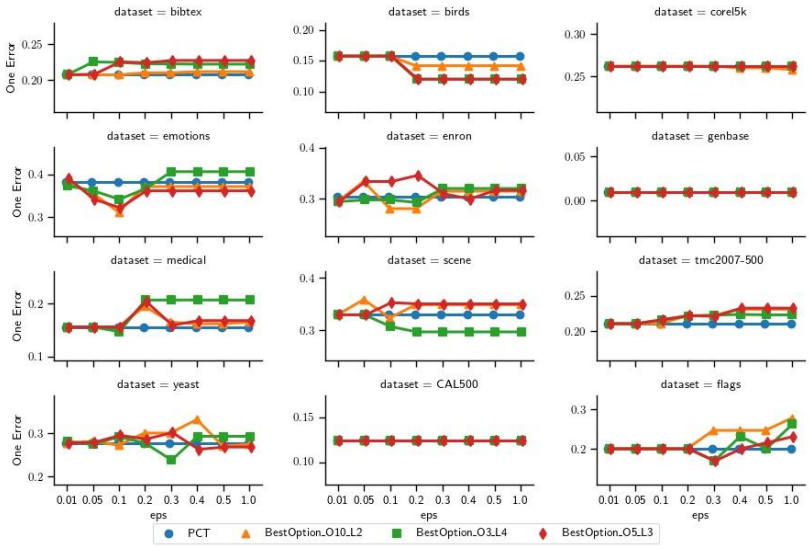

Figure 14

Comparison of PCTs and BestOption trees selected based on the validation set performance using the one error measure

Feature Ranking for Hierarchical Multi-Label Classification with Tree Ensemble Methods

Matej Petković, Sašo Džeroski, Dragi Kocev

Jožef Stefan Institute, Jamova 39, 1000 Ljubljana, Slovenia
Jožef Stefan Postgraduate School, Jamova 39, 1000 Ljubljana, Slovenia
{matej.petkovic, saso.dzeroski, dragi.kocev}@ijs.si

Abstract: In this work, we address the task of feature ranking for hierarchical multi-label classification (HMLC). The task of HMLC concerns problems with multiple binary variables, organized into a hierarchy of target attributes. The goal is to train a model to learn and accurately predict all of them, simultaneously. This task is receiving increasing attention from the research community, due to its wide application potential in text document classification and functional genomics. Here, we propose a group of feature ranking methods based on three established ensemble methods of predictive clustering trees: Bagging, Random Forests and Extra Trees. Predictive clustering trees are a generalization of decision trees, towards predicting structured outputs. Furthermore, we propose to use three scoring functions for calculating the feature importance values: Symbolic, Genie3 and Random Forest. We test the proposed methods on 30 benchmark HMLC datasets, show that Symbolic and Genie3 scores return relevant rankings, that all three scores outperform the HMLC-Relief ranking method and are computed in very time-efficient manner. For each scoring function, we find the most appropriate ensemble method and compare the scores to find the best one.

Keywords: hierarchical multi-label classification; feature ranking; ensemble methods; Relief

1 Introduction

Classification is a task in predictive modelling, where we develop a model that takes a vector $\boldsymbol{x}$ of descriptive variables (features) x_i as the input, and predicts the class value y, for a given example. If y can take two different values, the task at hand is referred to as binary classification. Otherwise (y can take more than two values), the task at hand is multi-class classification. In both cases, every example is assigned precisely one value. For example, one can predict whether a person is sick, where $y \in \{yes, no\}$ (binary), or what is the blood type of a person where $y \in \{A, B, AB, 0\}$ (multi-class). In both cases, class values are mutually exclusive. A related task is multi-label classification (MLC). As opposed to the standard

classification, a MLC predictive model predicts which labels l from a predefined set $\mathcal{L}$ are *relevant* for a given example. For example, one can predict which of the genres from the set $\mathcal{L} = \{romance, drama, comedy\}$ are relevant for a given film. Clearly, a film can be *drama* and *comedy* at the same time.

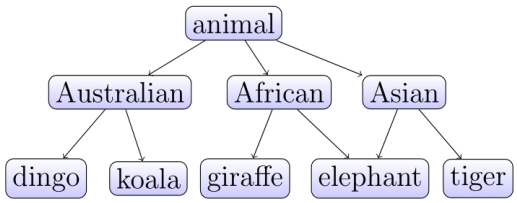

Figure 1
An exemplary hierarchy of animals

Hierarchical MLC (HMLC) is a generalization of MLC, where the labels are organized into a hierarchy that is given as a binary relation $\prec$, which partially orders the set $\mathcal{L}$. If $l_1 \prec l_2$, we say that l_1 is a predecessor of l_2. This relation imposes the *hierarchical constraint*: If l is relevant for a given example then all the predecessor labels are also relevant for the example. Fig. 1 shows a toy hierarchy of groups of animals. For example, $animal \prec l$ for all labels $l \in \mathcal{L}$, $Asian \prec tiger$ etc. The label *elephant* has two parents (*African* and *Asian*) and one additional predecessor (*animal*). Thus, if an example is an *elephant*, then it is also an *African*, *Asian* and an *animal*. If every label has, at most, one parent, the hierarchy is tree-shaped. Otherwise (as it is the case in the toy hierarchy), it is a general directed acyclic graph (DAG). In this paper, DAG refers only to the hierarchies that are not also tree-shaped.

HMLC is a practically relevant task with problems occurring in life sciences (e.g., gene function prediction, disease classification), environmental sciences (e.g., habitat modelling, remote sensing), multimedia (e.g., image classification and retrieval) and semantic web (classification and analysis of text and web pages). Furthermore, many of the datasets used in this study (the data with -GO in their names) are from functional genomics - the goal there is to assign to each gene the multiple functions it has. In turn, the gene functions are organized into an ontology that takes the form of a DAG known as Gene Ontology (GO) [7].

It has been shown in several studies that use of a hierarchy improves the performance as compared to MLC in a variety of domains. For example, [29] show that the task of HMLC is beneficial to exploit the interdependencies among the labels. In [18] it is shown that the use of hierarchy helps obtain better single tree models. Moreover, [20] shows that MLC can be approached as HMLC by constructing hierarchies of the labels by clustering the label co-occurrences.

However, it is still possible to approach HMLC problems by ignoring the hierarchy at the learning phase and use any of the MLC methods, such as binary relevance or power set approach [28]. Binary relevance is a simple method that

converts a MLC task to several binary classification tasks with y ∈ {*yes*, *no*} where we predict the relevance of each label separately. This approach is often criticized for it cannot make use of the interactions among the labels. In the label power set approach, the task of predicting a subset of $\mathcal{L}$ is converted to the task of predicting an element of the power set $2^{\mathcal{L}}$, and thus converting a MLC task to a multi-class classification task. However, the number of classes can be as high as $2^{|\mathcal{L}|}$ which results in a very sparse dataset. At prediction stage, predecessors of the labels predicted as relevant, must be added to the set of relevant labels, so that the hierarchical constraint is met. A similar two-step approach [1] learns support vector machines for each class separately, and then combines the predictions using a Bayesian network model so that the hierarchical constraint is met. However, method adaptation techniques where an existing method is adapted to a new problem may be more appropriate. This can be done with predictive clustering trees (PCTs), which were shown to outperform their basic versions that follow the binary relevance approach [29].

In this paper, we do not address the task of building predictive models for HMLC. Rather, we propose a feature ranking method that is useful in this context. Feature ranking is another important task in machine learning, where the goal is to assess the importance of every descriptive attribute (feature) by using some scoring function. The output of a feature ranking algorithm is a list of features that is sorted with respect to the scores.

Feature ranking is typically considered a part of data preprocessing, since it can be used to reduce the dimensionality of the input space, so that only the features that contain the most information about the labels (or target(s) in general) are kept in the dataset. By doing this, we decrease the computational cost of building a predictive model, while the performance of the model is not degraded. Another reason to compute a feature ranking is that dimensionality reduction typically results in models that are easier to understand, which is useful when a machine learning and domain experts collaborate. Predictive models, such as decision trees, are easier to interpret when a small number of the relevant features are used to learn them.

There is a plethora of feature ranking methods for the task of classification [27]. A possible approach to MLC feature ranking is to adapt the binary relevance approach from predictive modelling, where at the first stage, feature importance values are computed for every label $l \in \mathcal{L}$ separately as in the classification case. After that, the feature importance values are averaged over the different labels and a single ranking is returned. However, the landscape of methods for feature ranking for HMLC is not well populated, due to the complexity of the task.

This work contains the following contributions:

a) We propose a group of novel feature ranking approaches for HMLC that base on the Symbolic, Genie3 [13] and Random Forest [4] scoring

functions, coupled with Bagging, Random Forests and Extra Trees ensembles of PCTs for HMLC [16, 25]

b) We develop the parameter-less version of the Symbolic score. The earlier version has been (as well as the other two scores) previously evaluated in the context of multi-target regression [22]

c) We evaluate the proposed approaches on 30 HMLC benchmark datasets by using kNN model that uses feature importance scores in the distance function: we compare them to two baselines and show that the proposed scoring functions outperform i) the non-informed ranking where all features have equal importance; ii) the adaptation of Relief algorithm to HMLC [26]

The rest of the paper is organized as follows. In part 2, we describe predictive clustering trees, ensembles thereof and the proposed feature ranking scores. Then, we proceed to the HMLC-Relief description. In part 3, the experimental design is given. In part 4, the results are presented and finally, we summarize in the Conclusion Section.

2 Methods

We first present the ensemble-based feature rankings and then proceed to the Relief ranking. Both PCT framework and the Relief family of algorithms is implemented in the CLUS system (http://source.ijs.si/ktclus/clus-public).

2.1 Predictive Clustering Trees and Ensembles Thereof

PCTs generalize decision trees and can be used for a variety of learning tasks, including clustering and different types of structured output prediction tasks, e.g., multi-target regression, multi-label classification, hierarchical multi-label classification, time series prediction etc. [3] [16]. PCTs are induced with the standard greedy top-down induction of decision trees algorithm [5]. The heuristic h that is used for selecting the tests guides the algorithm towards small trees with good predictive performance. If there are no candidate tests, a leaf is created and the prototype of the instances belonging to that leaf is computed.

In the HMLC case, the heuristic function is defined as follows. First, a label subset $S \subseteq \mathcal{L}$ is converted into 0/1-vector $\boldsymbol{s}$ of length $|\mathcal{L}|$, where $\boldsymbol{s_j} = 1 \Leftrightarrow l_j \in S$. We denote the variance of $\boldsymbol{s_j}$ over subset of examples $E \subseteq \mathcal{D}_{\text{TRAIN}}$ as $var_j(E)$. Additionally, each label l_j is assigned a weight w_j that is defined as $w_j = \alpha\ \overline{w}(Parents(l_j))$ if the set of parents $Parents(l_j)$ is not empty and $w_j = 1$ otherwise (in the root(s) of the hierarchy). The function $\overline{w}(P)$ returns the average weight of the

label set P, and the parameter $\alpha \in (0, 1)$ is user-defined. Then, the impurity function is defined as $impurity(E) = \sum_{j=1}^{|\mathcal{L}|} w_j var_j(E)$, hence the labels l_j that are closer to the root of the hierarchy have bigger influence on the heuristic function. Motivation for this is - considering the example in Fig. 1 - that one can only correctly predict leaf labels (*dingo* versus *koala*) if the correct predictions are made for their predecessors (*Australian* versus *African*). Heuristic h is defined as the decrease of the impurity after applying the test. In a leaf L, the prototype function returns a vector whose j-th component equals the average value of s_j of the examples belonging to L.

To calculate feature importance scores (i.e., feature rankings), we grow ensembles of PCTs instead of growing a single one. An ensemble is a set of base predictive models, whose prediction for each new example is made by combining the predictions of the models from the ensemble. In HMLC tasks, this is typically achieved by taking the average of the base-model predictions. In our experiments, we used the following three approaches.

Random Forests, Bagging. In the Random Forests ensemble, instead of being derived from the original dataset $\mathcal{D}_{\text{TRAIN}}$, each tree in the ensemble is learned from a different bootstrap replicate B of the dataset $\mathcal{D}_{\text{TRAIN}}$, called bag. Additionally, we choose a random subset S of features in every internal node of the tree, and consider only the tests that are yielded by the features in S when looking for the best test. Typical size of the set S is of the order $log\ F$ or $root(F)$, where F is the number features in $\mathcal{D}_{\text{TRAIN}}$. If $|S| = F$, we obtain the Bagging procedure.

Extra Trees. Each tree is being developed directly from $\mathcal{D}_{\text{TRAIN}}$, but the candidate tests for each node are now extremely randomized. Again, we chose a random subset S of features in every internal node of the tree, and consider only one randomly chosen test per chosen feature, when looking for the best test.

2.2 Ensemble Scores

Once we build an ensemble of PCTs, we can exploit the ensemble structure to compute the feature ranking in three different ways. In the following, we denote a tree as TR, whereas $N \in TR$ denotes a node. Trees form a forest FO. Its size (the number of trees in the forest) is denoted as $|FO|$. The set of all internal nodes of a tree TR in which the feature x_i appears as part of a test is denoted as $\text{TR}(x_i)$.

Symbolic Ranking. In the simplest version of the score, we would count how many times a given feature occurs in the tests in the internal nodes of the trees. Since the features that appear closer to the root are intuitively more important than those that appear deeper in the trees, we weight these occurrences by the number of examples $e(N)$ that reach a node N, and define the feature importance as

$$importance_{SYMB}(x_i) = \frac{1}{|FO|} \sum_{TR \in FO} \sum_{N \in TR(x_i)} e(N) \,/\, |\mathcal{D}_{\text{TRAIN}}| \qquad (1)$$

Genie3 Ranking. The main motivation for Genie3 ranking is that splitting the current subset $E \subseteq \mathcal{D}_{\text{TRAIN}}$, according to a test where an important attribute appears, should result in high impurity reduction. The Genie3 importance of the feature x_i is thus defined as:

$$importance_{GENIE3}(x_i) = \frac{1}{|FO|}\sum_{TR\in FO}\sum_{N\in TR(x_i)} h^* \quad (2)$$

where h^* is the heuristic value of the variance reduction function. Since h^* is proportional to $e(N)=|E|$, greater emphasis is again put on the attributes higher in the tree, where $|E|$ is larger.

Random Forest Ranking. (To avoid confusion, we use the plural form (Random Forests) to refer to the ensemble method, and singular form to refer to the feature ranking score (Random Forest)). This feature ranking method tests how much the noise in a given feature decreases the predictive performance of the trees in the forest. The greater the performance degradation, the more important the feature is. In contrast to the first two feature rankings which can be computed for all three ensemble methods, this score cannot be used with ensembles of Extra Trees, since it uses the internal out-of-bag estimates of the error.

Once a tree *TR* is grown, the algorithm evaluates the performance of the tree by using the corresponding OOB_{TR} examples. This results in the predictive error $err(OOB_{TR})$, where lower error value corresponds to better predictions. To assess the importance of the feature x_i for the tree *TR*, we randomly permute its values in the set OOB_{TR} and obtain the set OOB_{TR}^{i}. Then, the error $err(OOB_{TR}^{i})$, is computed and the importance of the feature x_i for the tree *TR* is defined as the relative increase of error after noising. The final Random Forest score of the feature is the average of these values over all trees in the forest, namely:

$$importance_{RF}(x_i) = \frac{1}{|FO|}\sum_{TR\in FO}\frac{err\left(OOB_{TR}^{i}\right)-err(OOB_{TR})}{err(OOB_{TR})} \quad (3)$$

2.3 HMLC-Relief Ranking

The Relief family of feature ranking algorithms calculates the feature importance scores by considering differences in the feature values between pairs of examples (an example and its nearest neighbors). More specifically, if the values of features of a pair of examples from the same class are different then the features' importance decreases. Conversely, if the feature values are different for examples from different classes then the features' importance increases.

The values of the importance $importance_{Relief}(x_i)$ in the Relief can be written in a probabilistic fashion [17]: simplified to some extent, we have a relation:

$$importance_{Relief}(x_i) = \frac{P_{diffAttr,\ diffTarget}(i)}{P_{diffTarget}} - \frac{P_{diffAttr}(i)-P_{diffAttr,\ diffTarget}(i)}{1-P_{diffTarget}} \quad (4)$$

where we define the probabilities $P_{ev} = P(ev)$ and $P_{ev1,ev2} = P(ev1 \wedge ev2)$ that base on the events *diff/sameAttr* (two instances have different/same value of x_i) and *diff/sameTarget* (two instances have different/same target value). The probabilities in Eq. (4) are modeled as the distances in the corresponding spaces: $P_{diffAttr}$ is modeled by the distance d_i on the domain of feature x_i, $P_{diffTarget}$ is modeled by the distance $d_{\mathcal{L}}$ between two label subsets of $\mathcal{L}$, and $P_{\text{diffAttr,diffTarget}}$ is modeled as their product $d_i \, d_{\mathcal{L}}$. This enables the generalization not only to numeric attributes and targets, but also to more complex target types, such as hierarchies as described in [26]. However, it must be assured that the upper bound of all distances is 1, which was overlooked in [26]. There, they proceed as follows:

First, the distances d_i on the feature domains X_i, and the distance d_X on whole descriptive domain X are defined as:

$$d_i(\boldsymbol{x}^1, \boldsymbol{x}^2) = \begin{cases} \mathbf{1}[x_i^1, x_i^2] & : X_i \notin \mathbb{R} \\ \frac{|x_i^1 - x_i^2|}{\max_{\boldsymbol{x}} x_i - \min_{\boldsymbol{x}} x_i} & : X_i \subseteq \mathbb{R} \end{cases} \qquad d_X = \frac{1}{F} \sum_{i=1}^{F} d_i(\boldsymbol{x}^1, \boldsymbol{x}^2) \tag{5}$$

where $\mathbf{1}$ is the indicator function defined as $\mathbf{1}[true] = 1$ and $\mathbf{1}[false] = 0$. The distance between two label sets S_1 and S_2 is defined as a weighted Euclidean distance between the corresponding 0/1-vectors $\boldsymbol{s}^1$ and $\boldsymbol{s}^2$ where $s_j^{1,2}$ and w_j are defined as in Sec. 2.1. We correct this and define as:

$$\mu = 1 / \max_{S, S'} d_E(S, S') \quad \text{and} \quad d_{\mathcal{L}}(S_1, S_2) = \mu \, d_E(S_1, S_2) \tag{6}$$

The algorithm iteratively estimates the probabilities in Eq. (4) by randomly sampling the training dataset and comparing the chosen example r to its nearest neighbors $\boldsymbol{n}_j$. This is repeated m times and the estimate for $P_{diffTarget}(i)$ is thus,

$$P_{diffAttr}(i) = \frac{1}{mK} \sum_{r} \sum_{k=1}^{K} d_i(\boldsymbol{r}, \boldsymbol{n}_j).$$

The other probabilities are estimated analogously. The weight *1/mK* ensures that the computed importance values are between -1 and 1. The values of the two parameters are set as follows. Typically, we iterate over the whole dataset, i.e., $m = |\mathcal{D}_{\text{TRAIN}}|$. By doing this, the estimates of probabilities are expected to be more accurate. The value of K is typically set small enough to capture the local structure in the data. In that way, we implicitly capture the interactions between features [17]. Previous experiments [17] [21] have shown that $K = 10$ or $K = 15$ give the best performance.

The normalization factor in the numeric part of the definition of d_i in Eq. (5) is trivial to compute. However, this is not the case with the μ in Eq. (6), if we want to do that efficiently. For tree-shaped hierarchies, we developed an efficient algorithm for computing μ that recursively finds the distance-maximizing pair of the labels in $O(|\mathcal{L}|)$ time. If hierarchy is a general DAG we could not do considerably better than computing the maximizing pair by exhaustive search.

3 Experimental Design

3.1 Experimental Questions

The experiments were designed to answer the following experimental questions:

1) Given an ensemble feature ranking score, after which number of trees in the ensemble the quality of the ranking saturates?
2) Do the proposed ensemble feature ranking scores yield relevant rankings, i.e., can the additional information captured in the feature ranking boost the performance of the non-informed baseline classifier?
3) Do the proposed ensemble feature ranking scores outperform the improved version of HMLC-Relief algorithm?
4) Given an ensemble feature ranking score, which ensemble method is the most suitable?
5) Which ensemble feature ranking score yields the best rankings?

3.2 Datasets

We use 30 HMLC benchmark problems whose characteristics are summarized in Tab. 1. Most of the datasets have a few thousand of examples while the number of features could be as high as 74435. The label set typically contains a few hundred elements. Approximately 25% of the hierarchies are DAGs. Many of the datasets are microarray data and come from the field of functional genomics. They describe the connection between description of proteins and their functional classes that are taken from Gene Ontology [7] (the corresponding hierarchies are DAGs), or the MIPS functional hierarchy (http://mips.helmholtz-muenchen.de/funcatDB) (the corresponding hierarchies are tree-shaped). Some other datasets are about text categorization of the processed news (reuters), patent classification according to the World International Patent Organization (wipo) etc.

Table 1
Properties of the datasets: data size $|\mathcal{D}|$ given as the sum $|\mathcal{D}_{\text{TRAIN}}| + |\mathcal{D}_{\text{TEST}}|$ of training and test set sizes, number of features F, shape of the hierarchy, label set size, depth of the hierarchy (max d), and average leaf depth (average d) of the hierarchy

Dataset	$\|\mathcal{D}\|$	F	**shape**	$\|\mathcal{L}\|$	**max d**	**avg d**
cellcycle-yeast-FUN [6]	2482+1284	77	tree	751	4	4
church-yeast-FUN [6]	2480+1284	27	tree	751	4	4
clef07a-is [9]	10000+1006	80	tree	152	3	3
derisi-yeast-FUN [6]	2455+1278	63	tree	751	4	4

diatoms [11]	726+372	200	tree	81	2	2
eisen-yeast-FUN [6]	1588+837	79	tree	751	4	4
enron-corr [14]	988+660	1001	tree	67	3	2.2
expr-yeast-FUN [6]	2494+1294	552	tree	751	4	4
exprindiv-ara-FUN [6]	2314+1182	1251	tree	424	4	2.8
exprindiv-ara-GO [6]	7161+3679	1251	DAG	627	6.5	5.6
gasch1-yeast-FUN [6]	2486+1287	173	tree	751	4	4
hom-ara-FUN [6]	2260+1213	72869	tree	420	4	2.8
hom-ara-GO [6]	7119+4002	72869	DAG	623	6.5	5.6
hom-yeast-FUN [6]	2549+1318	47034	tree	751	4	4
icpr2010 [11]	4913+2999	4000	tree	76	3	2.5
interpro-ara-FUN [6]	2455+1264	2815	tree	427	4	2.8
interpro-ara-GO [6]	7778+3985	2815	DAG	630	6.5	5.6
pheno-yeast-FUN [6]	1010+582	69	tree	751	4	4
reuters [19]	3000+3000	47236	tree	143	4	2.5
scop-ara-FUN [6]	2055+1042	2003	tree	407	4	2.8
scop-ara-GO [6]	6507+3336	2003	DAG	572	6.5	5.7
seq-ara-FUN [6]	2455+1264	4450	tree	424	4	2.8
seq-ara-GO [6]	7778+3985	4450	DAG	630	6.5	5.6
seq-yeast-FUN [6]	2590+1342	478	tree	751	4	4
spo-yeast-FUN [6]	2442+1269	80	tree	751	4	4
struc-ara-FUN [29]	2455+1264	14804	tree	427	4	2.8
struc-ara-GO [29]	7778+3985	14804	DAG	630	6.5	5.6
struc-yeast-FUN [29]	2535+1316	19628	tree	751	4	4
wipo [24]	1352+358	74435	tree	528	4	4
yeast-GO [1]	2310+1155	5930	DAG	133	7.3	4.7

3.3 Evaluation Procedure

In our experiments, we use the same train/test splits of the datasets as the original authors, for all the data sets. First, a feature ranking is computed from the training set $\mathcal{D}_{\text{TRAIN}}$. Its quality is assessed by the k-nearest neighbor (kNN) algorithm in which the weighted version of Euclidean distance is used instead of the standard one, i.e., $d_E(\boldsymbol{x}^1, \boldsymbol{x}^2) = \sqrt{\sum_i w_i d_i^2(\boldsymbol{x}^1, \boldsymbol{x}^2)}$, where $\boldsymbol{x}^{1,2}$ are the input vectors of nominal/numeric feature values and d_i is defined by Eq. (5). Since the rankings that base on the Random Forest score and HMLC-Relief could contain negative relevance scores, which in both cases means that the feature is more irrelevant that a random feature would be, the weights are defined as $w_i = \max\{0, importance(x_i)\}$.

This evaluation procedure was chosen because kNN classifier is a distance-based model that can directly make use of feature importance values, learned in the first

phase of procedure. The second reason for our choice was kNN's simplicity: its only parameter is the number of neighbors, which we set to 10.

The rationale for using kNN as an evaluation model is as follows. If a feature ranking is meaningful, then when the feature importance values are used as weights in the calculation of the distances kNN should produce better predictions as compared to kNN without using these weights [30]. Once the kNN model is trained on $\mathcal{D}_{\text{TRAIN}}$, its performance on $\mathcal{D}_{\text{TEST}}$ is measured in terms of the area under the average precision-recall curve $AU\overline{PRC}$ [29] which is computed as follows. First, we define multi-set $P = \{(v_{i,l}, p_{i,l}) \mid l \in \mathcal{L}, (\boldsymbol{x}_i, S_i) \in \mathcal{D}_{\text{TEST}}\}$ where $v_{i,l} = \mathbf{1}[l \in S_i]$ and $p_{i,l} \in [0, 1]$ is the predicted probability of $l \in S_i$. After that, the numbers of true positives tp_θ, false positives fp_θ and false negatives fn_θ are computed, for all $\theta \in [0, 1]$, e.g., $tp_\theta = |\{(v, p) \in P \mid v = 1, p \geq \theta\}|$. From these, we compute recall $r_\theta = tp_\theta / (tp_\theta + fn_\theta)$ and precision $p_\theta = tp_\theta / (tp_\theta + fp_\theta)$, define the curve $PRC = \{(r_\theta, p_\theta) \mid \theta \in [0, 1]\}$, and compute the area under it.

It might seem that another possible approach to evaluation is extending a dataset with some randomly generated features and then see whether they are ranked at the bottom of the ranking. However, this approach is more suitable for synthetic data where the ground truth is known and all features can be made relevant. In the real world data, it may very well happen that some of the high-dimensional datasets indeed contain completely irrelevant features, hence, using this approach would yield incorrect performance estimates.

3.4 Statistical Analysis of the Results

We use the Wilcoxon's test for comparing two algorithms, and Friedman's test for comparing more than two. In both cases, the null hypothesis is that all considered algorithms have the same performance. If it is rejected by the Friedman's test, we additionally apply Nemenyi's post-hoc test to investigate where the statistically significant differences between the algorithms occur. A detailed description of all tests is available in [8]. When performing Wilcoxon's tests whose outcomes are not independent, we control the false discovery rate by the Benjamini-Hochberg procedure [2]: let p_i be the i-th smallest among the obtained p-values, and t the number of tests. Let i_0 be the largest i, such that $p_i \leq \alpha_i^* := (i / t)\, \alpha$. Then, we can reject the hypotheses belonging to p-values p_i, for $1 \leq i \leq i_0$.

The results of the Nemenyi's tests are presented on average ranks diagrams. Each diagram shows the average rank of the algorithm over the considered datasets, and the critical distance, i.e., the distance for which average ranks of two considered algorithms must differ to be considered statistically significantly different. Additionally, the groups of algorithms among which no statistically significant differences occur are connected with a line. If Friedman's test did not reject the null hypothesis, all algorithms on the average rank diagram are connected with the same line, and no critical distance is given.

Before proceeding with the statistical analysis, we round the performances to three significant digits. In the analysis, the significance level was set to $\alpha = 0.05$.

3.5 Parameter Instantiation

First, we give the parameters used in the process of obtaining the ensemble-based rankings. Afterwards, we give those for HMLC-Relief.

We consider the following ensemble sizes: $|FO| \in \{10, 25, 50, 75, 100, 150, 250\}$. Since 100 trees is a typical recommended value [15], this should be enough. This is the only parameter for Bagging, while Random Forests and Extra Trees method need another one: the number of features F considered in each internal node as described in Sec. 2.1. The recommended value for Random Forests is F' = *root(F)* [15] and F' = F for Extra Trees [15]. However, if we carefully examine the data, we see that are some datasets, e.g., enron-corr and struc-ara-GO, for which the diversifying mechanism of the Extra Trees algorithm does not work if we set F' = F, since every single one of the attributes takes, at most, two values, which results in only one possible split per attribute. Thus, we rather choose F' = root(F) for Extra Trees also, since a necessary condition for an ensemble to be more accurate than any of its individual members, is that the members are diverse models [12].

If we fix the ensemble size and feature ranking score and compare the quality of the rankings from the ensembles of Extra Trees that use *root(F)*- and F-feature subsets via Wilcoxon's test, the results show that *root(F)*-version of the ensemble statistically significantly outperforms the F-version on the problematic datasets, and that there are no statistically significant differences on the other datasets.

As for Relief algorithm, it has been shown in the previous experiments that the Relief algorithm is quite robust regarding the value of the number of neighbors K and that no other value outperforms K = 15 [17] [21], hence we will adhere to this value. Since the datasets are not all of equal size, the number of iterations m in HMLC-Relief algorithm is given as the proportion of the size of $\mathcal{D}_{\text{TRAIN}}$. The considered values are $m \in \{1\%, 5\%, 10\%, 25\%, 50\%, 100\%\}$.

4 Results

Feature rankings, and the extended results (for every dataset separately) are available at http://source.ijs.si/mpetkovic/hmlc-ranking.

4.1 Saturation of the Ranking Quality

Influence of the Ensemble Size. We analyze each ranking score and ensemble separately. While these two are fixed, we let the number of the trees in the ensemble vary, and apply Friedman's test to discover whether some differences among them occur.

The resulting *p*-values are all bigger than 0.05, which means that the rankings can be computed very efficiently since it suffices to grow only 10 trees. Therefore, the ensemble size in the subsequent experiments is fixed to 10. Fig. 2a shows the resulting average rank diagram for Genie3 score, computed from a Bagging ensemble. Similar conclusions can be made using the other ensembles and scores.

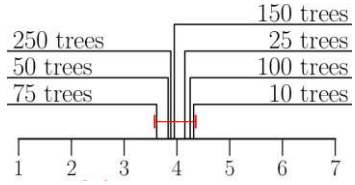

Figure 2a

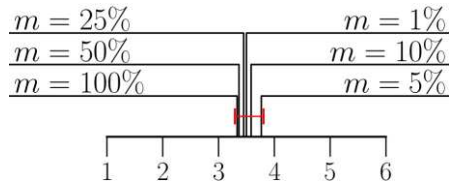

Figure 2b

Saturation of the rankings: Friedman's test discovered no statistically significant differences among different (a) ensemble sizes in the ensemble rankings (Genie3 score, coupled with the Bagging ensemble is shown), (b) considered proportions of the dataset by HMLC-Relief

Influence of the HMLC-Relief's Number of Iterations. Similarly, to previous setting, we let the value of the parameter *m* vary and compare the quality of the corresponding HMLC-Relief rankings by applying Friedman's test. Again, there are no statistically significant differences among the algorithms ($p = 0.96$) and the differences among quality of the rankings are now even smaller. As shown in Fig. 2b, no two average ranks differ by more than 0.43. Since the most time-efficient setting is $m = 1\%$, this is the considered number of iterations in the subsequent HMLC-Relief experiments.

4.2 Are the Ensemble-based Rankings Relevant?

To answer this question, we compare the predictive performance of the kNN classifier which uses the importance values from a particular feature ranking, to a non-weighted kNN baseline by using Wilcoxon's test. This pair-wise comparison is made for every admissible pair of feature ranking score and ensemble method, which results in 8 (not independent) comparisons. After we compute the *p*-values, the Benjamini-Hochberg correction is applied.

It turns out that all weighted kNN classifiers perform better than the baseline. However, the differences are statistically significant in 5 out of 8 cases, as assessed after applying the Benjamini-Hochberg correction after the Wilcoxon's test results: (Symbolic, RandomForests), (Genie3, RandomForests), (Symbolic, Bagging), (Genie3, ExtraTrees), and (Genie3, Bagging). Here, the p-values range from $2.14 \cdot 10^{-4}$ to $2.63 \cdot 10^{-2}$. The remaining three cases (with p-values at least $4.17 \cdot 10^{-2}$) are both feature rankings that are computed using Random Forest score and the feature ranking computed from Symbolic score and Extra Trees ensemble. Thus, using Genie3 score always results in relevant rankings, while Symbolic score fails to yield relevant rankings when used in combination with Extra Trees. The fact that Random Forest ranking fails to yield relevant rankings in all cases, may be at least partially explained by the sparsity of the data, since in that case, the differences of the error estimates on the out of bag examples and out of bag examples with permuted values of a feature, may not be that significant.

4.3 The most Appropriate Ensemble for a Given Score

Here, we fix the remaining parameter of the ensemble-based rankings, i.e., we find the most appropriate ensemble method for each feature ranking score. This is done by first fixing a feature ranking score, and then comparing the quality of the rankings obtained using this score and one of the possible ensemble methods. In the case of Symbolic and Genie3 score, Friedman's test is applied, since they can be used in combination with three ensemble methods. In the case of Random Forest score which cannot be paired with Extra Trees, Wilcoxon's test is used.

In the case of Symbolic ranking, the differences are not statistically significant ($p = 0.106$), as shown in Fig. 3a. Following the rationale from the previous section, Random Forests ensemble is proclaimed as the optimal one, since this method is considerably more time-efficient than Bagging. Since the majority of attributes is numeric (or can be considered numeric, because they are nominal and binary), Extra Trees i) have the same O time complexity of inducing one node as Random Forests, ii) typically result in bigger trees than Random Forests, the Random Forests ensemble is the most time efficient.

We observe a similar situation when comparing different ensemble methods when the feature ranking score is fixed to Genie3, as shown in Fig. 3b. Again, no statistically significant differences are found ($p = 0.705$), hence Random Forests ensemble is again chosen as the most appropriate one.

As for the Random Forest feature ranking score, Wilcoxon's test detects that Bagging ensemble statistically significantly ($p = 0.030$) outperforms Random Forests ensemble, hence Bagging is the most appropriate one for this feature ranking score.

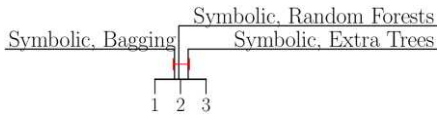

Figure 3a

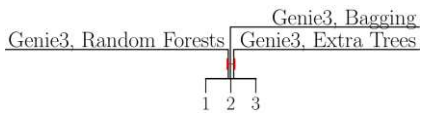

Figure 3b

The quality of different feature rankings as assessed by Friedman's test, when ensemble method varies, and feature ranking score is fixed to (a) Symbolic and (b) Genie3. No statistically significant differences were found.

4.4 Comparison of the Scores

In Sec. 4.1, we have shown that we obtain as good as it gets ensemble-based feature rankings when we grow 10 trees, and as good as it gets HMLC-Relief feature rankings when we set then number of iterations to $m = 1\%$ of the training set size $|\mathcal{D}_{\text{TRAIN}}|$. In the previous section, we additionally found the most appropriate ensemble method for a given feature ranking score. Now, we first check whether the three ensemble scores computed with the optimal parameters outperform the HMLC-Relief score, computed with the optimal parameters. This is done in a similar fashion to the Sec. 4.2 by applying three pairwise comparisons via Wilcoxon's test and Benjamini-Hochberg correction.

The differences reported here are always in favor of the ensemble-based scores. The obtained p-values are (sorted in the increasing order): $p_1 = 4.86 \cdot 10^{-5}$ (Symbolic, Random Forests), $p_2 = 1.74 \cdot 10^{-4}$ (Genie3, Random Forests), $p_3 = 1.59 \cdot 10^{-3}$ (Random Forest, Bagging). After applying the correction, all three differences are statistically significant, hence all three ensemble-based rankings outperform the HMLC-Relief ranking.

Next, we investigate which of the ensemble-based scores performs best. To this end, we apply Friedman's test. The obtained p-value equals $2.33 \cdot 10^{-3}$ and we can proceed to the Nemenyi's post-hoc test to discover where the differences occur. The results are shown in the Fig. 4. There are two groups of scores that do not perform statistically significantly different. The first group consist of Symbolic and Genie3 score, and the second one consists of Genie3 and Random Forest score. The graph also reveals Symbolic score (with the average rank of 1.55) performs statistically significantly better than Random Forest score (with the average rank of 2.42). Since the Random Forest score has the worst time complexity, we prefer the other two over it.

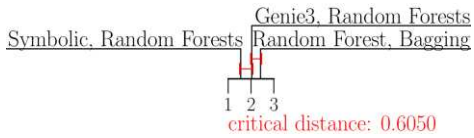

Figure 4
Comparison of the three ensemble-based feature ranking scores

4.5 A Closer Look to Some Other Rankings' Characteristics

A high number of benchmark problems allows for a statistical analysis performed in the previous sections. However, when averaging the performances, some information is always lost, therefore we now take a closer look at two characteristics of the obtained feature rankings in addition to the one already mentioned: the quality of the ranking stabilizes quite quickly (after growing ten trees). We will use the graphs in Figs. 5a and 5b which show the results for hom-ara-FUN dataset, as a running example. One of the reasons for choosing this dataset is that it is high dimensional and is also one the datasets where considering all features when inducing the trees in the Extra Trees ensemble does not work. This is visible from Fig. 5a, which shows the qualities of the Symbolic ranking, computed from different ensembles. Considering only a subset of features in each node (Extra Trees, SQRT) as compared to considering all the features (Extra Trees, all), pushes the quality of the rankings over the baseline.

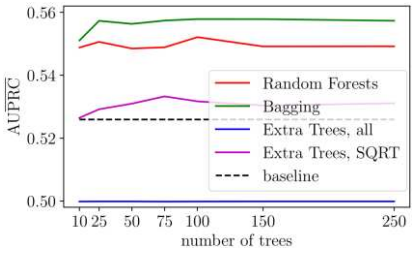

Figure 5a

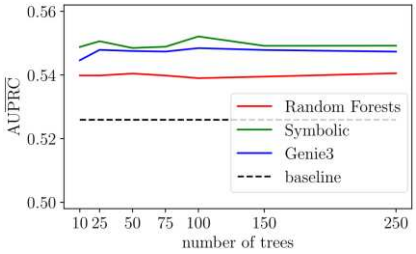

Figure 5b

Quality of the feature rankings on the hom-ara-FUN dataset when number of trees varies and (a) feature ranking score is fixed to Symbolic, (b) ensemble method is fixed to Random Forests. In the figure (a), all and SQRT denote the number of features considered in the Extra Trees algorithm.

The order of the rankings. Fig. 5b depicts typical situation with respect to the order of the feature ranking scores when an ensemble method is fixed. More precisely, only in 4 out of 30 cases, the ranking that belongs to the Random Forest score is placed in between those that belong to Symbolic and Genie3 score. This can be explained by the fact that the mechanisms for computing feature relevance values in the latter two scores, are more similar to each other than to the mechanism of Random Forest score: Symbolic score (number of examples) and Genie3 score (variance reduction) both consider statistics that are somewhat related since number of examples is also part of the variance reduction statistic. Random Forest score, on the other hand, takes a look at the error reduction values.

Efficiency of the rankings. Under efficiency of a ranking, we mean the (relative) number of the features that have a positive feature importance. The lower the number, the more efficient the ranking. In Fig. 5b, all three scores result in

relevant feature rankings, since all three curves lie above the baseline. The dataset at hand has the second highest number of features (72869) and it is surprising that the weighted kNN algorithms which make use of the weights from the rankings, wipo ignores more than 90% of the features - those that were proclaimed irrelevant and have weight 0 (or negative): In the case of Genie3 and Symbolic score, approximately, 8% of the features are being used, whereas in the in the case of the Random Forest score, this number is even lower: 3%. Similar situation was observed for the other extremely high dimensional datasets, e.g., wipo where Random Forest rankings proclaim 99% of the features irrelevant, and reuters. On the other hand, the rankings seem to be less efficient on lower-dimensional datasets. For example, in the case of cellcycle, clef07a-is and gasch1-yeast-FUN datasets, all features have positive importance.

By carefully inspecting the results, we make three main observations. First, Symbolic and Genie3 score columns are equal, but this can be explained by the fact that they are computed from the same ensemble (Random Forests) and the terms in Eq. (1) and Eq. (2) are always positive which is obvious for the Symbolic score, and can be proven with simple algebra for the Genie3 score.

A more interesting observation is that Random Forest ranking is consistently more efficient that the other two ensemble rankings (on 28 of 30 datasets). The reason for this is most likely the fact that Random Forest rankings are computed from the Bagging ensemble which always considers all features when inducing a new node of a tree. If the relevant features can be told apart from the irrelevant ones, then, always one of the relevant features would be chosen in a test split. This does not hold for the Random Forests ensembles which Genie3 and Symbolic scores are computed from, since they consider only a subspace of features, so all (or most of the) relevant ones can be skipped by chance. In addition to that, bootstrapping may also play an important role in this process, especially when the data is sparse which is true for many of the datasets, e.g., yeast-GO, it can happen, that different features are important, for different bootstrap replicates.

The last observation is that HMLC-Relief feature rankings are typically more efficient than the ensemble-based feature rankings. This is another proof that data is sparse, since the second term in Eq. (4) - which can make the relevance negative - should converge to zero when the domain is populated with more and more examples (a sketch of a proof can be found in [17]). However, the efficiency is not correlated with the ranking quality as shown in Sec. 4.4.

The other view on efficiency relates to time efficiency. We can estimate the time complexities $O(F\, m^2 + n\, |\mathcal{L}|)$ for HMLC-Relief and $O(F\, m\, log\, m\, (log\, m + |\mathcal{L}|))$ in the worst case of ensemble-based rankings (using bagging ensemble), where $m = |\mathcal{D}_{\mathrm{TRAIN}}|$. This reveals that ensemble-based rankings are typically more time-efficient than HMLC-Relief rankings (unless the hierarchy size $|\mathcal{L}|$ is sufficiently larger than the other quantities).

Ranking Similarity. The similarity of the two feature rankings is measured in terms of their Fuzzy Jaccard Index (FUJI) score [23] which is defined as follows. Given two rankings $r_i = (x_{(1)}^{i}, \ldots, x_{(F)}^{i})$, i = 1, 2, where $x_{(j)}^{i}$ denotes the j-th top-ranked feature in ranking r_i, accompanied by the feature importance score f_j^i, we define the sets $F_j^i = \{x_{(1)}^{i}, \ldots, x_{(j)}^{i}\}$ as the sets of top-ranked features of ranking r_i. Finally, the fuzzy membership function μ of the feature $x_{(k)}^{i}$ for the set F_j^i is defined as $\mu(F_j^i, x_{(k)}^{i}) = min\{1, f_k^i / f_j^i\}$, and $FUJI(F_j^1, F_j^2)$ is defined as:

$$FUJI\left(F_j^1, F_j^2\right) = \left(\sum_{x \in F_j^1 \cup F_j^2} \min_i \mu(F_j^i, x)\right) / \left(\sum_{x \in F_j^1 \cup F_j^2} \max_i \mu(F_j^i, x)\right)$$

This score is computed for $1 \leq i \leq F$ and the final similarity measure is the area under the FUJI curve consisting of the points (j, $FUJI(F_j^1, F_j^2)$). We compute this for all 6 pairs of the feature ranking scores and for all datasets. In Fig. 6, we present the distance $d = 1 - FUJI$ between the scores, averaged over the datasets.

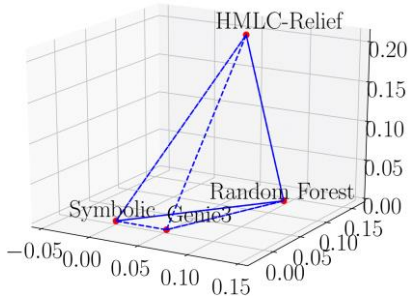

Figure 6

Tetrahedron whose vertices correspond to the feature ranking scores. The length of a side between two vertices equals the average distance $d = 1 - FUJI$ between the corresponding two feature ranking scores.

We can see that the Symbolic and Genie3 score produce the most similar rankings which is explained by the fact that they both consider tree node statistics. The closest to these two scores is the Random Forest score which reflects the fact that HMLC-Relief is the only non-ensemble-based score among the analyzed scores.

Conclusions

In this work we proposed three feature ranking scores, Symbolic, Genie3 and the Random Forest score, for the task of HMLC. The proposed feature ranking methods can be computed very efficiently, since it suffices to grow only 10 trees in the ensemble. The first two scores yield relevant feature ranking, while Random Forest score, fails. For the Symbolic and Genie3 score, the most suitable ensemble method is Random Forests, whereas bagging is the most suitable for Random Forest score. When coupled with the suitable ensemble method, all three scores outperform the HMLC-Relief feature ranking. Moreover, the Random Forest score is statistically and significantly, outperformed by the Symbolic score. Therefore, we recommend using either the latter or Genie3 score, since there are no

statistically significant differences among these two (but the Symbolic score has the lowest rank on average). We have also shown that Symbolic and Genie3 score are more closely related to each other than to Random Forest score. Especially on the extremely high-dimensional datasets, all three feature ranking scores successfully filtered out a majority of the features and still outperform the baseline that uses all of them. The HMLC-Relief feature rankings are even more efficient in that sense, but they are of lower quality.

This work can be extended in at least two directions. First, we could improve the HMLC-Relief, so that its performance would be comparable to the ensemble-based rankings. Second, we could extend the ensemble-based scores to the gradient boosting ensemble technique, which is inherently different from those presented herein, since, the trees are not independent of each other, which also allows for the analysis of the development of the ranking through the iterations.

Acknowledgement

We acknowledge the financial support of the Slovenian Research Agency (grant P2-0103 and a young researcher grant to MP), the European Commission (the grants MAESTRA (Learning from Massive, incompletely annotated, and Structured Data) and HBP (The Human Brain Project), SGA1 and SGA2. SD also acknowledges support by Slovenian Research Agency (via grants J4-7362, L2-7509, and N2-0056), the European Commission (project LANDMARK) and ARVALIS (project BIODIV). The experiments presented here were executed on the computing infrastructure from the Slovenian Grid (SLING) initiative.

References

[1] Barutcuoglu, Z., Schapire, R. E., & Troyanskaya, O. G. (2006) Hierarchical multi-label prediction of gene function. Bioinformatics, 22, 830-836

[2] Benjamini, Y., & Hochberg, Y. (1995) Controlling the False Discovery Rate: A Practical and Powerful Approach to Multiple Testing. Journal of the Royal Statistical Society, 57, 289-300, doi:10.2307/2346101

[3] Blockeel, H. (1998) Top-down Induction of First Order Logical Decision Trees. Ph.D. dissertation, Katholieke Universiteit Leuven, Leuven

[4] Breiman, L. (2001) Random Forests. Machine Learning, 45, 5-32

[5] Breiman, L., Friedman, J., Olshen, R. A., & Stone, C. J. (1984) Classification and Regression Trees. Chapman & Hall/CRC

[6] Clare, A. (2003) Machine learning and data mining for yeast functional genomics. Ph.D. dissertation, University of Wales Aberystwyth, Aberystwyth

[7] Consortium, T. G. (2000) Gene Ontology: tool for the unification of biology. Natural Genetics, 25, 25-29

[8] Demšar, J. (2006) Statistical comparisons of classifiers over multiple data sets. Journal of Machine Learning Research, 7, 1-30

[9] Dimitrovski, I., Kocev, D., Loskovska, S., & Džeroski, S. (2008) Hierchical annotation of medical images. Proceedings of the 11th International Multiconference - Information Society IS 2008 (str. 174-181) IJS, Ljubljana

[10] Dimitrovski, I., Kocev, D., Loskovska, S., & Džeroski, S. (2010) Detection of Visual Concepts and Annotation of Images Using Ensembles of Trees for Hierarchical Multi-Label Classification. Recognizing Patterns in Signals, Speech, Images and Videos (str. 152-161) Springer

[11] Dimitrovski, I., Kocev, D., Loskovska, S., & Džeroski, S. (2011) Hierarchical Classification of Diatom Images using Predictive Clustering Trees. Ecological Informatics

[12] Hansen, L. K., & Salamon, P. (1990) Neural network ensembles. IEEE Transactions on Pattern Analysis and Machine Intelligence, 12, 993-1001

[13] Huynh-Thu, V. A., Irrthum, Wehenkel, L., & Geurts, P. (2010) Inferring Regulatory Networks from Expression Data Using Tree-Based Methods. PLoS One, 5, 1-10

[14] Klimt, B., & Yang, Y. (2004) The Enron Corpus: A New Dataset for Email Classification Research. ECML '04: Proceedings of the 18th European Conference on Machine Learning -- LNCS 3201 (str. 217-226) Springer

[15] Kocev, D. (2011) Ensembles for predicting structured outputs. Ph.D. dissertation, IPS Jožef Stefan, Ljubljana

[16] Kocev, D., Vens, C., Struyf, J., & Džeroski, S. (2013) Tree ensembles for predicting structured outputs. Pattern Recognition, 46, 817-833

[17] Kononenko, I., & Robnik-Šikonja, M. (2003) Theoretical and Empirical Analysis of ReliefF and RReliefF. Machine Learning Journal, 55, 23-69

[18] Levatić, J., Kocev, D., & Džeroski, S. (2015) The Importance of the Label Hierarchy in Hierarchical Multi-label Classification. Journal of Intelligent Information Systems, 45, 247-271

[19] Lewis, D. D., Yang, Y., Rose, T. G., & Li, F. (2004) RCV1: A New Benchmark Collection for Text Categorization Research. Journal of Machine Learning Research, 5, 361-397

[20] Madjarov, G., Gjorgjevikj, D., Dimitrovski, I., & Džeroski, S. (2016) The use of data-derived label hierarchies in multi-label classification. Journal of Intelligent Information Systems, 47, 57-90

[21] Petković, M., Džeroski, S., & Kocev, D. (2018) Feature Ranking with Relief for Multi-label Classification: Does Distance Matter? V L.

Soldatova, J. Vanschoren, G. Papadopoulos, & M. Ceci (Ured.), Discovery Science (str. 51-65) Springer

[22] Petković, M., Kocev, D., & Džeroski, S. (2019) Feature ranking for multi-target regression. Machine Learning

[23] Petković, M., Lucas, L., Kocev, D., Džeroski, S., Boumghar, R., & Simidjievski, N. (2019) Quantifying the effects of gyroless flying of the Mars Express Spacecraft with machine learning. 2019 7th International Conference on Space Mission Challenges for Information Technology (SMC-IT)

[24] Rousu, J., Saunders, C., Szedmak, S., & Shawe-Taylor, J. (2006) Kernel-Based Learning of Hierarchical Multilabel Classification Models. Journal of Machine Learning Research, 7, 1601-1626

[25] Schietgat, L., Vens, C., Struyf, J., Blockeel, H., Kocev, D., & Džeroski, S. (2010) Predicting gene function using hierarchical multi-label decision tree ensembles. BMC Bioinformatics, 11

[26] Slavkov, I., Karcheska, J., Kocev, D., & Džeroski, S. (2018) HMC-ReliefF: Feature Ranking for Hierarchical Multi-label Classification. Computer Science and Information Systems, 15, 187-209

[27] Stańczyk, U., & Jain, L. C. (Ured.) (2015) Feature Selection for Data and Pattern Recognition. Springer

[28] Tsoumakas, G., & Katakis, I. (2007) Multi-label classification: An overview. International Journal of Data Warehousing and Mining, 1-13

[29] Vens, C., Struyf, J., Schietgat, L., Džeroski, S., & Blockeel, H. (2008) Decision trees for hierarchical multi-label classification. Machine Learning, 73, 185-214

[30] Wettschereck, D. (1994) A study of distance based algorithms. Ph.D. dissertation, Oregon State University, USA

Modelling, Forecasting and Testing Decisions for Seasonal Time Series in Tourism

Cvetko Andreeski[1], Daniela Mechkaroska[2]

Faculty of Tourism and Hospitality – Ohrid, University „St. Kliment Ohridski" – Bitola, 7000 Bitola[1]
Faculty of Computer Science and Engineering, Skopje, Ss. Cyril and Methodius University, 1000 Skopje, Macedonia[2]
cvetko.andreeski@uklo.edu.mk[1], daniela.mechkaroska@finki.ukim.mk[2]

Abstract: Time series analysis for basic tourism parameters, in the countries of the Balkan Peninsula, have been emphasized in recent research. Moreover, some of them have also shown a trend, aside from the rising variance during the period-heteroscedasticity. All of these characteristics of a time series of tourist demand, result in them being a great challenge for modeling. Therefore, there are different types of models that can be implemented for the modeling of a time series, which include accentuated seasonal components. Throughout this paper, multiple tests are performed using several parameters of the time series, with the ARIMA model, in an attempt to find any influence on the fit and validity of the model. For the accepted models, series are predicted for a year in advance and, in addition, a method of testing the decisions made by authorities in the field of tourism is presented.

Keywords: time series; modelling; parameters; forecasting; testing; decisions

1 Introduction

The modeling and forecasting of a time series plays a vital role in the process of planning and decision making in the tourism industry, which accounts for the vast number of papers on these issues. In the paper [15], modeling and forecasting is made for basic tourism parameters, from 1953-2014, sampled as annual data. This series is a challenge for modeling, as it contains two structural breaks. For the modeling, a standard ARIMA model is implemented according to what can be found in [2]. Alternatively, in paper [20], the authors used several competing models, mainly based on models for time series analysis and commenting on the results of modeling and forecasting of a series of arrivals in Australia. On the other hand, in paper [1] and [6] the main aim of research is the comparison between linear ARIMA models and non-linear models based on artificial neural networks. In paper [1] we can find an exploration of their performances for modeling time

series with existing break(s). Nevertheless, many authors have worked on time series modeling with seasonal components by using neural networks [3] [6] [13] [19], as time series with a significant seasonal component are important in different areas of research like economy [7], climate forecast [17], biology [18], medicine [8], etc. Aside from their performances in modeling, especially in modeling time series with occurring structural break(s), these models are much more complex than linear models. They have the potential problem of getting values of weights from the local minimum, so the results of forecasting can be disappointing, or fail to meet previous expectations based on the results of modeling [6] [3]. In this paper, we have analyzed time series of arrived domestic and foreign tourists with monthly data from two landlocked countries on the Balkan Peninsula: The Republic of Macedonia and the Republic of Serbia for a period of nine years. Whilst all the analyzed series have accentuated seasonal behavior, an upward trend is present, as well. All those characteristics of the series present a significant challenge for successful modeling and forecasting. ARIMA models will be used in the process of modeling and accordingly, different parameters of them will be tested to choose the best one. Correspondingly, the final chosen model will be tested for validity and forecast performance. Additionally, a forecast of future values of arrived tourists for the current year has been created. This paper presents a way of testing the decisions made in both countries aimed at supporting the growth of tourism. A few of them will be tested in different intervals for the impact that they have on the progress of tourism via increment on number of arrived tourists.

2 Analysis of Time Series

For the modeling, two different time series are used for each country: one concerns the domestic tourists visiting the Republic of Macedonia for the period from 01:2010 until 08:2017, and the other a series of arrived foreign tourists during the same interval. Despite the similarities of the two, we can detect different characteristics and behavior of the series. Both series have been presented for the analyzed time increment, in the Republic of Macedonia in Figure 1. From the graphical representation of the time series, several features may be noticed.

For the series of arrived domestic tourists we can conclude the following:

- The series has an accentuated seasonal component, much more heightened than is the case for the series of arrived foreign tourists at the same time.
- This series does not have a trend, although there is variation around an average value. It can be visible if we present data on an annual level.
- It has weak heteroscedasticity that should be tested.

For the series of arrived foreign tourists from the graphical representation, we can conclude that:

- It has an accentuated seasonal component.
- Furthermore, it has a heightened upward trend at the time.
- Likewise, it also has prominent heteroscedasticity, which implies the necessity of logarithmic transformation on the original time series in order to remove the influence of the heteroscedasticity. In addition, the last analyzed year significantly differs from the behavior of the rest of the series, which warrants further testing for hypothetical structural changes.

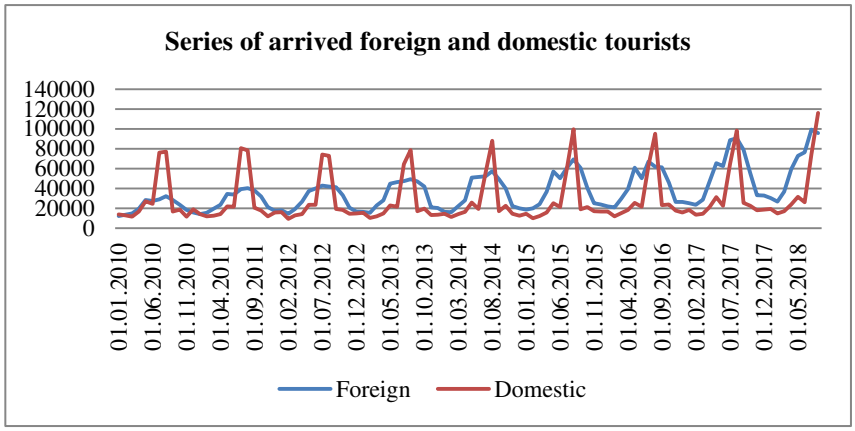

Figure 1

Graphical representation on series of arrived domestic and foreign tourists in the period 01:2010 - 8:2018. Source: State institute for statistics - Republic of Macedonia

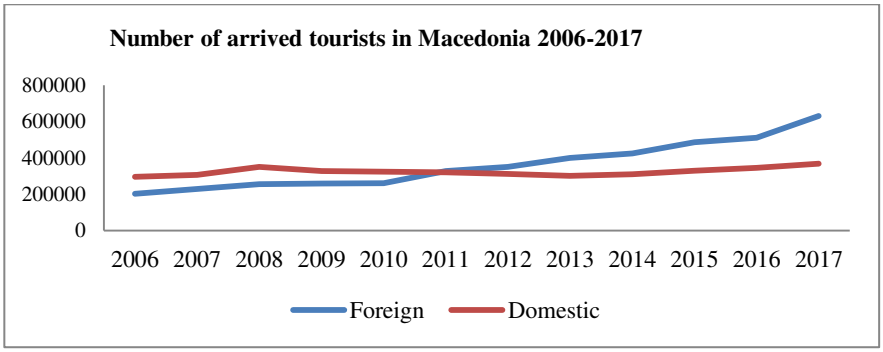

Figure 2

Number of arrived domestic and foreign tourists in the Republic of Macedonia, annual data. Source, State institute for statistics of the Republic of Macedonia

Series with annual data of arrived domestic and foreign tourists from 2006 to 2017 are shown in Figure 2. Similarly, the upward trend of the number of foreign tourists for the analyzed period can correspondingly be noticed in Figure 2, as well as, the variation of the number of arrived domestic tourists in the same timeframe. Leading up to 2011, the number of arrived foreign tourists was lower than the arrived domestic tourists, whereas their number significantly increased for the last six years, which leads to a 71% increase in the number of visiting domestic tourists in 2017. From the period of visa liberalization for Schengen countries in 2009 until 2013, the number of arrived domestic tourists decreases, and at the last four years, it encounters a slight increment. To conclude, in the series of arrived foreign tourists, an upward trend is present between 2006 and 2017.

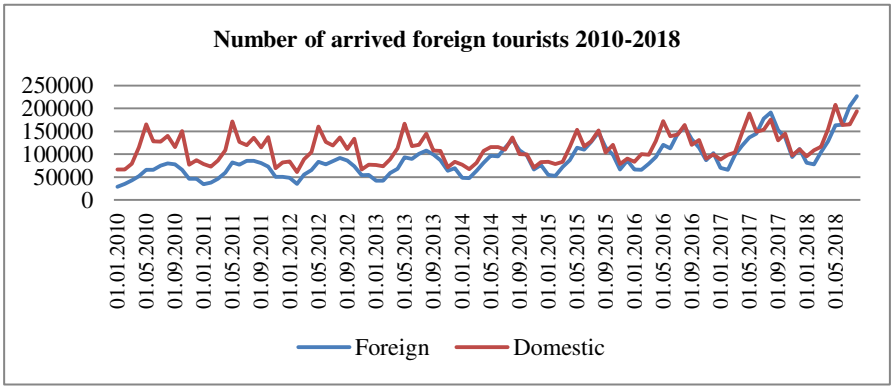

Figure 3

Graphical representation on series of arrived domestic and foreign tourists in the period 01:2010 - 8:2018. Source: State institute for statistics - Republic of Serbia

For the series of arrived domestic tourists in Serbia we can conclude that:

- The Series has a heightened seasonal component
- This series does not have a trend, but variation around an average value
- We should test for potential heteroscedasticity
- It changes its behavior (shape) in this phase of the analyzed time series

The series of arrived foreign tourists in Serbia suggests that:

- An accentuated seasonal component with a different pattern can be noted
- A prominent upward trend during the years is visible
- The presence of heteroscedasticity indicates the necessity of a logarithmic transformation of the original series in order to decrease that influence.

Each series should be tested for possible structural breaks[1].

Figure 4 portrays the series with annual data of arrived domestic and foreign tourists between 2010 and 2017 – Republic of Serbia, from which the upward trend of the number of foreign tourists can be observed.

On the other hand, the number of arrived domestic tourists does not show a specific trend, as it has variations around the average number of arrived tourists. Beside the fact that the series of arrived foreign tourists has a constant upward trend, the number of domestic tourists is greater than the number of arrived foreign tourists.

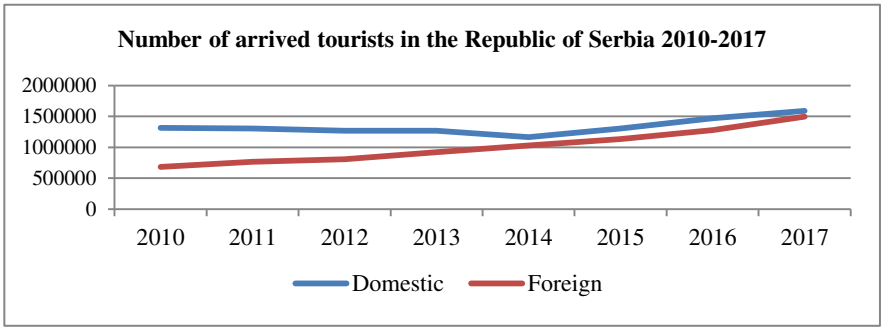

Figure 4
Number of arrived domestic and foreign tourists in the Republic of Serbia, annual data. Source, State institute for statistics of the Republic of Serbia

3 Modeling of Time Series

Autoregressive moving average model (ARMA) for stationary time series is a linear structure of two polynomials, one for the auto-regression (AR) and the second for the moving average (MA).

A stationary ARMA(p,q) model is defined as a linear sequence of autoregressive random variables X_t, and moving average random variables Y_t with zero mean value and constant variance provided by (1):

$$X_t - \varphi_t X_{t-1} - \ldots - \varphi_p X_{t-p} = Y_t + \theta_1 Y_{t-1} + \ldots + \theta_q Y_{t-q} \quad (1)$$

If the time series is non-stationary, we need to differentiate the series in order to get a stationary one. In this case we have an ARIMA(p,d,q) process where d is a

[1] Structural break is an abruptly change of time series at a point in time. This variation could involve a change in mean or a change in the other parameters of the process that produce(s) the series.

non-negative integer such that $(1-B)^d X_t$ is a causal ARMA(p,q) process [5]. All the analyzed time series in this paper are sampled by monthly data.

A series of arrived domestic tourists in the Republic of Macedonia will be the first analyzed time series, which has a seasonal component, without a trend. We have made one differencing of the series and we have tested the resulting series in order to conclude if it is stationary, as this is necessary for modelling. Augmented Dickey Fuller test was performed to check the status of the series and the results can be observed in Table 1.

Table 1

Unit root test for number of domestic tourists in the Republic of Macedonia

Null Hypothesis: D_DOMESTIC has a unit root, Exogenous: Constant
Lag Length: 10 (Automatic - based on SIC, maxlag=12)

		t-Statistic	Prob.*
Augmented Dickey-Fuller test statistic		-59.39975	0.0001
Test critical values:	1% level	-3.503049	
	5% level	-2.893230	
	10% level	-2.583740	

The critical values are much higher than the test statistics and the probability of rejection on null hypothesis is close to 0 as table one suggests, which indicates that the differenced time series is stationary.

At the beginning of the modeling, a Correlogram should be consulted for the lags of the series in order to detect the most significant parameters. The values of the autocorrelation of the lags and the partial autocorrelation are stated in Figure 5.

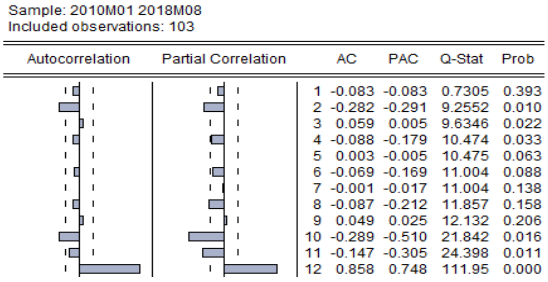

Figure 5

Autocorrelation and partial autocorrelation values of the lags of series

From the values of the Correlogram, we can conclude that the 12 lag has a significant value of correlation, furthermore, the variation of the values can be deduced from the partial autocorrelation values, or potential serial correlation of the lags. ARIMA(1,1,1) model can be proposed, the results are reported in Table 2.

From the results gathered from Table 2, we can conclude that:

- The probability that chosen variables will be rejected is low
- The fit of the model is good, so we can expect to have a suitable forecast
- According to Durbin-Watson statistics, the result is not conclusive, so we need to test the residuals in order to identify if they are uncorrelated.

Table 2
Model of series AR(12), MA(1)

Dependent Variable: D_DOMESTIC
Method: ARMA Maximum Likelihood (OPG - BHHH)
Date: 12/09/18 Time: 13:47, Sample: 2010M02 2018M08
Included observations: 103, Convergence achieved after 14 iterations
Coefficient covariance computed using outer product of gradients

Variable	Coefficient	Std. Error	t-Statistic	Prob.
AR(12)	0.990949	0.003742	264.8407	0.0000
MA(1)	-0.922846	0.051716	-17.84435	0.0000
SIGMASQ	12678529	1188167.	10.67066	0.0000
R-squared	0.979357	Mean dependent var		994.7282
Adjusted R-squared	0.978944	S.D. dependent var		24903.88
S.E. of regression	3613.708	Akaike info criterion		19.72877
Sum squared residuals	1.31E+09	Schwarz criterion		19.80551
Log likelihood	-1013.032	Hannan-Quinn criter.		19.75985
Durbin-Watson stat	1.579279			

In Figure 6, we can see the Correlogram of the residuals. From it, we can conclude that the residuals are uncorrelated, and they are inside the range of ±2 SE.

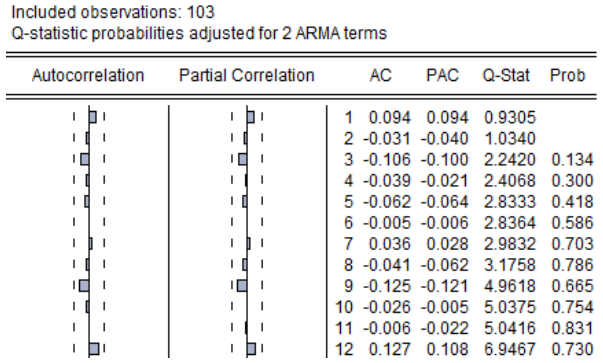

Figure 6
Correlation analysis on residuals of the model

The results provided in Table 3 imply that there is no heteroscedasticity of the residuals, and the model is valid. Hence, the residuals are uncorrelated and there is no heteroscedasticity in this series. This model grants us an opportunity to forecast future values of the series, aside from covering almost 98% of the variance of differenced series.

Table 3

Heteroscedasticity White Test on residuals

Heteroskedasticity Test: White		
F-statistic	172.8046 Prob. F(6,96)	0.0000
Obs*R-squared	94.27140 Prob. Chi-Square(6)	0.0000
Scaled explained SS	305.8439 Prob. Chi-Square(6)	0.0000

Figure 7 portrays an in sample forecast of the values 01-08.2018.

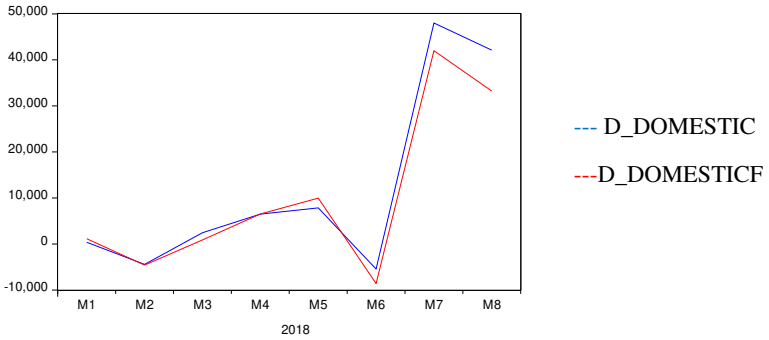

Figure 7

In sample forecasting of the series for 2018

Figure 8 represents the forecast of values for the analyzed series of arrived domestic tourists in 2019, and illustrates a comparison of the values with the previous year.

From there, we can deduct that the series of arrived domestic tourists in 2018 and the predicted values for 2019 are almost identical. The difference within the entire predicted timeframe is minor, but taking into consideration the fact that a trend was not present in the series, this result is to be expected.

The second modeled series, is the series of arrived foreign tourists in the Republic of Macedonia in the period between 01.2010 and 08.2018. This series is more complex for identification, taking into consideration the fact that this series has a trend, seasonal component, and evident heteroscedasticity. As can be seen by these characteristics of the series, a logarithmic transformation on the original series has been conducted, as well as differencing the series in order to create a stationary one.

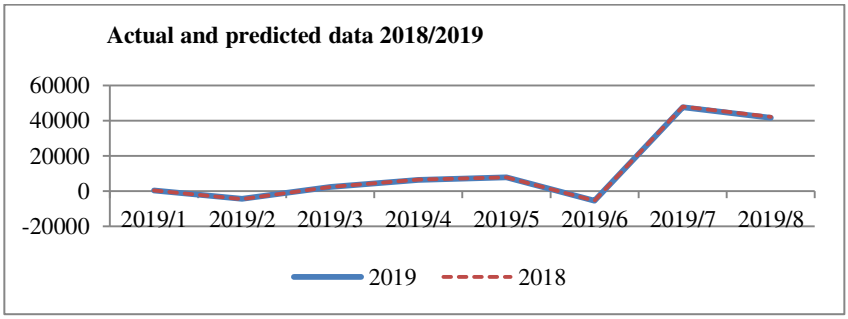

Figure 8

Graphical presentation of original series 01-08.2018 and predicted data 01-08.2019

Prior to modeling, a unit root test was performed on the transformed series in order to test whether the series is stationary. The results of the aforementioned testing are conveyed through Table 4.

Table 4

Unit root test results for the series of foreign tourists in the Republic of Macedonia

Null Hypothesis: LOG_FOREIGN_D has a unit root Exogenous: Constant
Lag Length: 11 (Automatic - based on SIC, maxlag=11)

		t-Statistic	Prob.*
Augmented Dickey-Fuller test statistic		-4.945204	0.0001
Test critical values:	1% level	-3.511262	
	5% level	-2.896779	
	10% level	-2.585626	

The test results indicate that one differencing of the series is enough to create stationary series. Hence, the modeling of the series should be commenced. A matrix of autocorrelation and partial autocorrelation values of the series lags were performed as is depicted in Figure 9.

The results of the Correlogram indicate (autocorrelation-AC and partial autocorrelation-PAC) patterns of serial correlation of the lags in both columns. Consequently, in the model of the series by itself, two parameters can be found. While the first one MA(1) is engaged for modeling serial correlation, the 12^{th} lag explains the seasonality of the series. Correspondingly, it is to be expected that these two lags will be very significant for this model.

During the phase of testing different models for validity, we have checked whether the series itself has different behaviors in different periods.

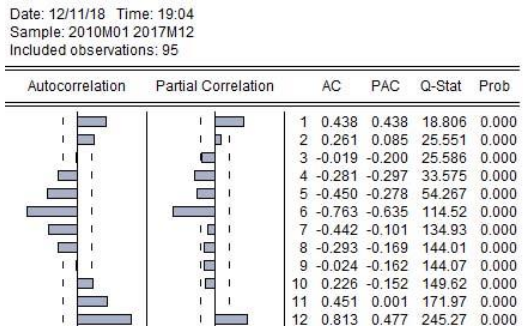

Figure 9

Autocorrelation and partial autocorrelation values of the lags of series – foreign tourists

Both models will be presented, from which the initial model consists of the first and 12th lag of the series, whilst the second model contains the first, 12th and 5th lag. Table 5 below introduces the comparison of the models.

Table 5

Models for series of foreign tourists in the Republic of Macedonia 01:2010-08:2018

Dependent Variable: LOG_FOREIGN D
Method: ARMA Maximum Likelihood (OPG - BHHH)
Date: 12/11/18 Time: 19:28
Sample: 2010M02 2018M08
Included observations: 103
Convergence achieved after 96 iterations
Coefficient covariance computed using outer product of gradients

Variable	Coefficient	Std. Error	t-Stat	Prob.
AR(12)	0.9883	0.0095	103.51	0.00
MA(1)	-0.7032	0.0545	-12.904	0.00
MA(12)	-0.2391	0.0564	-4.239	0.00
SIGMASQ	0.0072	0.0013	5.5099	0.00
R-squared	0.88962	Mean dependent var		0.01994
Adjusted R-squared	0.88628	S.D. dependent var		0.25665
S.E. of regression	0.08654	Akaike info criterion		-1.626
Sum sqr residuals	0.74155	Schwarz criterion		-1.52379
Log likelihood	87.7450	Hannan-Quinn criter.		-1.58467
DW stat	1.79844			

Model 1

Dependent Variable: LOG_FOREIGN D
Method: ARMA Maximum Likelihood (OPG - BHHH)
Date: 12/11/18 Time: 22:08
Sample: 2012M01 2018M08
Included observations: 80
Convergence achieved after 30 iterations
Coefficient covariance computed using outer product of gradients

Variable	Coefficient	Std. Error	t-Stat	Prob.
AR(12)	0.946817	0.03131	30.2346	0.0000
MA(1)	-0.535643	0.07428	-7.2110	0.0000
MA(5)	-0.357282	0.08642	-4.1341	0.0001
SIGMASQ	0.007650	0.00189	4.02862	0.0001
R-squared	0.894424	Mean dependent var		0.02150
Adjusted R-squared	0.890256	S.D. dependent var		0.27088
S.E. of regression	0.089738	Akaike info criterion		-1.5973
Sum sqr residuals	0.612021	Schwarz criterion		-1.4782
Log likelihood	67.89400	Hannan-Quinn criter.		-1.5495
DW stat	2.07777			

Model 2

Several conclusions can be deducted from the results of the preparation of model 1:

- Incorporated independent variables have low probability of rejection from the model, or high value of t-statistics
- The displayed model covers more than 88% of the variance of the series
- Durbin-Watson - DW statistics has a value close to 2 which can be an indicator for absence of serial correlation of residuals. However, further testing is necessary for assessing the hypothetical correlation of the residuals.

To conclude, the Correlogram stated in Figure 10 for model 1 clarifies that the fifth lag is outside the confidence interval. This prompted a search for another model appropriate for the series, including an examination of the series for a possible break.

Date: 12/11/18 Time: 19:32
Sample: 2010M01 2018M08
Included observations: 103
Q-statistic probabilities adjusted for 3 ARMA terms

Autocorrelation	Partial Correlation		AC	PAC	Q-Stat	Prob
		1	0.089	0.089	0.8464	
		2	0.084	0.077	1.6001	
		3	0.069	0.056	2.1191	
		4	-0.125	-0.144	3.8332	0.050
		5	-0.247	-0.244	10.577	0.005
		6	-0.101	-0.056	11.722	0.008
		7	-0.064	0.008	12.184	0.016
		8	-0.014	0.030	12.207	0.032
		9	0.021	-0.022	12.258	0.056
		10	0.017	-0.064	12.293	0.091
		11	0.100	0.062	13.477	0.096
		12	-0.004	-0.026	13.479	0.142

Model 1

Date: 12/11/18 Time: 22:11
Sample: 2012M01 2018M08
Included observations: 80
Q-statistic probabilities adjusted for 3 ARMA terms

Autocorrelation	Partial Correlation		AC	PAC	Q-Stat	Prob
		1	-0.100	-0.100	0.8236	
		2	0.000	-0.010	0.8236	
		3	-0.031	-0.032	0.9046	
		4	-0.172	-0.180	3.4583	0.063
		5	0.012	-0.026	3.4714	0.176
		6	-0.047	-0.055	3.6708	0.299
		7	0.054	0.030	3.9310	0.415
		8	0.002	-0.023	3.9313	0.559
		9	-0.020	-0.029	3.9684	0.681
		10	0.026	0.007	4.0314	0.776
		11	0.094	0.115	4.8634	0.772
		12	-0.140	-0.131	6.7429	0.664

Model 2

Figure 10

Correlogram on residuals for analyzed time series of arrived foreign tourists in Macedonia

The values from Table 6 and the graphical presentation in Figure 11 based on the Dickey-Fuller t-stat reveal that there is a structural break in the series of arrived tourists at the end of 2011. Thus, in order to have a stationary series without occurring structural breaks, a resampling of the series for the period 2012-2018 was conducted. The preceding data is enough to make a valid model (more than 50 samples) and this new series can be modeled as concluded from previous tests and results.

Table 6

Structural break at a time series of arrived foreign tourists

Null Hypothesis: LOG_FOREIGND has a unit root
Trend Specification: Intercept only
Break Specification: Intercept only
Break Type: Innovational outlier

Break Date: 2011M10

Break Selection: Minimize Dickey-Fuller t-statistic
Lag Length: 11 (Automatic - based on Schwarz information criterion, maxlag=12)

		t-Statistic	Prob.*
Augmented Dickey-Fuller test statistic		-5.781147	< 0.01
Test critical values:	1% level	-4.949133	
	5% level	-4.443649	
	10%level	-4.193627	

Results on modeling for this series can be subtracted from Table 5, model 2. This model has the following characteristics:

- Incorporated independent variables have low probability of rejection from the model, or high value of t-statistics
- The represented model covers more than 89% of the variance of the series
- The Durbin-Watson statistics has a value close to 2 which can be an indicator for the absence of serial correlation of residuals, however, further testing of the residuals is required

A comparison of Akaike and Hannan Quinn information criterion indicates that model 2 has lower values for both criteria, which consequently suggests that this model is more applicable than model 1. As models have the same number of independent variables, this does not affect the results of criteria. Furthermore, the results of the Correlogram on the residuals of model 2 imply that residuals are uncorrelated, and subsequently, there are no values outside the confidence interval, thus model 2 is a valid model for this series.

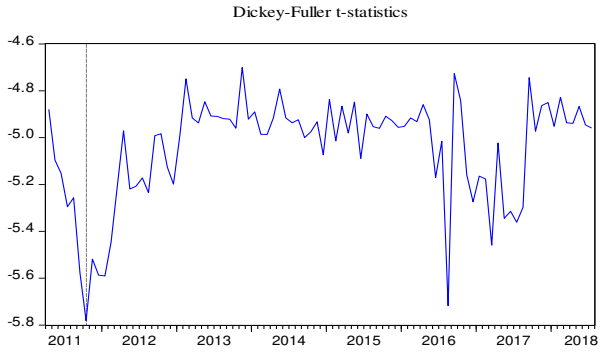

Figure 11
Structural break graph at the end of 2011 – series of foreign tourists

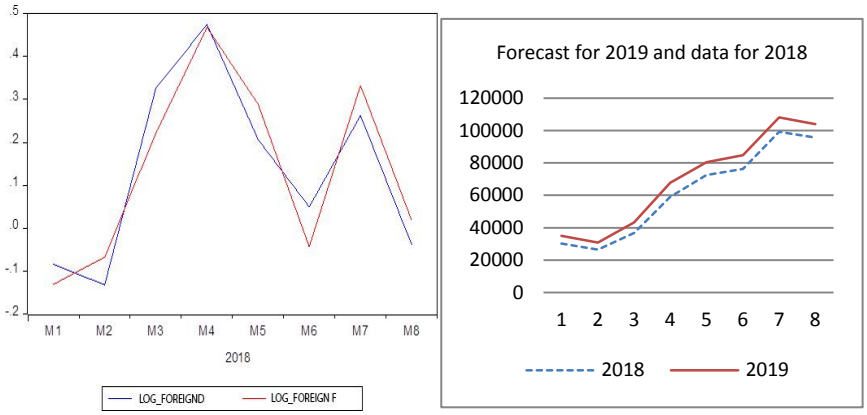

Figure 12
Original and predicted time series – arrived foreign tourists, Republic of Macedonia

Implementing the model that has proven to be superior, we can make a forecast for 2019. The results acquired from the use of the aforementioned model are portrayed in Figure 12. In addition, from the two graphs showcased in Figure 12, the first one is an in-sample forecast on-log and differenced series, while the second one is the forecast for 2019 vs 2018.

The following analysis and modeling on the series of arrived tourists in the Republic of Macedonia is about the first series of domestic tourists.

Before undertaking the analysis, the series should be tested for conceivable break point(s). The graphical presentation of the series in Figure 3 shows different behaviors of the series during the analyzed period. The completed unit root break test is documented in Figure 13.

Null Hypothesis: D_DOMESTIC has a unit root
Trend Specification: Intercept only
Break Specification: Intercept only
Break Type: Innovational outlier
Break Date: 2015M05
Break Selection: Minimize Dickey-Fuller t-statistic
Lag Length: 10 (Automatic - based on Schwarz information criterion, maxlag=12)

	t-Stat	Prob.*
ADF test	-25.4579	< 0.01
Test critical values:	1% level	-4.9491
	5% level	-4.4436
	10%level	-4.1936

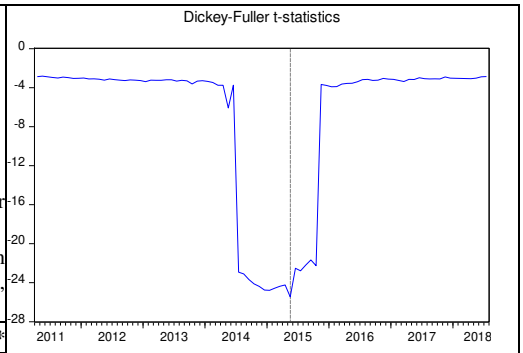

Figure 13
Unit root break test on the time series of arrived domestic tourists

The results in Figure 13, suggest that there is a break point in the series detected in 2015. Resampling the series 01:2015-08:2015 reveals that the number of data in the new series is slightly higher than the minimum series of 30 samples. The resampling and differencing of the series in order to get a stationary one was performed, from which results can be noted from Table 7.

Table 7

Unit root test results for the series of domestic tourists in the Republic of Serbia

Null Hypothesis: D_DOMESTIC has a unit root, Exogenous: Constant
Lag Length: 8 (Automatic - based on SIC, maxlag=9)

		t-Statistic	Prob.*
Augmented Dickey-Fuller test statistic		-6.220455	0.0000
Test critical values:	1% level	-3.588509	
	5% level	-2.929734	
	10% level	-2.603064	

As can be seen by the results from Table 7, the differenced time series is a stationary one. This concludes that the probability of rejection of null hypothesis is quite low. At this point, a Correlogram can be created in order to detect the crucial lags in the series. It has an evident trend and heteroscedasticity, which has prompted both a logarithmic transformation, and first lag differencing on the series. The Correlogram for the transformed and differenced series is presented in Figure 14.

The Correlogram in Figure 14, indicates that the 12^{th} lag is significant, which suggests that there is a serial correlation, meaning that the first and 12^{th} lag should be involved in the model. The proposed model, along with its associate statistics is showcased in Table 8.

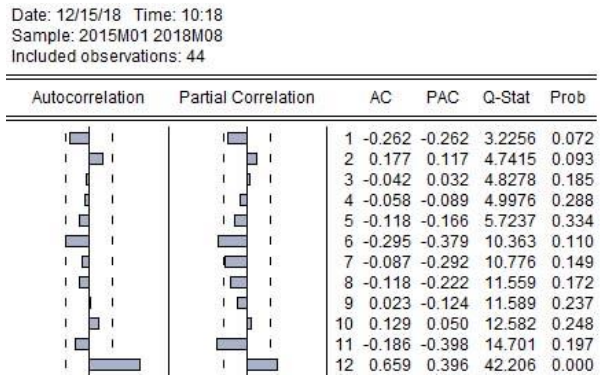

Figure 14

Correlogram for the transformed and differenced time series of arrived domestic tourists

Table 8
Models for series of domestic tourists in the Republic of Serbia

Dependent Variable: DLOG_DOMESTIC
Method: ARMA Maximum Likelihood
Date: 12/15/18 Time: 10:25
Sample: 2015M01 2018M08
Included observations: 44
Convergence achieved after 18 iterations
Coefficient covariance computed using outer product of gradients

Variable	Coefficient	Std. Error	t-Statistic	Prob.
AR(12)	0.98130	0.00868	113.05	0.000
MA(1)	-0.85245	0.10141	-8.405	0.000
SIGMASQ	0.00043	6.27E-05	6.9697	0.000
R-sqr	0.94942	Mean dependent var		0.008452
Adj R-sqr	0.94696	S.D. dependent var		0.094046
S.E. of regression	0.02165	Akaike info criterion		-3.83978
Sum sqr residuals	0.01923	Schwarz criterion		-3.71813
Log likelihood	87.47527	Hannan-Quinn criter.		-3.79467
DW stat	1.68946			

Dependent Variable: DLOG_DOMESTIC
Method: ARMA Maximum Likelihood
Date: 12/15/18 Time: 11:34
Sample: 2015M01 2018M08
Included observations: 44
Convergence achieved after 40 iterations
Coefficient covariance computed using outer product of gradients

Variable	Coefficient	Std. Error	t-Statistic	Prob.
AR(12)	0.992810	0.003790	261.9713	0.000
SAR(12)	-0.45479	0.113553	-4.00511	0.000
MA(1)	-0.85910	0.124190	-6.91767	0.000
SIGMASQ	0.00035	5.84E-05	6.007008	0.000
R-sqr	0.959437	Mean dependent var		0.00845
Adj R-sqr	0.956395	S.D. dependent var		0.09404
S.E. of regression	0.0196	Akaike info criterion		-3.8925
Sum sqr residuals	0.0154	Schwarz criterion		-3.7303
Log likelihood	89.636	Hannan-Quinn criter.		-3.8324
DW stat	1.6682			

The results from Table 8 reveal that:

- Included independent variables have low probability of rejection from the model, or high value of t-statistics
- The stated model covers more than 94% of the variance of the series
- DW statistics has a value close to 2 which can be an indicator of absence of serial correlation of residuals, however, the residuals should be tested.

The Correlogram in Figure 15 for model 1 indicates that the 12^{th} lag is outside of the confidence interval. An attempt was made to contain a seasonal component in order for a model with uncorrelated residuals to be created.

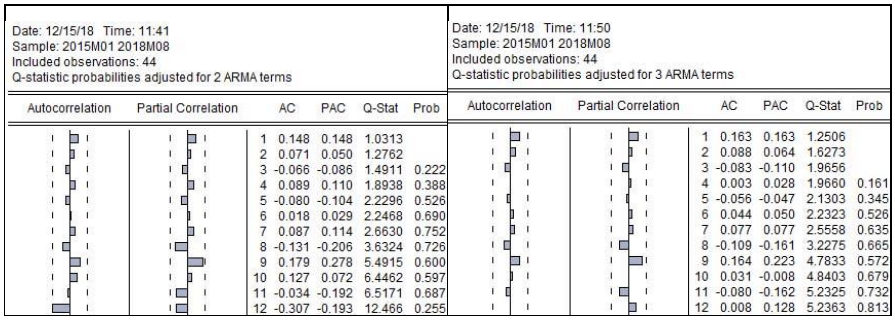

Date: 12/15/18 Time: 11:41
Sample: 2015M01 2018M08
Included observations: 44
Q-statistic probabilities adjusted for 2 ARMA terms

	Autocorrelation	Partial Correlation		AC	PAC	Q-Stat	Prob
1			1	0.148	0.148	1.0313	
2			2	0.071	0.050	1.2762	
3			3	-0.066	-0.086	1.4911	0.222
4			4	0.089	0.110	1.8938	0.388
5			5	-0.080	-0.104	2.2296	0.526
6			6	0.018	0.029	2.2468	0.690
7			7	0.087	0.114	2.6630	0.752
8			8	-0.131	-0.206	3.6324	0.726
9			9	0.179	0.278	5.4915	0.600
10			10	0.127	0.072	6.4462	0.597
11			11	-0.034	-0.192	6.5171	0.687
12			12	-0.307	-0.193	12.466	0.255

Date: 12/15/18 Time: 11:50
Sample: 2015M01 2018M08
Included observations: 44
Q-statistic probabilities adjusted for 3 ARMA terms

	Autocorrelation	Partial Correlation		AC	PAC	Q-Stat	Prob
1			1	0.163	0.163	1.2506	
2			2	0.088	0.064	1.6273	
3			3	-0.083	-0.110	1.9656	
4			4	0.003	0.028	1.9660	0.161
5			5	-0.056	-0.047	2.1303	0.345
6			6	0.044	0.050	2.2323	0.526
7			7	0.077	0.077	2.5558	0.635
8			8	-0.109	-0.161	3.2275	0.665
9			9	0.164	0.223	4.7833	0.572
10			10	0.031	-0.008	4.8403	0.679
11			11	-0.080	-0.162	5.2325	0.732
12			12	0.008	0.128	5.2363	0.813

Figure 15

Correlation of residuals for both models: series of arrived domestic tourists – Serbia

The residuals of the second model are not correlated, which indicates that it is to be rendered as valid for representing this time series. Suitably, the results of modeling given in Table 8 specify that Akaike and Hannan Quinn criteria have lower values for the first model, due to the number of independent variables. Then again, model 1 cannot be selected, as it is not relevant for this time series. What follows is a forecast calculated by the model. Figure 16 is presenting an in sample forecast.

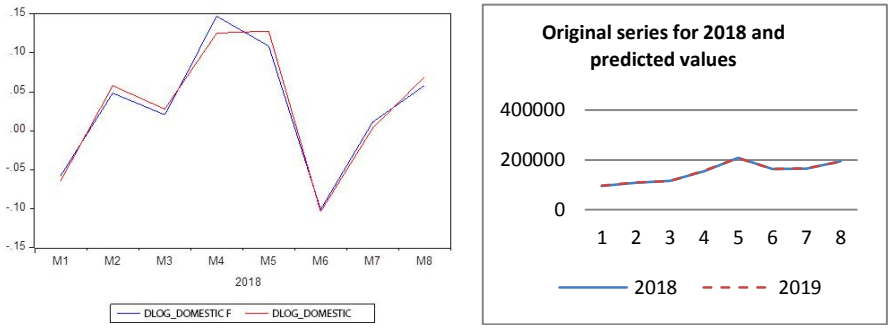

Figure 16

In sample and out of sample forecast for time series of arrived domestic tourists – Serbia

The last time series analyzed in this paper is the series of arrived foreign tourists in the Republic of Serbia, as can be deducted from Figure 3. As concluded earlier, this series should be tested for impending structural breaks, as there are evident differences in the behavior of the series over a longer period. This time series has an accentuated trend and heteroscedasticity. As means to eliminate the heteroscedasticity and trend a transformation on the series was performed, which contained a differentiation and log transformation. Likewise, whether the time series is stationary was tested with a unit root test.

The results specified in Table 9 indicate that the value of t-statistics is lower than the critical values, and the probability to reject null hypothesis of stationary series is very low. Henceforth, the resulting time series is stationary.

Table 9

Results of unit root test for the series of arrived foreign tourists – Republic of Serbia

Null Hypothesis: LOGD_FOREIGN has a unit root, Exogenous: Constant
Lag Length: 10 (Automatic - based on SIC, maxlag=10)

		t-Statistic	Prob.*
Augmented Dickey-Fuller test statistic		-14.92968	0.0001
Test critical values:	1% level	-3.528515	
	5% level	-2.904198	
	10% level	-2.589562	

As depicted in Figure 17, a test was performed to examine the series for potential structural breaks.

Null Hypothesis: LOGD_FOREIGN has a unit root
Trend Specification: Intercept only
Break Specification: Intercept only
Break Type: Innovational outlier

Break Date: 2017M02
Break Selection: Minimize DF t-statistic
Lag Length: 10 (Automatic - based on Schwarz information criterion, maxlag=10)

		t-Statistic	Prob.*
ADF test		-15.823	< 0.01
Test critical values:	1% level	-4.9491	
	5% level	-4.4436	
	10% level	-4.1936	

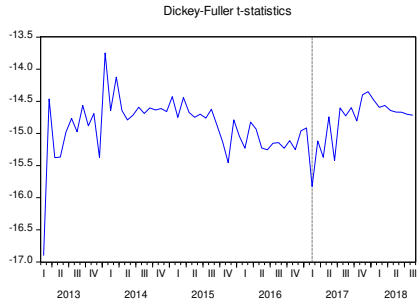

Figure 17

Structural break unit root test. Time series of foreign tourists in the Republic of Serbia

Additionally, the results represented in Figure 17 show that this series has a structural break at the beginning of 2017, meaning that, there is not enough sample data to serve as basis for a valid model. Models for identification of time series with existing structural breaks can be found in literature, such as models based on Artificial Neural Networks, yet their structure is very complex. In these models, the number of variables is much higher than the variables from ARIMA, and the forecasting is not as accurate as those created with linear models [3] [4].

Some authors [6] propose a combination of linear and non-linear models to get the best results, even though these models are more complex, and in most cases are hardly superior to linear models. They test in [9] [6] [19], the models going by the values of the residuals and the error between the original series and model with calculated MAPE and MAE errors.

In this paper, the accuracy of the models is between 88% and 97%, although that is not the main issue, but only one aspect of designing a valid model. The reasons for changes of the behavior of the series, as well as the period of the changes need to be identified. That is why the design of the model for this series will not be continued.

4 Analysis of Government Decisions Concerning Tourism

For the analyzed countries in the Balkans, the government decisions for the improvement of tourism have been considered as well. Both of these countries have subsidies for tourism. Granted, both countries have different approaches toward the type of subsidies, the choices for each of them were tested. Subsequently, the analysis of the implemented strategies in the Republic of Macedonia was conducted first, in which the period 2011-2018 was considered in order to make an appropriate analysis.

The unit root test for structural break(s) was selected as a valid methodology on testing decisions, where structural break(s) in time series is an abrupt change at a point in time. This change could involve a change in mean or the other parameters of the process that produce time series, such as variance or trend.

The most important assumption under the unit root [11] is that the random shocks have permanent effects on the long-run level of series. Correspondingly, these findings were challenged by [14], who argues that in the presence of a structural break, the standard ADF tests are biased towards the non-rejection of the null hypothesis [10]. Evidence of such an example can be found in the analyzed series of arrived foreign tourists in the Republic of Serbia, within this paper. According to the ADF test, the series is stationary after the first difference, but that shock is not on the long-run level of the series as can be concluded after the unit root break test.

Contrarily, Perron proposes a modified Dickey Fuller - (DF) unit root test with included dummy variables, to test the known or exogenous structural break. There are three types of possible structural breaks: First, changes in level of the series, second, changing of the trend (slope) in the series and third, a combination of the first and second break. Those three types are summed in the following equations:

$$x_t = \alpha_0 + \alpha_1 DU_t + d(DTB)_t + \beta t + \rho x_{t-1} + \sum_{i=1}^{p} \phi_i \Delta x_{t-1} + \varepsilon_t \quad (2)$$

$$x_t = \alpha_0 + \gamma DT_t + \beta t + \rho x_{t-1} + \sum_{i=1}^{p} \phi_i \Delta x_{t-1} + \varepsilon_t \quad (3)$$

$$x_t = \alpha_0 + \alpha_1 DU_t + d(DTB)_t + \gamma DT_t + \beta t + \rho x_{t-1} + \sum_{i=1}^{p} \phi_i \Delta x_{t-1} + \varepsilon_t \quad (4)$$

Where DU_t is the intercept dummy which tests the change in the level; DT_t is the slope dummy which tests the slope in some interval of the series and TB is a date of a structural break. All models have a unit root with a break under the null hypothesis [10].

The first analyzed time series is the time series of arrived Dutch tourists in the Republic of Macedonia in 2011. This is the first year after the decision of the government to give subsidies in order for tour-operators to bring tourists from the Benelux region. Figure 11 shows that there is a structural break in the series of arrived foreign tourists. Therefore, the series of arrived foreign tourists from the Netherlands were tested next to show whether there is a structural break after the applied strategies.

Null Hypothesis: D(DUTCH) has a unit root
Trend Specification: Intercept only
Break Specification: Intercept only
Break Type: Innovational outlier

Break Date: 2011M07
Break Selection: Minimize DF t-statistic
Lag Length: 11 (Automatic - based on Schwarz information criterion, maxlag=12)

		t-Statistic	Prob.*
ADF test		-4.6350	0.029
Test critical values:	1% level	-4.9491	
	5% level	-4.4436	
	10% level	-4.1936	

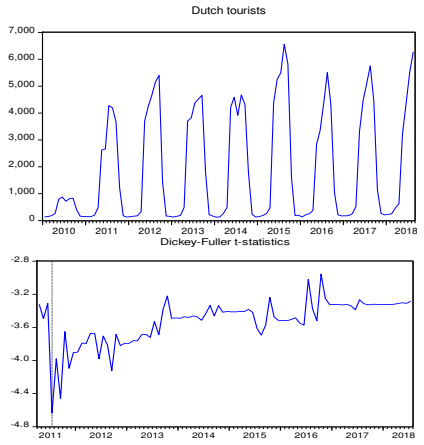

Figure 18

Time series and unit root structural break test for series of arrived tourists from Netherlands

Figure 18 reveals the time series of arrived Dutch tourists in the Republic of Macedonia and the corresponding structural break test for the series. Consequently, the results of the presentation and unit root structural break test indicate that:

- There is a difference in the level of arrived Dutch tourists in and after 2010
- The series is a seasonal, although a different behavior is present in different years, due to the different measures taken by the government, this series will be tested for another potential break
- From the results received from the break test we can conclude that there is a break in 2011, as expected based on different levels in the series

After 2010 a specific trend is not present and additionally there is a variation of the values around the mean value of the series

Another time series of arrived tourists from Scandinavian countries will be tested as well. A time series of arrived tourists from Sweden was taken as an example. In the Official Gazette of the Republic of Macedonia, No 53 published on 11 of April 2013, the government of the Republic of Macedonia has announced subsidies for tourists from Sweden amounting to 25 euros per tourist. Figure 19 presents the time series of arrived tourists from Sweden, including a unit root break test for this series. The graph of the series indicates that:

- This time series has a trend and an accentuated heteroscedasticity.What is more, the increase in the number of foreign tourists arrived in 2017 compared to 2010 is 363%
- Different behavior of the series in different years is evidenced, however, a proper test should be conducted such as a unit root test for a structural break
- There is no significant change in the level of the series in 2013, or 2014 as noted in the series of arrived tourists from the Netherlands.

The results given in the table of the unit root break test reveal that there is a structural break in the series in 2017. Contrarily, this structural break cannot be connected with the decision of the government in 2013. This leads to a conclusion that this decision did not bring the expected results measured by the increment in the number of arrived tourists from Sweden in the Republic of Macedonia. Moreover, the positive trend in the series can also be a result of the number of established direct air lines from Sweden to the Republic of Macedonia.[2] An added difference between the decision made for tourists from Benelux and one for tourists from Scandinavian countries is that subsidies for Scandinavian tourists is 25 euros per tourist, despite the amount of 65 euros for the arrived tourists from Benelux.

Nonetheless, subsidies in the Republic of Serbia have a different character and purpose in relation to subsidies in the Republic of Macedonia.

In Serbia, judging by the annual competitions for tourism subsidies envisaged under the established Strategy for development of tourism in the Republic of Serbia for the time between 2016 and 2025[3], subsidies may be received by domestic legal entities for the following purposes: promotion of tourism products, progress of satellite account statistics, education and training in tourism, arrangement of space, creation of planning documentation, arrangement of public areas, etc.

[2] In 2013 airline company Wizzair established direct lines from Skopje to Stockholm and Goteborg

[3] http://mtt.gov.rs/download/3/strategija.pdf

Null Hypothesis: D(SWEDISH) has a unit root
Trend Specification: Intercept only
Break Specification: Intercept only
Break Type: Innovational outlier

Break Date: 2017M05
Break Selection: Minimize DF t-statistic
Lag Length: 11 (Automatic - based on Schwarz information criterion, maxlag=12)

		t-Statistic	Prob.*
ADF test statistic		-6.7050	< 0.01
Test critical values:	1% level	-4.9491	
	5% level	-4.4436	
	10% level	-4.1936	

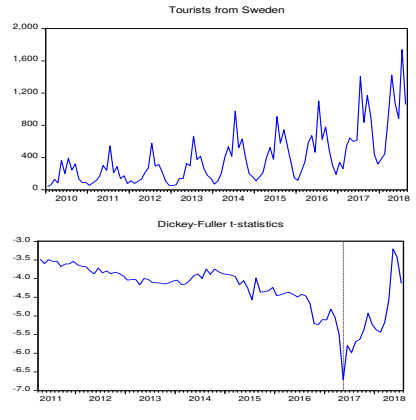

Figure 19
Time series and unit root structural break test for time series of arrived tourists from Sweden

This diverts the attention to the previous analysis of the series of arrived tourists in the Republic of Serbia. Subsequently, for foreign tourists, the structural break is at the beginning of 2017, which may indicate a result of the measures provided for the Tourism Development Strategy 2016-2025.

Conclusions

From our conducted analysis on time series of the number of visiting tourists in two neighboring countries in the Balkans, we can conclude, that in spite of the similarities in the characteristics of the series, the generated models can differ. Even though all of them have seasonal components and a significant serial correlation, each model has unique characteristics. What is more, all models are tested for validity, adding to the attempt at creating a concurrent model, which is chosen as per the results of the accompanied information criteria. Moreover, one of the essential parts in the analysis is the presence of any structural break(s) in the time series, which can influence choices, or events that have happened during a given period of the analysis. Likewise, they can serve as a basis for testing decisions of the Government or other Governmental body, that are responsible for any strategies and assessments designed to improve Tourism in their country. As deduced from the analysis, some implemented strategies have an impact on the advancement of Tourism, whereas some of them do not. However, the main goals in the development of Tourism, is the growth of the number of arriving foreign tourists and to ensure that the target has been reached for the concerned country.

References

[1] Andreeski, Cvetko, and Pandian Vasant. "Comparative analysis on time series with included structural break." *Proceedings of the Second Global*

Conference on Power Control and Optimization. Bali: American Institute of Physics, 2009, 217-224

[2] Baldigara, Tea, and Maja Mamula. "Modelling International Tourism Demand." *Tourism and Hospitality Management, Vol. 21, No. 1*, 2015: 19-31

[3] Benkachca, S, J Behra, and H El Hassani. "Causal Method and Time Series Forecasting model based on Artificial Neural Network." *International Journal of computer Applications (0975-8887)*, August 2013: 37-42

[4] Benkachcha, S, S Benhra, and H El Hassani. "Seasonal Time Series Forecasting Models based on Artificial Neural Network." *International Journal of Computer Applications (0975-8887) Vol. 166*, 2015: 9-14

[5] Brockwell, Peter J, and Richard A Davis. *Introduction to Time Series and Forecasting, Second Edition.* New York: Springer, 2002

[6] Chen, K. Y. "Combining linear and nonlinear model in forecasting tourism demand." In *Expert Systems with Applications*, 10368-10376, Vol. 38, 2011

[7] Ette, Etuk Harrison. "A Seasonal Arima Model for Nigerian Gross Domestic Product." *Developing Country Studies, Vol. 2, No. 3*, 2012: 50-62

[8] Fazekas, Mária. "Time Series Models on Medical Research." *Periodica Polytechnica Ser. El. Eng. Vol. 49, No. 3-4*, 2005: 175-181

[9] Fong-Lin, Chu. "Forecasting tourism demand: a cubic polynomial approach." *Tourism Management 25*, 2004: 209-218

[10] Glynn, J, N Perera, and R Verma. "Unit root tests and structural breaks: a survey with applications." *Journal of Quantitative Methods for Economics and Business Administration, 3(1)*, 2007: 63-79

[11] Nelson, C R, and C I Plosser. "Trends and random walks In Macroeconomic Time Series." *Journal of Monterey Economics, 10*, 1982: 139-162

[12] O'Hare, Colin, and Youwei Li. "Identifying Structural Breaks in Stochastic Mortality Models." *SSRN electronic Journal*, 2015

[13] Oscar, Claveria, Monte Enric, and Torra Salvador. *Tourism demand forecasting with different neural networks models.* Barcelona: Research Institute of Applied Economics, 2013

[14] Perron, P. "The great crash, the oil price shock, and the unit root hypothesis." *Econometrica 57*, 1989: 1361-1401

[15] Petrevska, Biljana;. "Predicting tourism demand by A.R.I.M.A. models." *Economic Research, doi 10.1080/1331677X.2017.1314822*, 2015: 939-950

[16] Ruey-Chyn, Tsaur, and Kuo Ting-Chun. "Tourism demand forecasting using a novel high precision fuzzy time series model." *International Journal of Innovative Computing, Information and Control*, 2014: 695-701

[17] Shengwei, Wang, Feng Juan, and Liu Gang. "Application of seasonal time series model in the precipitation forecast." *Mathematical and Computer Modelling, Volume 58, Issues 3-4*, 2013: 677-683

[18] Shitan, Mahedran, Pauline Mah Jin Wee, Lim Ying Chin, and Lim Ying Siew. "Arima and Integrated Arfima Models for Forecasting Annual Demersal and Pelagic Marine Fish Production in Malaysia." *Malaysian Journal of Mathematical Sciences 2(2)*, 2008: 41-54

[19] Teixeira, J p, and P O Fernandes. "Teixeira, J. P., & Fernandes, P. O. (2014). Tourism time series forecast with artificial neural networks. " *Tékhne, 12(1-2), 26-36, doi:10.1016/j.tekhne.*, 2014: 26-36

[20] Victor Wong, Anand Tularam and Hamid Shobeir Nejad. "Modeling Tourist Arrivals Using Time Series Analysis: Evidence From Australia. "*Journal of Mathematics and Statistics 8 (3)*, 2012: 348-360

2020 Reviewers

Ádám, Norbert
Adamne Major, Andrea
Agbinya, Johnson
Andoga, Rudolf
Arahal, Manuel R.
Atanasova – Pachemska, Tatjana
Baklanov, Alexander
Bakucz, Peter
Baranyi István
Bednar, Peter
Belina, Károly
Berke, Szilárd
Bobrov, Leonod
Bonilla, Javier
Choroś, Kazimierz
Csobán, Attila
Czakó, Bence Géza
Czifra, Árpád
de la Calle, Alberto
Dömötör, Ferenc
Drexler, Dániel András
Erdélyi, Viktor
Fábián, Enikő Réka
Főző, Ladislav
Fülöp, Zoltan
Garai-Fodor, Monika
Gašpar, Vladimír
Gonda, Viktor
Grion, Valentina
Gyarmati, Gábor
Györök, György
Hargitai, Hajnalka
Horecky, Jan
Horváth, Richárd
Hrabovsky, Jan
Ispány, Márton
Jelacic, Denis
Jukic, Samed
Juříková, Martina
Karpov, Alexey
Kasanicky, Tomas
Katona, Attila
Katona, Jozsef
Kaya, Heysem
Kopacek, Peter
Kovács, László
Kucharcikova, Alzbeta
Laššák, Miroslav
Lipovský, Pavol
Lucka, Maria
Machová, Kristína
Magyar, Attila
Mankovits, Tamás
Matis, Martin
Mikó, Balázs
Molnár, György
Myskova, Renata
Nagy, Dénes Ákos
Pál Ex Apró, Magdolna
Paniti, Imre
Papcun, Peter
Paralic, Jan
Pawel Dobrzanski
Pedro, Rodriguez
Pokorádi, László
Polishchuk, Volodymyr
Precup, Radu-Emil
Prochazka, Ales
Reicher, Regina Zsuzsánna
Rövid, András
Schreiner, Michal

Schrötter, Martin
Simandi, Szilvia
Smieszek, Miroslaw
Stachová, Katarína
Steingartner, William
Svec, Marek
Szabó, Attila
Szénási, Sándor
Takács, Árpád
Tar, József
Toth, Janos
Tóth, János
Vaispacher, Tomas
Vajdova, Iveta
Vámossy, Zoltán
Vascak, Jan
Venkatraman, Praburaj
Woda, Marek
Wójcik, Waldmar
Závadský, Jan
Zsidai, László